

70-14,430

SAMIMI, Jalal, 1940-
AN EMULSION STUDY OF PION-NUCLEON INTERACTIONS
AT 16.2 BEV.

The University of Oklahoma, Ph.D., 1970
Physics, elementary particles

University Microfilms, Inc., Ann Arbor, Michigan

THE UNIVERSITY OF OKLAHOMA
GRADUATE COLLEGE

AN EMULSION STUDY OF PION-NUCLEON INTERACTIONS AT 16.2 BEV

A DISSERTATION
SUBMITTED TO THE GRADUATE FACULTY
in partial fulfillment of the requirements for the
degree of
DOCTOR OF PHILOSOPHY

BY
JALAL SAMIMI
Norman, Oklahoma
1969

AN EMULSION STUDY OF PION-NUCLEON INTERACTIONS AT 16.2 BEV

APPROVED BY

M. Burwell
G. M. Canfield
William H. Huff
John C. ...
Dennis Shery

DISSERTATION COMMITTEE

ACKNOWLEDGMENTS

The author would like to express his deepest appreciation to Dr. James R. Burwell for his invaluable advice, assistance, and personal encouragements throughout the course of this research.

The help of many individuals involved in this project, in particular Miss Katie Royal, has been instrumental and is sincerely appreciated.

The author is also grateful to NASA for the fellowship which supported most of this work.

TABLE OF CONTENTS

	Page
LIST OF TABLES	vi
LIST OF ILLUSTRATIONS	vii
CHAPTER	
I. INTRODUCTION	1
II. KINEMATICS OF THE INTERACTIONS	7
A. Notations	7
B. Lab and C.M. Systems	8
C. Pion-Nucleon Interaction	8
1. Maximum Secondary-Nucleon Momentum	9
2. Maximum Angle of the Secondary Nucleon	11
3. Momentum vs. Angle of the Recoil Nucleon	15
a- Elastic Collisions	15
b- Inelastic Collisions	15
III. EQUIPMENT AND EXPERIMENTAL PROCEDURES	18
A. Emulsion	18
B. Microscopes	19
C. Experimental Techniques	21
1. Scanning	21
2. Selection of Events	23
3. Angle Measurements	28
4. Momentum Measurements	31
a- Range Measurement	31
b- Blob Counting	32
c- Multiple Coulomb Scattering	37
c1- Multiple Cell Calculations	42
c2- Calculations of Errors	43
d- Variable Cell Scattering Measure- ment	45
IV. PRESENTATION AND ANALYSIS OF DATA	47
A. Cross Sections and Pion Multiplicity Distributions	47
B. Elastic π^- -p Interactions	54
C. Inelastic π^- -N Interactions	58
1. Momentum Distribution of the Recoil Protons	59
2. Angular Distributions in the C.M. System	61
3. Transverse Momentum of Pions	68
a- Overall p_t -distribution	69
a1- Boltzmann Distribution	72

TABLE OF CONTENTS (Cont.)

	Page
a2-Linear Distribution	73
b-Dependence of p_t on θ and n_s	74
c-Dependence of p_t on C.M. Angle of Emission	78
4. Target Mass and Effective Target Mass	80
a-Target Mass	80
b-Effective Target Mass	85
5. Complete Events	92
a-Missing Mass	92
b-Kinematical Fitting	94
6. Search for Resonances	97
 V. SUMMARY AND CONCLUSIONS	 107
 APPENDICES	
A. NOISE ELIMINATION IN MULTIPLE COULOMB SCATTERING	115
B. EQUATIONS USED TO CHECK COMPLETE EVENTS	128
C. DATA ON INELASTIC π^- -N INTERACTIONS	133
 LIST OF REFERENCES	 182

LIST OF TABLES

Table	Page
1. Maximum Lab Angle and Minimum Momentum of the Recoil Nucleon	14
2. Mean Free Paths and Cross Sections	48
3. Data on Elastic π^- -p Events	56
4. Average Transverse Momentum	77
5. Average Effective Target Mass	91
6. Effective Target Mass for Complete Events	96
C1. Data on Inelastic π^- -p Events	134
C2. Data on Inelastic π^- -n Events	165

LIST OF ILLUSTRATIONS

Figure	Page
1. Maximum Lab Angle of the Recoil Nucleon vs. its C.M. Angle	13
2. Maximum Lab Momentum of the Recoil Nucleon vs. its Lab Angle	17
3. Lab Angles Definition	28
4. Range--Momentum-- g/g_m Plot	33
5. Scattering Factor vs. Cell Length	39
6. Distribution of Number of Charged Pions	50
7. Corrected Distribution of Number of Charged Pions	53
8. Momentum vs. Angle Plot for Protons from Elastic π^- -p Events	57
9. C.M. Angular Distribution of Protons from Elastic π^- -p Events	57
10. Recoil Proton Momentum Spectrum	60
11a C.M. Angular Distribution of All the Measured Secondary Pions from Inelastic π^- -p Events	63
11b C.M. Angular Distribution of All the Measured Secondary Pions from Inelastic π^- -n Events	64
12. C.M. Angular Distributions of the Measured Secondary Pions for Different Pion Multiplicities: π^- -p Events	66
13. C.M. Angular Distributions of the Measured Secondary Pions for Different Pion Multiplicities: π^- -n Events	67
14. Overall Transverse Momentum Distribution of the Measured Secondary Pions: π^- -p Events	70
15. Overall Transverse Momentum Distribution of the Measured Secondary Pions: π^- -n Events	71

LIST OF ILLUSTRATIONS (Cont.)

Figure	Page
16. Transverse Momentum Distributions for Angular Intervals: π^- -p Events	75
17. Transverse Momentum Distributions for Angular Intervals: π^- -n Events	76
18. Average Transverse Momentum vs. C.M. Angle Intervals	79
19. Target Mass Distributions	84
20. Effective Target Mass Distributions	87
21. Two-pion and Three-pion Invariant Mass Distributions	100
22. Pion-proton and Pion-pion-proton Invariant Mass Distributions	101
23. Invariant Mass Distributions for Combinations with $2800 < M_{\pi\pi p} < 3400$ MeV	105

AN EMULSION STUDY OF PION-NUCLEON
INTERACTIONS AT 16.2 BEV

CHAPTER I

INTRODUCTION

Although it is the most studied, the strong interaction is the least understood of the interactions in high energy particle physics. Strong interactions, which are responsible for the nuclear forces and processes, together with gravitational, electromagnetic, and weak interactions comprise the four known basic interactions which occur between elementary particles. In addition to nucleons (protons and neutrons), all the baryons (particles of half-odd-integral spin which, except for proton, decay either directly or via a chain of decays into a proton plus lighter particles) and all the mesons (particles of integral spin and non-zero mass which decay directly or via other mesons into leptons and photons) participate in strong interactions. ~~Although mesons~~ and baryons also participate in the other interactions, because of the very large

strength of the strong interaction, in processes in which this interaction participates, effects of the other interactions, if they occur simultaneously, are usually unobserved.

In the past few decades theoretical studies and experimental observations of the interactions between mesons and baryons have been used as a probe to the nature of strong interaction. One of the most important such features at high energies is the prolific production of particles, mainly mesons, but including baryon-antibaryon pairs. The threshold kinetic energy for single pion production is less than 200 MeV and at energies in the BeV region many-particle production processes become dominant. Because of this, any theory which is to explain the strong interaction at high energies must allow for the production (and also annihilation) of particles. Naturally, quantum field theory becomes a prime candidate. However, field theoretical treatments such as the propagator approach in quantum electrodynamics (which explains very well the electromagnetic interactions between elementary particles) fail for strong interactions. This is due to the fact that the coupling constant, which characterizes the strength of an interaction, is ~ 1 for the strong interactions, while it is $\ll 1$ for electromagnetic interactions. In quantum electrodynamics one expands the S-matrix in a pow-

er series in the coupling constant and then calculates the first few terms only, since the series converges very rapidly. This approach cannot be applied to strong interactions since the expansion parameter is greater than unity and the size of the higher order terms remains large and they cannot be ignored. For these reasons field theoretical treatments have been confined to the calculations of specific terms in the expansion which correspond to such particular dynamical models for the interaction as the isobaric model⁽¹⁾ or the one-pion-exchange model⁽²⁾. Other more intuitive models such as the statistical⁽³⁾ and fireball⁽⁴⁾ models have had partial success in correlating the observations in strong interaction experiments.

Due to the lack of a complete theory in the study of strong interactions, it has become common practice to start from the experimentally observed effects and to try to interpret them phenomenologically. Due to this rather unique situation experimental high energy physics has acquired an unusual role in pointing the way to an understanding of elementary particles and their interactions. For example, experimentalists who have studied the interactions of strongly interacting particles have discovered a great number of very unstable (lifetime of the order of 10^{-23} sec) particles. The discovery of these unpredicted particles (called resonances) in addition to making

the constantly growing list of the elementary particles more complete, has revolutionized the basic understanding of the elementary particles and strong interactions and has opened many avenues for research in this field. Many other important features of strong interactions such as the characteristics of the emission of the secondary particles, facts concerning the dynamics of certain interactions, constancy of the average transverse momentum, etc., have been revealed by experimental observations.

Although in the past two decades a great amount of experimental information has been collected and published on this subject, many of the published results are neither confirmed nor well established. Also many open questions regarding the characteristic features of strong interactions at high energies still exist. It is the purpose of this dissertation to describe an experimental observation on strong interactions at high energies conducted in an attempt to confirm some of the already observed results and effects, and, more important, to reveal other characteristic features of strong interactions. Due to the availability of the facilities at the University of Oklahoma, interactions of 16.2 BeV negative pions with nucleons have been examined with nuclear emulsion being the target and detector. Some of the specific concerns of this investigation can be outlined as follows:

- i--Measurements of cross sections for various pion-nucleon interactions.
- ii--Measurement and detailed observations on interaction parameters which are believed to be constant such as the average transverse momentum of secondary particles and effective target mass.
- iii--Observation of some of the aspects of the dynamics of the interactions and in particular exploring the question of centrality and/or peripherality of the collisions.
- iv--Comparison of the findings of this experiment with the results of previous experiments and with theories when such information is available.

Since the examination of the kinematics of the interactions requires an accurate determination of the momenta of the secondary particles, some of the existing emulsion techniques have been critically studied, and at times revised, in an attempt to improve the accuracy of the data. In the course of this research a new formalism for the interpretation of the data of multiple Coulomb scattering measurements has been developed which results in more reliable and more consistent values for the measured momenta.

A complete relativistic kinematical analysis of

pion-nucleon collisions have been carried out and used along with other selection rules as a criterion for the selection of the pion-nucleon collisions from the pion-nucleus collisions. This analysis is shown in Chapter II. The descriptions of the experiment, the emulsion stack, the equipment, and the experimental techniques and the formalisms used to extract the final data from the measurement data are given in Chapter III. The analysis and interpretation of the data, together with the full description of the approaches used in the analysis is contained in Chapter IV. A summary of the results and the conclusions are given in Chapter V. Appendix A contains the derivation of the equation developed for the elimination of noise in the multiple Coulomb scattering measurements together with an outline of all the research done as a part of this dissertation on this subject. Appendix B gives the equations developed and used for the identification of complete events, discussed in Chapter IV. The complete data of this experiment in its final form is presented in Appendix C.

CHAPTER II

KINEMATICS OF THE INTERACTIONS

A. Notations

Natural units ($c = 1$) will be used; mass, energy, and momentum will be given in units of MeV. β will denote the velocity of a particle with $\gamma = 1/\sqrt{1-\beta^2}$. The mass difference of protons and neutrons and that of charged and uncharged pions will be neglected.

M = nucleon mass

m = pion mass

E_N, \vec{p}_N = energy, momentum of the secondary nucleon

E_i, \vec{p}_i = energy, momentum of the i th secondary pion

θ_i = angle between \vec{p}_i and the direction of the incident pion

W = total energy of the reaction

E_0, \vec{p}_0 = energy, momentum of the incident pion

E_{TN}, \vec{p}_{TN} = energy, momentum of the target nucleon

B. Lab and C.M. Systems

The lab system is referred to as the coordinate system in which the target nucleon is at rest. The C.M. system is defined as the system in which the total momentum of all the particles is zero. Quantities in the lab system will be denoted by unprimed quantities and those in the C.M. system by primed quantities. Denoting the lab velocity of the C.M. system as β_c , taken along the z-axis, and using the Lorentz transformation, the primed quantities and the unprimed quantities can be written in terms of one another.

$$E' = \gamma_c (E - \beta_c p \cos \theta), \quad (1)$$

$$p' \cos \theta' = \gamma_c (p \cos \theta - \beta_c E), \quad (2)$$

$$p' \sin \theta' = p \sin \theta. \quad (3)$$

C. Pion-Nucleon Interaction

For the pion-nucleon reaction $\pi + N \rightarrow N + n\pi$, with $n = 1, 2, 3, \dots$, some useful relations will be derived. The elastic scattering (and charge exchange) are the special case of $n = 1$.

Taking \vec{p}_0 along the z-axis and using Eq. 2 for \vec{p}'_0 and \vec{p}'_{TN} we get

$$\beta_c = \frac{p_0}{E_0 + M}. \quad (4)$$

The total energy of the reaction in the lab and C.M. sys-

tems, W and W' , are

$$W = E_0 + M \quad (5)$$

$$W' = E_0' + E_{TN}' = \gamma_c (M + E_0 - \beta_c p_0) \quad (6)$$

$$= \frac{1}{\sqrt{1 - \left[\frac{p_0}{E_0 + M} \right]^2}} (M + E_0 - \frac{p_0^2}{E_0 + M}) = \sqrt{M^2 + m^2 + 2ME_0}$$

1-Maximum Secondary-Nucleon Momentum

In the C.M. system one has

$$\vec{p}_N' = -\sum \vec{p}_i' \quad (7)$$

To find the condition for maximum momentum transfer to the recoil nucleon (i. e., $p_N' = \max.$), the expression for p_N' is first written using Eq. 7

$$p_N' = \sqrt{(-\sum \vec{p}_i') \cdot (-\sum \vec{p}_i')} = \sqrt{\sum p_i'^2 + \sum_{i>j} 2p_i' p_j' \cos \theta_{ij}'} \quad (8)$$

In this equation the p_i' are not independent because of the restriction of constant total energy. However, the θ_{ij}' can all be chosen independently compatible with this restriction. Therefore the first condition for p_N' to be maximum is obtained by setting $\frac{\partial p_N'}{\partial \theta_{ij}'} = 0$ for all i and j .

Carrying out the differentiation, one immediately obtains $\theta_{ij}' = 0, \pi$. By inspection it is seen that $\theta_{ij}' = 0$ is the condition for p_N' being maximum. Therefore, the first con-

dition is that all the pions come out of the reaction together (in the same direction) and, naturally, opposite to the direction of the recoil nucleon. Setting $\theta'_{ij} = 0$, equation 7 or 8 becomes

$$p'_N = \sum p'_i. \quad (9)$$

To maximize p'_N with respect to p'_i , consistent with the energy restriction

$$W' = E'_N + \sum E'_i = \text{constant} \quad (10)$$

one normally uses Lagrange multipliers⁽⁵⁾ while setting $\delta p'_N = 0$. Taking the variations in Eqs. 9 and 10 and using the Lagrange multiplier λ ($\lambda = \text{constant}$), one gets

$$\sum \left(\frac{p'_i}{E'_i} - \lambda \right) \delta p'_i = 0. \quad (11)$$

From the above equation one immediately obtains the second

condition that $\beta'_i = \frac{p'_i}{E'_i} = \lambda = \text{constant}$ for all i . That is,

all pions must have the same velocity. Now, inserting this second condition, the maximum value of the recoil nucleon momentum can be calculated. From Eq. 9 using the same velocity λ for all pions, one obtains

$$\gamma'_N = \sqrt{1 + \left(\frac{nm}{M} \right)^2 \frac{\lambda^2}{1 - \lambda^2}}. \quad (12)$$

Putting this in Eq. 10, one can solve for λ , and in turn

for $E'_N = M\gamma'_N$ which yields

$$E'_N = \frac{W'^2 + M^2 - (nm)^2}{2W'} \quad (13)$$

Equation 13 gives the value of the maximum energy that the recoil nucleon can obtain in a reaction in which n pions are produced. For the special case of $n = 1$ (in which E'_N is greater than any other case) Eq. 13 together with Eq. 6 gives

$$E'_N = M(E_0 + M) / \sqrt{M^2 + m^2 + 2E_0M} = M\gamma_C, \quad (14)$$

indicating that the maximum velocity of the nucleon is the same as the C.M. velocity, β_C .

2-Maximum Angle of the Secondary Nucleon

It is useful for the selection of events (see Chapter III) to know the maximum value of the recoil nucleon angle in the lab system. Using the Lorentz transformation, Eqs. 2 and 3, the angle of the recoil nucleon in the lab system, θ_N , can be written in terms of its C.M. angle and velocity,

$$\tan \theta_N = \frac{\sin \theta'_N}{\gamma_C (\cos \theta'_N + \beta_C / \beta'_N)} \quad (15)$$

Since θ'_N and β'_N are two independent quantities, θ_N is maximized with respect to each independently. First setting $\partial \theta_N / \partial \theta'_N = 0$ gives $\cos \theta'_N = -\beta'_N / \beta_C$ for the condition of max-

imum θ_N , which yields for the maximum value

$$(\tan \theta_N)_{\max} = \frac{1}{\gamma_c \sqrt{(\beta_c/\beta_N^i)^2 - 1}} \quad (16)$$

Second, in regard to β_N^i , the maximum of θ_N occurs when β_N^i is maximum. Using the result of the previous section, Eq. 13, the maximum value of β_N^i can be obtained from the maximum value of γ_N^i . After inserting Eq. 6 in Eq. 13, one gets

$$\gamma_N^i = \gamma_c \left\{ 1 - \frac{(n^2 - 1)m^2}{2M(M + E_0)} \right\} \equiv K(n) \gamma_c, \quad (17)$$

$$\beta_c/\beta_N^i = K(n) \beta_c / \sqrt{\beta_c^2 + K^2(n) - 1} \quad (18)$$

In Table 1 the maximum value of the angle θ_N , along with the corresponding values of β_c/β_N^i and $K(n)$ have been tabulated for different values of the pion multiplicity n . A value of $p_0 = 16200$ MeV, for the case of this experiment has been used. The maximum multiplicity of the pions can be calculated by setting $\gamma_N^i = 1$ in Eq. 17. This gives a value of $n = 33$.

Figure 1 summarizes the results of this section. Here, the maximum value of θ_N (in regard to β_N^i) has been plotted against θ_N^i for a number of different pion multiplicities. The maximum values of the curves are the same as the values given in Table 1.

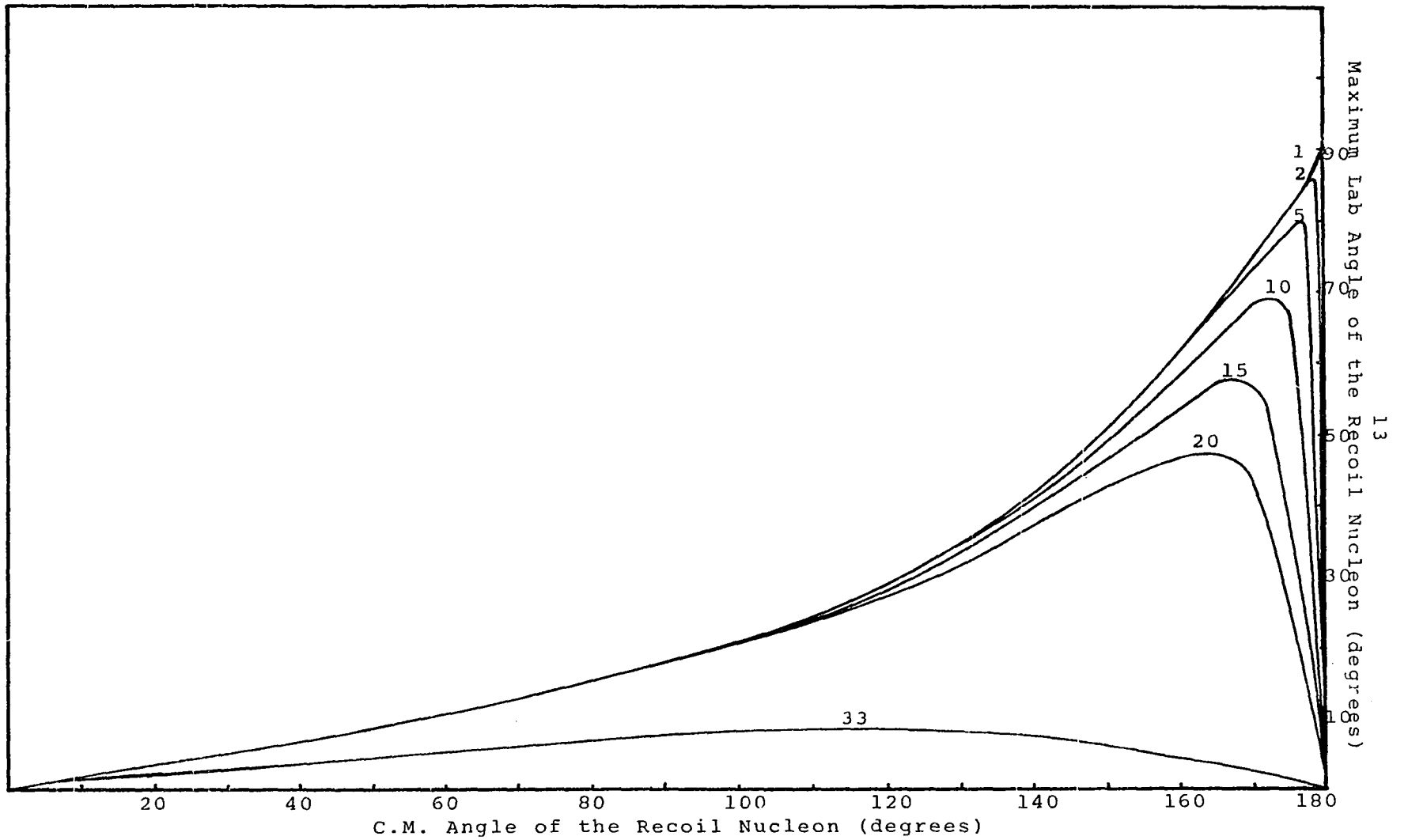


Fig. 1 Maximum Lab Angle of the Recoil Nucleon versus its C.M. Angle

TABLE 1

MAXIMUM ANGLE OF THE RECOIL NUCLEON
IN THE LAB SYSTEM

n	K(n)	β_C/β_N^i	$(\theta_N)_{\max}$ degrees	$(P_N)_{\min}$ MeV
1	1	1	90.0 ± .0	0 ± .0
2	.99822	1.00021	86.4 ± .0	2 ± .0
3	.99526	1.00057	84.1 ± .0	5 ± .0
4	.99112	1.00108	81.9 ± .0	9 ± .0
5	.98579	1.00174	79.7 ± .0	15 ± .0
6	.97928	1.00256	77.6 ± .0	21 ± .0
7	.97158	1.00356	75.5 ± .0	29 ± .1
8	.96270	1.00475	73.3 ± .0	38 ± .1
9	.95264	1.00614	71.2 ± .0	49 ± .1
10	.94139	1.00776	69.0 ± .0	61 ± .1
11	.92895	1.00962	66.9 ± .0	74 ± .2
12	.91534	1.01176	64.7 ± .1	89 ± .2
13	.90053	1.01422	62.6 ± .1	105 ± .3
14	.88455	1.01703	60.4 ± .1	124 ± .3
15	.86738	1.02025	58.2 ± .1	144 ± .4
16	.84903	1.02396	56.0 ± .1	166 ± .4
17	.82949	1.02822	53.7 ± .1	190 ± .5
18	.80877	1.03315	51.5 ± .1	216 ± .6
19	.78686	1.03889	49.2 ± .1	245 ± .7
20	.76377	1.04558	46.9 ± .1	277 ± .9
25	.63056	1.10494	34.8 ± .2	498 ± 2.1
33	.35585	2.38110	8.6 ± .8	1717 ± 51.8

3-Momentum versus Angle of the Recoil Nucleon

In the case of elastic scattering the angle of the recoil nucleon is uniquely determined by its momentum. However, this is not the case for the inelastic reaction, i.e., for $n > 1$. But for the inelastic case one can determine the maximum possible angle for a recoil nucleon of a given momentum (this is useful for the selection of the π -N interactions).

a-Elastic Collisions

In this case the energy of the recoil nucleon in the C.M. system is a constant (total energy, W' , is constant) and is the same as its maximum value given by Eq. 14. Putting this in Eq. 1, one gets a unique relationship between lab angle and momentum of the recoil nucleon. This is

$$\cos \theta_N = \frac{E_N - M}{\beta_C p_N} \quad (19)$$

b-Inelastic Collisions

In this case the energy of the recoil nucleon in C.M. is not a constant, and hence there is not a unique relationship between the lab angle and momentum of the nucleon. However, the limiting case of E'_N being maximum gives the maximum lab angle which could correspond to a fixed lab momentum. Putting the maximum value of E'_N

(Eq. 13) in Eq. 1, one can solve for the maximum lab angle of the recoil nucleon in terms of its lab momentum. This yields,

$$\cos \theta_N = \frac{E_N - MK(n)}{\beta_c p_N}, \quad (20)$$

where $K(n)$ is given by Eq. 17. Eq. 20 reduces to Eq. 19 for the case of elastic collision since $K(n=1) = 1$.

Figure 2 shows the graph of maximum lab angle (unique angle in the case of elastic collision) versus the lab momentum of the recoil nucleon for a number of pion multiplicities. As is seen in Figure 2 there is a minimum cut-off for recoil-nucleon momentum for all inelastic cases. The values of these cut-offs (minimum value of p_N) are given in the last column of Table 1. The errors calculated for $(\theta_N)_{\max}$ and $(p_N)_{\min}$, Table 1, are due to the error in the incident pion momentum which is 640 MeV.

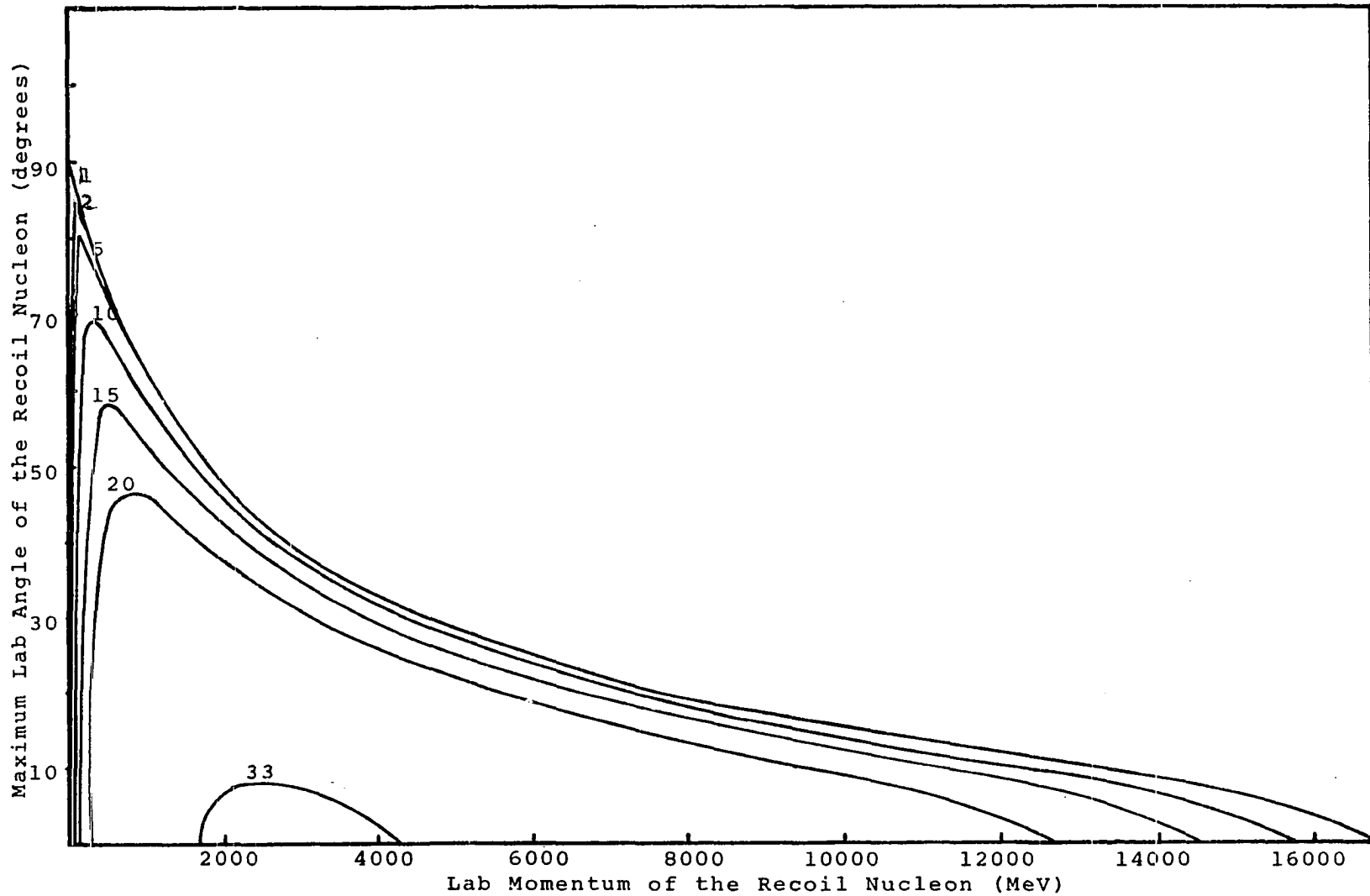


Fig. 2 Maximum Lab Momentum of the Recoil Nucleon versus its Lab Angle

CHAPTER III

EQUIPMENT AND EXPERIMENTAL PROCEDURES

A. Emulsion

Nuclear emulsion provided the target and detector for this experiment. The plates were Ilford K-5 emulsion which had been exposed to the negative pion beam from the CERN (Geneva) proton synchrotron, and which were developed and processed by W. H. Barkas at the University of California at Berkeley. Fifty-six plates, about one-third of the Berkeley \mathcal{A} -stack, are on loan to the high energy group at the University of Oklahoma and have been used for this experiment. The negative pion beam has a momentum of 16.2 ± 0.64 BeV/c and a particle contamination of less than 10%, the contaminant being chiefly muons. The pellicles of the emulsion stack were mounted on glass plates from which they receive support. On the bottom of each pellicle a one mm square grid with a set of two coordinate numbers was contact printed. This enables one to rapidly relocate positions in the emulsion. Each pellicle is 15 cm x 7.5 cm and had a nominal thickness of

600 microns before processing. The very careful processing yielded an excellent track visibility and very little distortion. The processing and shrinkage is extremely uniform. The shrinkage factor for this stack (the Berkeley A -stack) is 2.4. Since nuclear emulsion is extremely sensitive to changes in humidity and temperature, the laboratory in which the emulsion and the equipment are kept and the experiment was done was maintained at a constant temperature of $70 \pm 2^{\circ}\text{F}$ and constant relative humidity of $60 \pm 2\%$.

B. Microscopes

Four high precision microscopes have been used for detection of events and measurements in the emulsion. A Spencer binocular microscope was used for detection of the interactions in the emulsion, i.e., for scanning of the tracks of the beam particles. This microscope is mounted on an ordinary travelling stage. An electric motor with reduction gear system is attached to this stage to provide a uniform motion in one direction. Two other binocular microscopes have Leitz Wetzlar optics and are mounted on high precision travelling stages. These stages have two-dimensional motion in the plane perpendicular to the optical axis with travels of 18.5 cm x 14 cm in two perpendicular directions. The stages are driven by 1 mm

pitch screw drives and were constructed extremely carefully to insure that the motion, particularly in the 18.5 cm direction of travel, is as nearly linear as possible. The emulsion-plate holders on these stages allow for the rotation of the emulsion under the microscope in order to align any track with either direction of stage travel. One of these microscopes, which has extremely low stage noise, was used for the multiple Coulomb scattering measurements described below. The other one was used for range, projected angle, and other general measurements. The stage for these three microscopes were constructed in the machine shop of the physics department at the University of Oklahoma. A commercial Leitz Wetzlar Ortholox binocular microscope with travelling stage and high precision fine focus mechanism was used for dip angle measurements. These measurements are critical along the vertical direction, i.e., along the optical axis. Hence, an accurate fine focus mechanism is necessary.

Various Leitz Wetzlar and Koristka objectives and eyepieces were used for the different measurements. A Leitz Wetzlar screw-type eyepiece micrometer with extremely high setting accuracy (gives setting error of less than 0.05 microns when used with 100X objective) was used for multiple Coulomb scattering and accurate small-distance measurements. An eyepiece goniometer, whose

vernier allows measurement to the nearest minute of arc, was used for measuring projected angles. The two microscopes used for range and for multiple Coulomb scattering measurements are equipped with two precision micrometer dials (Ames gauges). The micrometers are calibrated in microns and allow accurate measurements of intervals along the two directions of stage motion.

Measurements were done at different magnifications: projected angle and range at 660X, scanning at 825X, dip angle at 1000X, grain density at 1250X, multiple Coulomb scattering at 1560X. All measurements were done with blue filtered light.

C. Experimental Techniques

Tracks of beam pions were followed in order to locate interactions in the emulsion stacks. Pion-nucleon interactions were identified and selected from among the many different types of interactions found. Most of the kinematical quantities of all the charged secondary particles of all the pion-nucleon interactions have been determined by various measurements. The following discussion describes in detail the techniques used.

1- Scanning

The interactions were located by systematically following the tracks of about 18400 beam pions. These tracks were located by volume scanning at about 3 mm from

the entering edge. The initial positions of these tracks in emulsion were carefully recorded to allow relocation of the tracks and to prevent rescanning of the same track. These precautions are necessary to accurately determine the total length of track scanned which is required for mean free path and cross section calculations. Selected entering tracks were followed until they either interacted or left the emulsion. About 75% of all tracks followed left the emulsion pellicle in which they entered without producing any interaction. Most of these traversed the entire length of the emulsion. If an interaction was found, its position and nature was carefully recorded by the scanner. On tracks which did not produce any interaction the location at which it left the emulsion was recorded.

The scanning was done primarily to locate electromagnetic interactions. These interactions involve one or two minimum ionizing secondary tracks and they are accompanied by a visually-undetectable direction change of the primary particle. This makes such interactions the most difficult ones to detect. All scanners were specifically trained to detect these interactions. A scanning efficiency test was carried out in which a total of 250 meters of track was rescanned by few of the scanners. Almost all of the pion-nucleon interactions recorded in

the original scanning were relocated in the rescanning. This gives a detection efficiency of almost 100%. Also, from the results of this efficiency test, it was possible to estimate that about 10% of the tracks have been erroneously scanned and recorded twice and hence the total length of track must be corrected accordingly.

The beam tracks in the stack of emulsion used in this experiment have an average divergence of ± 5 minutes of arc over the width of the pellicle. A divergence of approximately ± 8 minutes of arc exists in the beam over the entire emulsion at the entrance edge. In order to insure that the tracks scanned are beam tracks, the microscope was well aligned with the beam direction in each pellicle and then only tracks which were parallel to the direction of microscope traverse were scanned.

A total of 9000 man-hours was used to scan a total of about 1800 meters of beam track. Among other interactions a total of 970 "White-Stars" were located by the scanners. These events, which are probable pion-nucleon interactions, have any number of minimum-ionizing tracks but either zero or one greater-than-minimum ionizing tracks.

2-Selection of Events

The interaction $\pi^- + N \rightarrow N + m\pi$, with $m = 1, 2, 3, \dots$ is the subject of investigation in this experiment.

Therefore, an attempt has been made to select those events having only one secondary nucleon, any number of secondary pions, and no other secondary particles. There are other final states for the pion-nucleon interaction which are not of any interest for this experiment and an attempt has been made to eliminate such events. The following is a list of the possible final states for pion-nucleon interactions with their relative probability of occurrence as calculated by Laverriere and Grea⁽⁶⁾ based on the statistical theory at an energy of 5 BeV.

1--N + m π	88%
2-- Λ + k + m π	2.7%
3-- Σ + k + m π	3.0%
4-- Ξ + 2k + m π	0.05%
5--N + k + \bar{K} + m π	5%
6--2N + \bar{N} + m π	.8%

Due to the fact that the emulsion tracks of relativistic pions are indistinguishable from those of relativistic kaons, it is not possible to differentiate between emulsion events of final states 2 and 5 and those of final state 1 above. However, since the probability of these final states is very small compared to final state 1, this will introduce only a very small error in this experiment.

Pions with a momentum greater than 170 MeV leave

a track whose ionization density is visually indistinguishable from minimum. Out of 1650 secondary pion tracks from the interactions investigated only 2 had an ionization density greater-than-minimum. The momenta of these 2 were less than 160 MeV. The proton tracks, however, can be greater than minimum ionizing since the nucleons coming out of these interactions generally have a relatively low energy. "White Stars" satisfy these preliminary conditions, and have been carefully examined for further selection rules. In order to insure that the events are interactions of pions with "almost-free" nucleons the following points have been considered in the selection of the events:

i--Events with a blob at the interaction point have been ruled out. A blob normally is caused by the recoil of a nucleus in a pion-nucleus interaction. 401 events have been ruled out in this manner.

ii--When a heavy nucleus is involved in the interaction an Auger electron may be emitted from the reaction. Such an electron has sufficiently low energy for appreciable direction changes due to multiple Coulomb scattering. The visually-detectable scattering of such electron tracks allow their easy identification. 22 events with Auger electrons have been eliminated.

iii--In Chapter II it has been shown that

the secondary nucleon from the interaction of a pion with a single nucleon at rest cannot be emitted backward in the laboratory system. Therefore, proton tracks making angles greater than 90° with the direction of the incident pion must be caused by evaporation protons or protons from secondary reactions inside a heavier nucleus. 41 such events were found but not included. The existence of these 41 events, which is about 20% of the total number of events with a single proton in the final state, introduces an ambiguity into this experiment: from symmetry considerations, one expects that about 20% of the interactions with a neutron in the final state must have the neutron emitted backwards. These events which are not normally distinguishable* from the rest of the events having a secondary neutron are not interactions of pions with a single nucleon. This point will be discussed more in the next chapter.

Some of the events selected in the above manner have a greater-than-minimum ionizing track. These events were examined further.

i--Since the greater-than-minimum ionization track could belong to a hyperfragment or a particle

*This is because a neutron does not have a track and to determine its direction one can use a kinematical analysis only if complete data on all the other secondary particles of the interaction is available. Such data is generally exceedingly hard to obtain and in case secondary neutral pions are involved it is impossible.

other than proton, an attempt was made to identify these tracks. a) The ends of these tracks were carefully examined and compared to those of the known stopping particles⁽⁷⁾. b) Variable-cell scattering measurements (discussed later) were carried out on some of the stopping particles in order to estimate their mass. c) On some of the tracks grain density measurement was done along with range measurements to allow a determination of both energy and the mass of the particle.

ii--As shown in Chapter II, in the interaction of a pion with a single nucleon there exists a kinematical limitation on the energy of the secondary nucleon, this limit depending on the angle of emission. These kinematical limitations are given in Table 1 and by the curves of Figures 1 and 2 for a number of different pions produced. All protons have been tested and 12 events which did not meet the required limitations have been ruled out.

509 events have been selected which fulfill all the above-mentioned rules and requirements with the highest-achievable degree of confidence. 85 of these events have only one minimum ionizing track each. There is not much information which can be extracted from these events. Hence, they will be used only in certain distribution and cross section analyses. No more measurements have been made on these events. Measurements as complete as possi-

ble have been done on the remaining 424 events. Those measurements which have been done for the purpose of determining the direction of emission and the momentum of each of charged secondary particles are described below.

3-Angle Measurements

In order to determine the direction of emission of a particle one has to make two independent angle measurements. The two angles measured for each track are the projected angle ϕ and the dip angle δ . The projected angle refers to the angle between the projection of the track onto the plane of emulsion and the direction of the incident pion. The dip angle refers to the angle between the track and its projection onto the plane of the emulsion. The plane of the emulsion refers to the plane which is perpendicular to the line of sight (the optical axis) and contains the focused incident pion track. This geometry is illustrated by Figure 3.

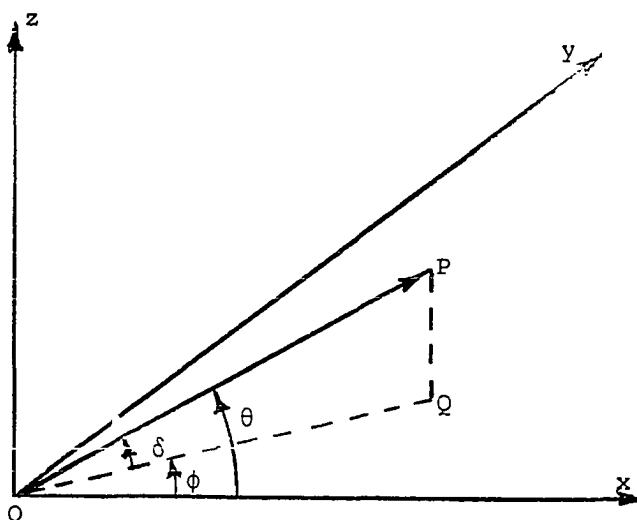


Fig. 3

Here z is taken along the direction of the optical axis. This is the same as the 600 micron dimension of the emulsion pellicle. x is taken to be along the direction of the incident pion which is perpendicular to z and along the 148 mm direction of the pellicle. y is taken to be perpendicular to x and z and is along the 75 mm direction of the pellicle. The x - y plane is called the plane of emulsion, and z is referred to as the line of sight. Now if OP refers to the direction of a track, with OQ as its orthogonal projection onto the x - y plane, then ϕ is called the projected angle and δ is called the dip angle of the track. θ , the angle between the direction of the track and the direction of the incident pion, is referred to as the space angle of the track. The positive sense of these angles is shown by the direction of the arrows.

Measurements of the projected angles were done directly with the help of an eyepiece goniometer. The goniometer cross-hair was first set on the direction of the track being measured and then on the direction of the incident pion track. The difference between the two readings is the projected angle of the track. This measurement is very accurate for minimum ionizing tracks since, when using the whole length of the cross hair, it is possible to accurately set the cross hair on the track. For

most of the greater-than-minimum ionizing tracks, in particular, those which are short and those which scatter appreciably, it is very hard to accurately set the cross-hair on the track. For such tracks the measurement was repeated five times and the average result was used.

The dip angle was measured indirectly by using the relation $\delta = \tan^{-1} \frac{PQ}{OP}$ (Figure 3) and measuring PQ and OP. A reticle containing a scale was set on the track (this when calibrated measures OQ) and the microscope was first focused on the event (point O) and then on the track at point P. The difference in the two vertical readings gives the distance PQ in microns. This must be multiplied by the shrinkage factor in order to get the distance before processing and hence the actual dip angle of the track. For dip angle measurement the track was carefully centered in the field of view such that the points O and Q were equidistant from the center of the cross hair. In this manner the error due to lens curvature is kept to a minimum. The accuracy in dip angle measurement mainly depends on the ability to focus on a grain in the emulsion and to make a vertical reading. This is limited by the accuracy of the fine focus mechanism of the microscope. In order to reduce the error the vertical measurement was repeated four to five times and averaged. A heat

absorbing glass plate was used in making these measurements in order to avoid an appreciable change in the thickness of the emulsion which would occur in the course of the measurements due to the concentrated heat in the field of view.

4-Momentum Measurements

Different techniques have been used for the measurement of the momenta of the particles depending on the degree of the ionization of their tracks. Multiple Coulomb scattering measurement has been attempted on all the minimum ionizing tracks. All the greater-than-minimum ionizing tracks have been followed through the many pellicles of the emulsion stack until they either stopped or left the stack. Range measurements were done on all those tracks which stopped in the emulsion, and grain density measurements were done on those which left the stack.

Grain density measurements also were made on some of those tracks which stopped in the emulsion for the purpose of calibration. These measurements are separately described below.

a-Range Measurement

The range of the tracks which stopped in the emulsion was determined by making coordinate measurements at numerous points along the track. These points include: beginning (at the event) and end of the track, the points

where the track enters and leaves each pellicle, intermediate points wherever the track changes direction more than about 2° . The residual range is then found by adding the length of the track segments between these points. Through repeating measurements on a group of sample tracks it was found that measurement error in the residual range is less than 1% for tracks longer than 1 cm with dip angle less than 5° . Although short tracks and tracks with large dip angles show large measurement errors in their ranges, all such errors were less than 5%. Standard tables⁽⁸⁾ were used to obtain the momenta of the tracks whose residual ranges had been measured. The standard tables which were used give momentum, velocity, kinetic energy, and grain density of different particles for a wide range of the residual range of the particle in Ilford K-5 emulsion. Figure 4 shows the variation of momentum and normalized grain density (grain density divided by the minimum grain density) of a pion and a proton with the respective residual range plotted from the data of the standard tables.

b-Blob Counting

A blob counting technique has been used to indirectly determine the residual range for all the greater-than-minimum ionizing tracks which do not stop in the emulsion stack. Blobs are resolvable clumps consisting of one

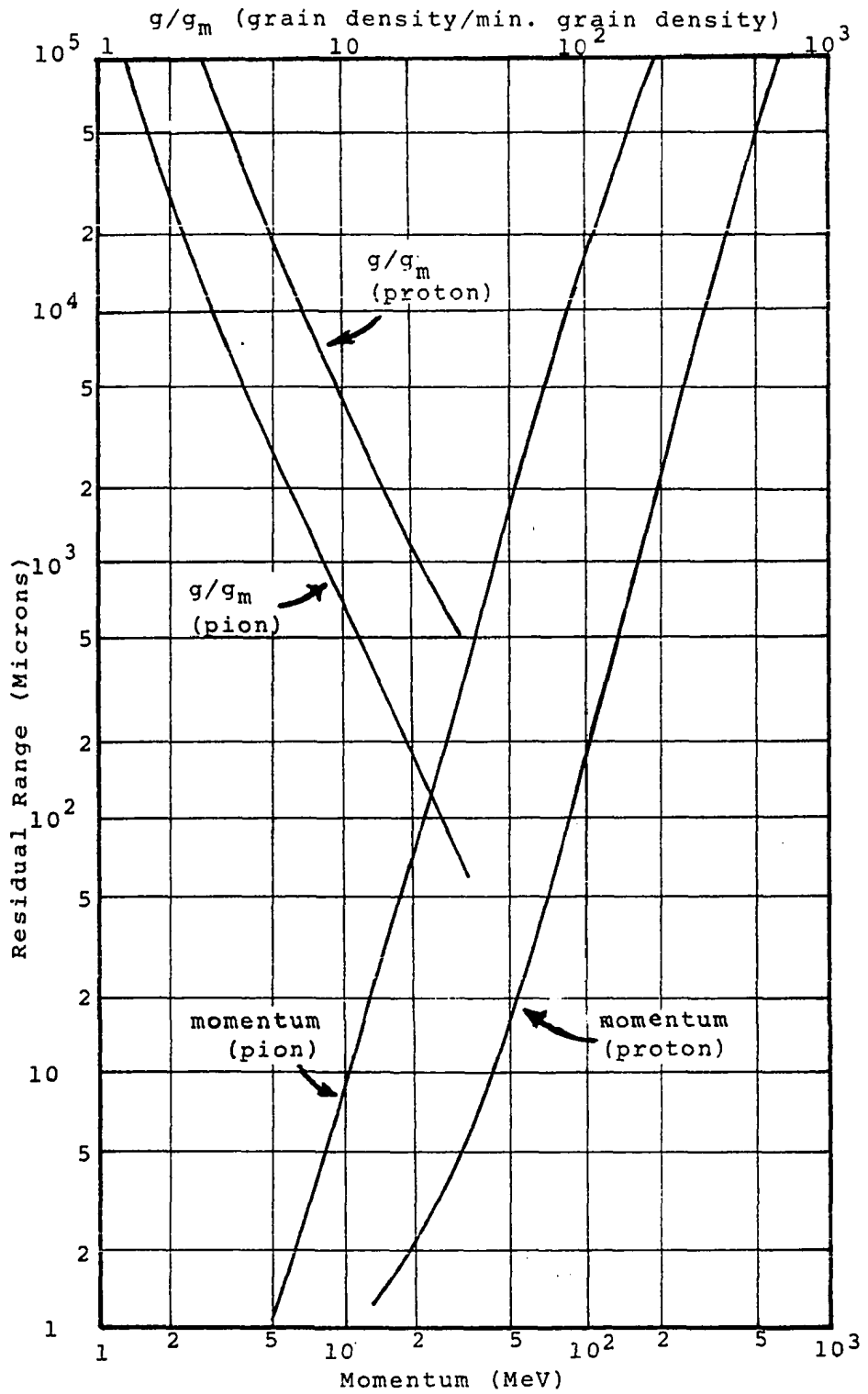


Fig. 4 Range--Momentum-- g/g_m Plot

or more unresolved, developed grains. Blob density B , the number of blobs (or equivalently number of gaps) per unit length of track, is related to the grain density, g , of a track by the equation^(9,10)

$$B = g \exp(-\alpha g \text{Sec } \delta) \quad (21)$$

where δ is the dip angle of the track and α is the projection on the plane of the emulsion of the average distance between centers of two grain images when the grains can just be resolved into two objects. α is one combined parameter describes the emulsion, the optical equipment and the observer characteristics. Grain density in turn is related to the residual range: from Figure 4 one obtains the relation

$$g \propto R^{-.42} \quad (22)$$

for protons in which the constant of proportionality depends on the minimum grain density g_m . This again depends on characteristics of the emulsion, the equipment and the observer. It is customary to determine the parameters α and g_m by numerous measurements of B and R on tracks of known particles. The use of these calibration values of α and g_m along with a measurement of B on any track allows one to obtain its residual range. However, a different technique has been used in this experiment. For each track blob density, dip angle of the track and the distance from the event were measured at three different

positions: at the beginning of the track (at the event), at the point where the track left the stack of emulsion, and at a point midway between the first two points. With three sets of data on each track a knowledge of α and g_m is not necessary. Upon eliminating g between Eqs. 21 and 22 for each measurement, we obtain

$$B_i = K(R-D_i)^{-.42} \exp(-\alpha K(R-D_i)^{-.42} \sec \delta_i), \quad i=1,2,3 \quad (23)$$

where D_i is the distance from the event to the i th point of measurement and K is the proportionality constant of the Eq. 22. Now α and K are eliminated between the three equations in Eq. 23 which results in a single equation relating the residual range and the measured quantities B_i , D_i , δ_i ($i=1,2,3$). This is

$$F(R) \equiv x_1 y_1 (x_2 - x_3) + y_2 x_2 (x_3 - x_1) + x_3 y_3 (x_1 - x_2) = 0, \quad (24)$$

with $x_i \equiv (R-D_i)^{.42} / \sec \delta_i$ and $y_i \equiv \ln\{B_i (R-D_i)^{.42}\}$. An iteration technique was used to compute R from $F(R) = 0$. From the form of this function it is observed that it has only one root in the physical region of R , i.e.; for $R > D_i$, $i = 1,2,3$. The error in R is calculated from the individual measurement errors using the relation

$$\Delta R = \left\{ \sum_{i=1}^3 \left\{ \left(\frac{\partial R}{\partial B_i} \Delta B_i \right)^2 + \left(\frac{\partial R}{\partial \delta_i} \Delta \delta_i \right)^2 + \left(\frac{\partial R}{\partial D_i} \Delta D_i \right)^2 \right\} \right\}^{1/2} \quad (25)$$

where, using the previous notations x_i and y_i , we have

$$\frac{\partial R}{\partial B_i} = 2.38x_i (x_j - x_k) / B_i S, \quad (26)$$

$$\frac{\partial R}{\partial \delta_i} = (2.38x_i \cot \delta_i) / S, \quad (27)$$

$$\frac{\partial R}{\partial D_i} = x_i \{ (1+y_i) (x_j - x_k) - x_j y_j + x_k y_k \} / (R - D_i) S, \quad (28)$$

where,

$$S = \sum_{i,j,k=1,2,3}^{\text{cyclic}} \{ (1+y_i) (x_j - x_k) - x_j y_j + x_k y_k \} \frac{x_i}{R - D_i}. \quad (29)$$

Blob counting was done with the help of an electric counter and foot switch. An average of 1000 blobs were counted for each measurement on flat tracks. On dipping tracks for each measurement all blobs of the segment of the track in a single pellicle were counted. The length of the segment of the track used in blob counting was measured as described in the section on range measurement. D_i was taken as the distance between the middle of ith segment used in blob counting and the event. The counting error in the technique was determined to be less than $\frac{1}{2}\%$ by repeated counting of the blobs. The error in blob density ΔB_1 was therefore taken to be the statistical error in B; i.e., $\Delta B_i = B_i / \sqrt{\text{No. of blobs}}$.

In order to use Eq. 22 it was assumed that the particle whose track was being measured is a proton. This assumption was checked for all the tracks by using the

blob counting data to estimate the minimum grain density, g_m , and requiring it to be within the experimental error of the value $g_m = 0.24 \pm .02$ for this emulsion.

c-Multiple Coulomb Scattering

This technique was used on about 65% of the minimum-ionizing tracks, for which range measurement and blob counting techniques fail. This method is based on the fact that as a fast charged particle travels through matter it is scattered repeatedly through small angles by the atomic Coulomb field of the emulsion matter. The mean value of the angle of this multiple scattering depends on the charge and the velocity of the particle for a given emulsion. The mean value of this angle is related to the observable scattering angle of the track of the particle⁽⁹⁾. In current practice angle measurements are seldom done and a coordinate method is used instead. The general procedure in the coordinate method is as follows: The track is aligned with the direction of microscope stage motion, which is taken to be the abscissa, x . If possible, the track is aligned well enough that over the interval of measurement it will remain within the microscope field without changing the y coordinate of the stage.

One selects a length, t , parallel to x as a cell length. A cell length of 250μ , which was found to be most convenient, was used for most of the tracks. A lower cell

length was used for tracks with lengths smaller than 2500μ , but not less than 1250μ , in one pellicle. The ordinate, y_0 , of the track at an arbitrary $x = 0$ point (this point was chosen close to the event) is measured by an eye-piece micrometer which had been accurately calibrated in microns. Then the plate is displaced a distance t along the x axis, and the ordinate y_1 is recorded. By successively displacing the plate and at each stop recording the track ordinate, a set of numbers, y_i , is obtained. The measurements are the distances of the track from a "straight line" that extends generally parallel to the track, at equal intervals of length t .

The second differences

$$D_k = (y_{k+2} - y_{k+1}) - (y_{k+1} - y_k) \quad (30)$$

are then calculated. The average absolute value of D_k when corrected for measurement noise (to take account of the fact the y_i 's are not the distances of the track from a true straight line) is related to the mean angle $\bar{\alpha}$ between successive chords to the track. Calling this D_t , we have

$$D_t = \frac{\langle \bar{\alpha} \rangle t}{57.3}$$

where $\bar{\alpha}$ is expressed in degrees and 57.3 is degrees to radians conversion factor.

In reference (9) the relation between the momen-

tum of the particle and $\bar{\alpha}$ is derived and given by

$$p\beta = \frac{Kz}{\bar{\alpha}} \left\{ \frac{t}{100} \right\}^{1/2} = \frac{Kzt^{3/2}}{573D_t} \quad (32)$$

where p is the momentum of the particle, β its velocity (in units of c), z its charge (in units of e) and K is the scattering factor. K is not strictly a constant. It varies slowly with particle velocity and cell length, and its numerical value depends somewhat on the theory used in its calculation and the cut-off procedure applied. Figure 5 shows the values of K used in this experiment as a function of t based on Moliere's scattering theory for a standard cut-off of four times the mean absolute second difference applied to the data, and taking $\beta \approx 1$.

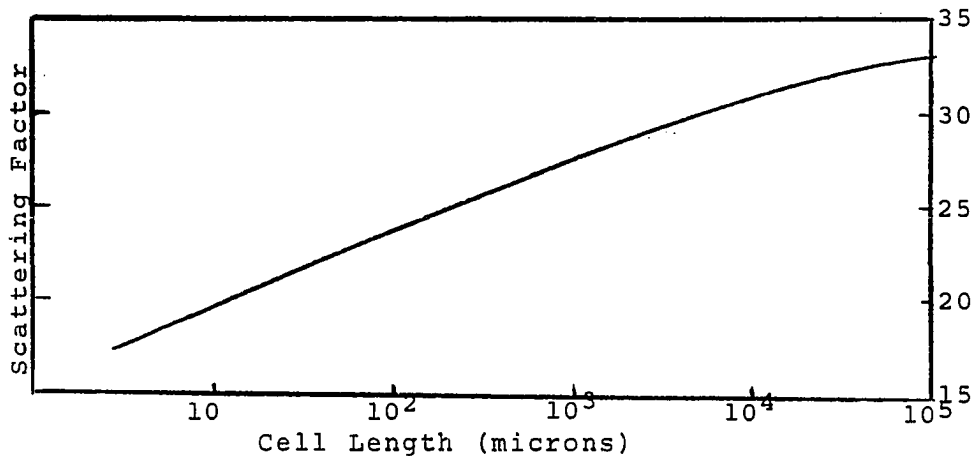


Fig. 5

The problem of obtaining D_t from the measured set of y_i is referred to as noise elimination. This process is of grave importance and extreme difficulty. Each

measurement y_i on the track is subject to several types of error. Two obvious ones are microscope stage noise and setting noise. In addition, the track only imperfectly defines the trajectory of the particle in emulsion because the grains are finite in size and are distributed randomly about the trajectory. The emulsion is also subject to distortion. The process of noise elimination by a direct determination of all the different noise levels is unachievable and has not been attempted in this experiment. Instead, the following procedure has been used for the purpose of noise elimination:

i--In order to eliminate all large angle nuclear scatterings any $|D_k|$ greater than four times the average of the other $|D_k|$'s has been eliminated. Other cut-offs were experimented with, but were not used. This one proved to be sufficient and more satisfactory.

ii--As a first approximation correction for simple curvature of the track and spurious scattering the average of the second differences* has been subtracted from all second differences.

iii--Products of the second differences, $D_k^2, D_k D_{k+1}, \dots, D_k D_{k+N-1}$ ($N =$ number of second differences) and their weighted averages were calculated. The

*The statistical average of the second differences must be zero in the absence of any noise.

weighting factor was taken to be proportional to the square of the number of each second difference product; other weighting factors were tried but they seemed to yield less consistent results. With the weighting factor the average of the ℓ th second difference product is calculated from the equation

$$\langle D_k D_{k+\ell} \rangle = \frac{N-\ell}{N^2} \sum_{k=1}^{N-\ell} D_k D_{k+\ell} \quad (33)$$

iv--Using Barkas⁽⁹⁾ notation and formalism on noise elimination and fully extending the modification introduced by Burwell⁽¹¹⁾, it is shown in Appendix A that the true (noise eliminated) mean square second difference, Δ_t^2 , is given by

$$\Delta_t^2 = 2/3 \{ \langle D_k^2 \rangle + 2 \sum_{\ell=1}^{N-2} (1 - \frac{\ell^2}{N^2}) \langle D_k D_{k+\ell} \rangle \} / (1 - \frac{1}{3N^2}) \quad (34)$$

where N is any large integer which satisfies the condition described in Appendix A, and $N \leq N+1$.

v--Finally, in order to calculate D_t from Δ_t^2 as defined in the previous step, the noise-eliminated absolute second differences have been assumed to have a Gaussian distribution. This gives the relation

$$\Delta_t^2 = (\pi/2) D_t^2. \quad (35)$$

This assumption has been used by other investigators and is consistent with the scattering theory.

cl Multiple Cell Calculations--Although the set of y_i ordinates were measured at a cell length of t , the base cell length, the momentum of the particle can be determined by a calculation based on higher cell lengths of M times t ($M = 1, 2, 3, \dots, M_{\max}$). This is done by calculating second differences at $M \cdot t$ cell length from

$$D_k^M = y_k - 2y_{k+M} + y_{k+2M} \quad (36)$$

This yields M sets of second differences calculated at $M \cdot t$ cell length, and hence M different values of $p\beta$ which are averaged to give one $p\beta$ for that cell length of calculation. The method of multiple cell calculations has two very important advantages: (1) For each track whose $p\beta$ is not known there is no way to decide a priori on the optimum cell length. By comparing the consistency of the results and considering the errors (discussed below) in $p\beta$ calculated at different cell lengths, the optimum cell length can be more realistically chosen. (2) The M different $p\beta$'s calculated at the cell length $M \cdot t$ must have only a statistical variation among them. This provides a good test of the consistency of the entire procedure.

In order to use the approximation made in the derivation of Eq. 34 (Appendix A) for all the multiple cell lengths, the maximum value of M has been chosen such that $M_{\max} \leq (N/10)+1$.

The entire calculation was repeated for two

different values of N of Eq. 34: once with $N=N+1$ and once with $N = \frac{1}{2}(N+1)$. As is shown in Appendix A, can have any value between a minimum (in order to satisfy the approximation) and its maximum $N+1$. In order to check this fact, for a group of test tracks of particles of known energies, calculations were repeated while changing N between its minimum and maximum values. The fluctuations in $p\beta$'s obtained were generally found to be well within statistical errors, occasionally there was a larger variation between $p\beta$'s calculated for high and low values of N .

Of all the many different $p\beta$'s calculated for each track from a single set of measured values, y_i , the one with the least relative error has been chosen as the final answer. This choice was made because the errors calculated by the method discussed below include a measure of the noise level in the measurement, the consistency of the data, and the statistical error.

c2-Calculations of Errors--Equation 34 gives Δ^2 as the sum of the averages of the second difference products, $\langle D_k D_{k+\ell} \rangle$, each of which, being averaged over many terms, has an inherent variance associated with it. Since $\langle D_k D_{k+\ell} \rangle$ terms generally are related to the measurement noise (in fact $\langle D_k D_{k+\ell} \rangle = 0$ for $\ell \geq 2$ for a noise-free measurement), their variance is a measure of the error

introduced in Δ^2 due to the measurement noise. The variance also depends on the number of terms averaged and hence is a measure of the statistical error. Denoting the variance in $\langle D_k D_{k+l} \rangle$ by σ_ℓ^2 and treating $\langle D_k D_{k+l} \rangle$'s as statistically independent quantities as is discussed in Appendix A, then for the variance in Δ^2 we have

$$\sigma_{\Delta^2}^2 = 2/3 \left\{ \sigma_0^2 + 2 \sum_{\ell=1}^{N-2} \left(1 - \frac{\ell^2}{N^2}\right) \sigma_\ell^2 \right\} / \left(1 - \frac{1}{3N^2}\right). \quad (37)$$

Now by taking the error in Δ^2 to be the square root of its variance and using Eqs. 32 and 35 we obtain the error in each calculation of $p\beta$ to be

$$\Delta p\beta = \frac{1}{2} p\beta \sqrt{\frac{\sigma_{\Delta^2}^2}{\Delta^2}}. \quad (38)$$

The error in the final answer which is the average of the M different $p\beta$'s calculated at the M th multiple cell length is then given by

$$\Delta p\beta = \frac{1}{2} \left\{ \sum_{i=1}^M \left(\frac{p\beta_i}{\Delta_i} \right)^2 \sigma_{\Delta_i^2}^2 / (M-1) \right\}^{1/2}. \quad (39)$$

In order to keep the statistical error in the measurements as low as experimentally feasible the number of measurements on each track, y_i 's, has been kept at 100 when possible. For dipping tracks which are not long enough for 100 measurements the whole length of the track

in one pellicle has been used in the measurement. However, tracks which were not long enough to yield at least 10 values of y_i were not measured.

d-Variable-Cell Scattering Measurement

This technique has been used to identify tracks which stop in the emulsion. For a stopping particle whose velocity changes considerably with residual range, one must use a variable cell length with length depending on the residual range in order to maintain the statistical constancy of the scattering sagitta. This is seen by using an approximate equation relating the energy, E , of a particle of mass M and charge z to its residual range $R(7,10)$,

$$E = 0.251z^{1.16}M^{.42}R^{.58}, \quad (40)$$

which along with Eq. 32 yields,

$$D_t = aM^{-.42}z^{-.73}R^{-.58}t^{1.587} \quad (41)$$

where a is a normalization constant. When measurements are made at residual range R using a cell length t which is adjusted so that $R^{-.58}t^{1.587}$ remains constant, then the scattering sagitta, D_t , is statistically constant. Therefore, making a large number of such y_i measurements along the track and calculating D_t , which is the noise-corrected mean absolute value of second differences of y_i 's, enables one to identify the particle which produced the track by determining its mass, since $M^{-.42}z^{-.073}$ re-

mains constant.

The variable-cell scattering measurements were made according to the Table 8.11.1 of reference (9) which is so prepared to keep $R^{-.58}t^{1.587}$ constant. Tracks of known particles (decaying pions and muons) were used for the calibration and testing of this technique.

CHAPTER IV

PRESENTATION AND ANALYSIS OF DATA

A. Cross Sections and Pion Multiplicity Distributions

Of the 509 pion-nucleon interactions analyzed, 472 events were located and measured in this laboratory, and the measurements on the remaining 37 events were done at the University of California, Berkeley. In compliance with charge conservation, events with an even number of tracks have been labeled as π^- -p', and those with an odd number of tracks π^- -n'. A total of 1830 meters of π^- beam track has been followed for locating the 472 events measured here. This length of track when corrected for the muon contamination of the beam and also for the scanning efficiency (correction for the duplicate recordings) becomes 1490 meters. The mean-free-path and cross sections for different final states of pion-nucleon collisions have been calculated and are given in Table 2.

The reaction π^- -n' refers to the reaction of the beam π^- with a loosely bound, almost free, neutron of

TABLE 2

Reaction	No of Events	MFP (Meter)	Cross Section(mb)	σ (corrected) (mb)	σ (J.Bartke) (mb)
π^- - 'n'	237	6.3	---	---	---
π^- - 'p'	235	6.6	---	---	---
π^- -p total	45	32.9	9.5	24.2 \pm 2.3	26
π^- -p Elastic	14	106.6	2.9	2.9 \pm .8	6
Charge Exchange	4	373.2	0.8	0.8 \pm .4	<1

an emulsion nucleus. The reaction π^- - 'p' refers to all the reactions which simulate pion-proton reactions; that is, the reaction of a π^- with a free proton (hydrogen nucleus) or with a loosely bound proton of an emulsion nucleus. The reaction π^- -p refers to the reaction of a π^- with an emulsion hydrogen nucleus. The total number of the π^- -p events, collisions with 'free' protons, has been estimated on the basis of the experimental number of π^- - 'p' and π^- - 'n' events in the following manner: The number of π^- -p events should be equal to the number of π^- - 'p' minus the number of collisions of π^- with bound protons (call π^- -b.p). This in turn is related to the number of collisions of π^- with bound neutrons modified by the ratio of the relative abundances of the bound protons and neutrons in the emulsion. Therefore, one

has the relation

$$\#(\pi^- - p) = \#(\pi^- - 'p') - \#(\pi^- - 'n') \cdot \frac{\langle z \rangle}{\langle A \rangle - \langle z \rangle}$$

where $\langle z \rangle$, $\langle A \rangle$ are the mean proton number, and the mean nucleon number of the emulsion. From the composition of Ilford K-5 emulsion, not including hydrogen in the averages, one obtains $\frac{\langle z \rangle}{\langle A \rangle - \langle z \rangle} = 0.80 \pm .03$.

The elastic $\pi^- - p$ events have been selected from the $\pi^- - 'p'$ events according to the criteria derived in Chapter 2. The charge exchange reactions $\pi^- + p \rightarrow \pi^0 + n$ have been identified after careful examination of beam tracks which suddenly disappear in the interior of an emulsion plate (no secondary tracks exist for these events).

In the last column of Table 2, the corresponding cross sections as obtained by J. Bartke, et. al.⁽¹³⁾ in emulsion with a 16 BeV incident negative pion beam is given.

The cross sections for different kinds of inelastic pion-nucleon interactions (processes with pion production) are normally not feasible to be obtained in an emulsion experiment (due to the existence of neutral particles). In Figure 6 the distribution of the pion-nucleon interactions, measured in this experiment, in the number of the secondary charged pions per event have been given. The average number of charged pions per event is $4.3 \pm .3$

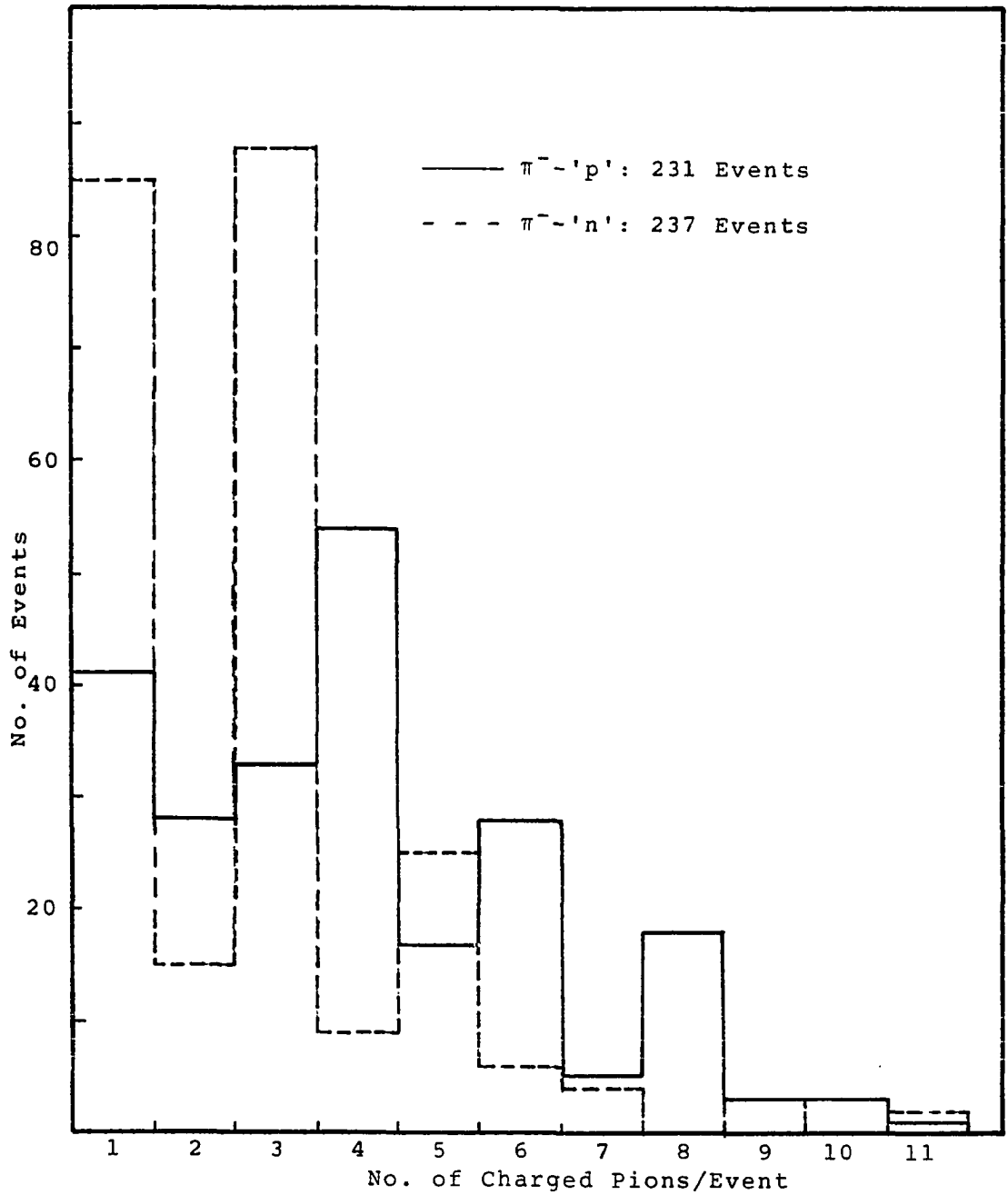


Fig. 6 Distribution of Number of Charged Pions

for the π^- -p' and $2.7 \pm .2$ for the π^- -n' events. In the histograms of Figure 6 one can observe an enhancement of the events with 4, 6, 8 charged pions in the case of π^- -p' and events with 1, 3, 5, 7 in the case of π^- -n' interactions. These events do not have an identifiable proton track and are assumed to have a secondary neutron (for both π^- -p' and π^- -n'). These enhancements of the events can be partially attributed to the uncertainty in the selection of such events (i.e., events with no proton tracks). It has not been possible to examine these events to see if they satisfy the kinematical limitations on the recoil nucleon (neutron), whereas about 27% of the events with a proton track had been rejected for not satisfying the kinematical limitations. In order to correct for this effect the number of the events with a recoil neutron must be reduced by a factor which could be taken as the ratio of the number of events whose recoil proton meets the kinematical limitations to the total number of events with a recoil proton. 29 of the 129 white stars with even numbers of tracks and an identifiable proton did not meet the kinematical requirements. This number for the corresponding events with odd number of tracks is 24 out of 54. These figures yield reduction factors of $\frac{100}{129}$ and $\frac{30}{54}$ for the π^- -p' and π^- -n', respectively, events with no proton track. With these corrections the number

of inelastic π^- -p' events becomes 188 and the total number of π^- -n' events would be 145. Assuming the ratio of elastic to total π^- -n (same as π^+ -p) cross sections to be $\sigma_{el}/\sigma_t \approx 6/26$ ⁽¹³⁾ it is estimated that 33 of the corrected number of π^- -n' events with one charged pion should be elastic scatterings. Taking all this into account, the histograms of Figure 6 are replotted for the inelastic events only. These results are shown in Figure 7. The crosses in Figure 7a indicate the number of events for each pion multiplicity calculated using the "multiplicity distribution functions" of reference 14. These distribution functions are obtained by assuming that pion production is related to Poisson processes with neutral production considered to be independent of charged pion production. Then the multiplicity distribution of the secondaries are given by some combinations of terms of the Poisson probability function.

From Figure 7a the proportion of protons present in inelastic π^- -p' collisions is found to be (46±5)%. This confirms the fact that the outgoing nucleon has about equal probability to be a proton or a neutron. However, for π^- -n' collisions this proportion is found from Figure 7b to be (27±5)%. The large discrepancy here cannot be entirely attributed to the experimental inaccuracies, although it should be remarked that some of the min-

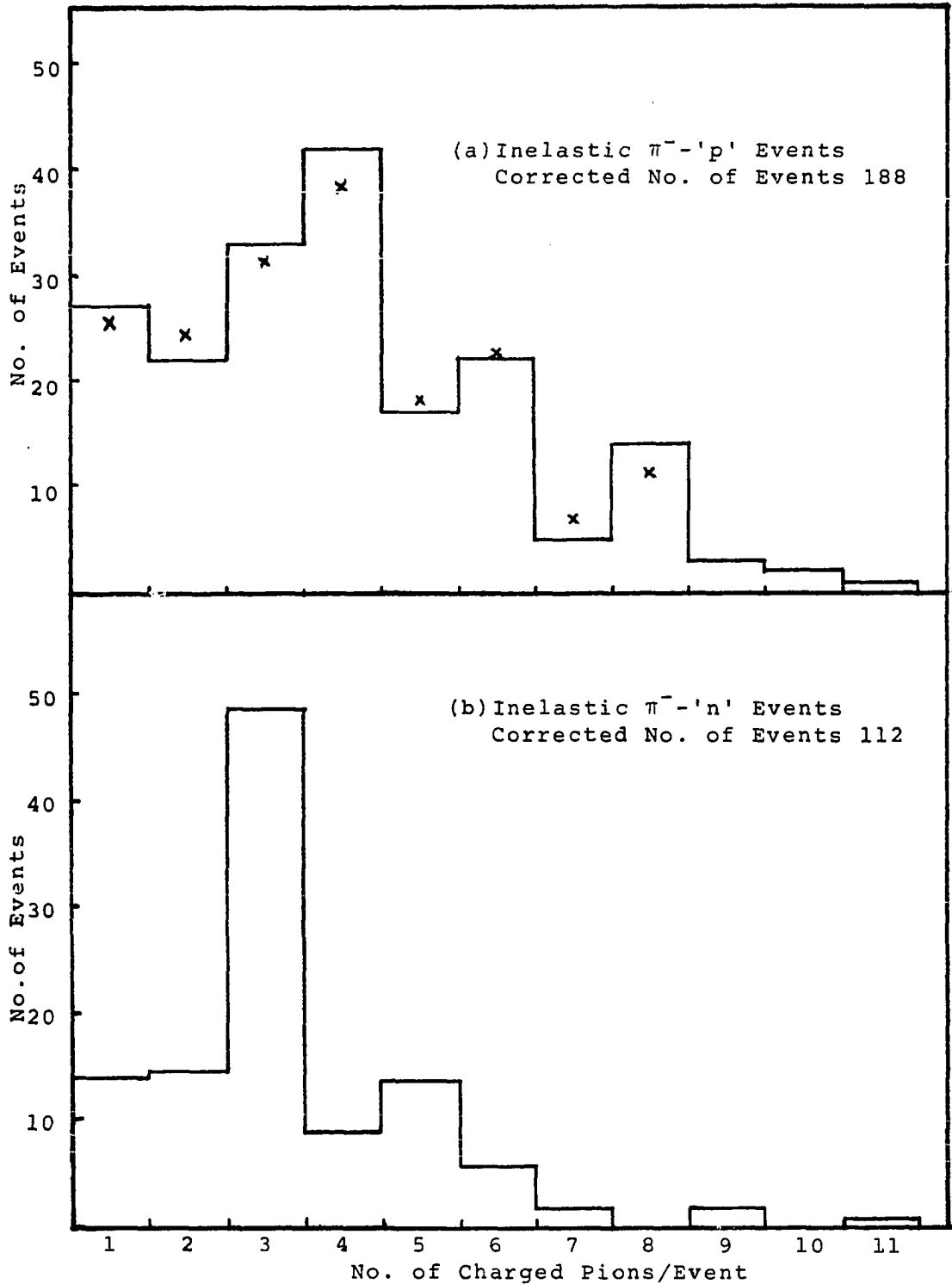


Fig. 7 Corrected Distribution of
Number of Charged Pions

imum ionizing tracks, taken to be pion tracks, could have been proton tracks. The fraction of such tracks is estimated to be about 13% (see Momentum Distribution of the Recoil Protons). Using the corrected number of π^- -p' and π^- -n' events, the corrected number of π^- -p events is calculated to be 116 ± 12 with a corrected mean free path of 12.8 meter. The corrected cross sections for the different types of events are given in Table 2. The agreement with the results of J. Bartke, et. al., is satisfactory. The corrected average number of charged pions per event is 4.0 ± 0.3 for the π^- -p' events and 3.7 ± 0.3 for the π^- -n' events.

B. Elastic π^- -p Interactions

The identification of the elastic π^- -p events is dependent only upon the measurements on the proton track. This is fortunate because in these events the secondary pion has a very high energy (of the order of the incident energy, 16 BeV) and the error associated with its measurement by the multiple Coulomb scattering technique is usually of order of few BeV. Also, since the secondary pion usually makes a very small angle with the incident pion, the angle measurements on the secondary pion track is not very accurate. The results of the measurements on 16 events which have been selected as elastic π^- -p inter-

actions are given in Table 3. The angles θ_p and θ_π refer to total angle that the recoil proton and the secondary pion, respectively, make with the direction of the incident pion. All these events meet the requirement of coplanarity, and are checked to meet the kinematical requirements derived in Chapter II. Figure 8 shows a plot of lab angle versus momentum of the recoil protons for these events. Most of these events fall on the curve of $P_{||} = 0$ within the limit of the experimental error. This curve is obtained on the assumption that the elastic collision is with a proton at rest. For the other two curves it has been assumed that the elastic collision is with a target proton whose parallel component of its momentum (parallel to the direction of incident pion) is -30 MeV and +30 MeV, respectively. It is observed that all of the events fall between the two curves ($P_{||} = -30$ and $P_{||} = 30$) within the experimental error. Noting that a value of 30 MeV for the momentum of the target proton is far below the average Fermi momentum of the nucleons in the nuclei, which is about 220 MeV⁽¹⁵⁾, it is concluded that all of these events are elastic collisions with free or almost free protons.

Due to the low statistics a detailed analysis of these elastic events is not done. However, in Figure 9 the C.M. angular distribution of the recoil protons is

TABLE 3

DATA ON ELASTIC π^- -p EVENTS

Event	Proton Momentum (MeV)	θ_p ($^\circ$)	θ_π ($^\circ$)
150175	261 \pm 3	81.6 \pm .1	.8 \pm .1
183249	380 \pm 200	78.2 \pm .3	1.2 \pm .1
190182	356 \pm 4	78.2 \pm .3	1.2 \pm .1
190194	370 \pm 90	74.7 \pm .3	2.1 \pm .1
350661	490 \pm 300	73.0 \pm .2	1.5 \pm .4
351285	500 \pm 300	73.3 \pm .4	1.1 \pm .1
370103	270 \pm 3	77.0 \pm .4	2.9 \pm .4
370327	439 \pm 5	81.1 \pm .3	1.2 \pm .1
380008	290 \pm 50	75.6 \pm .2	1.4 \pm .1
380053	408 \pm 90	79.1 \pm .4	1.7 \pm .2
400279	160 \pm 3	85.6 \pm .4	1.2 \pm .4
400347	134 \pm 2	87.0 \pm 1.0	.5 \pm .1
410015	333 \pm 4	74.4 \pm .2	1.4 \pm .2
461508	270 \pm 3	81.4 \pm .1	.9 \pm .1
481161	67 \pm 2	86.1 \pm .8	.1 \pm .1
560032	452 \pm 5	76.6 \pm .3	1.8 \pm .2

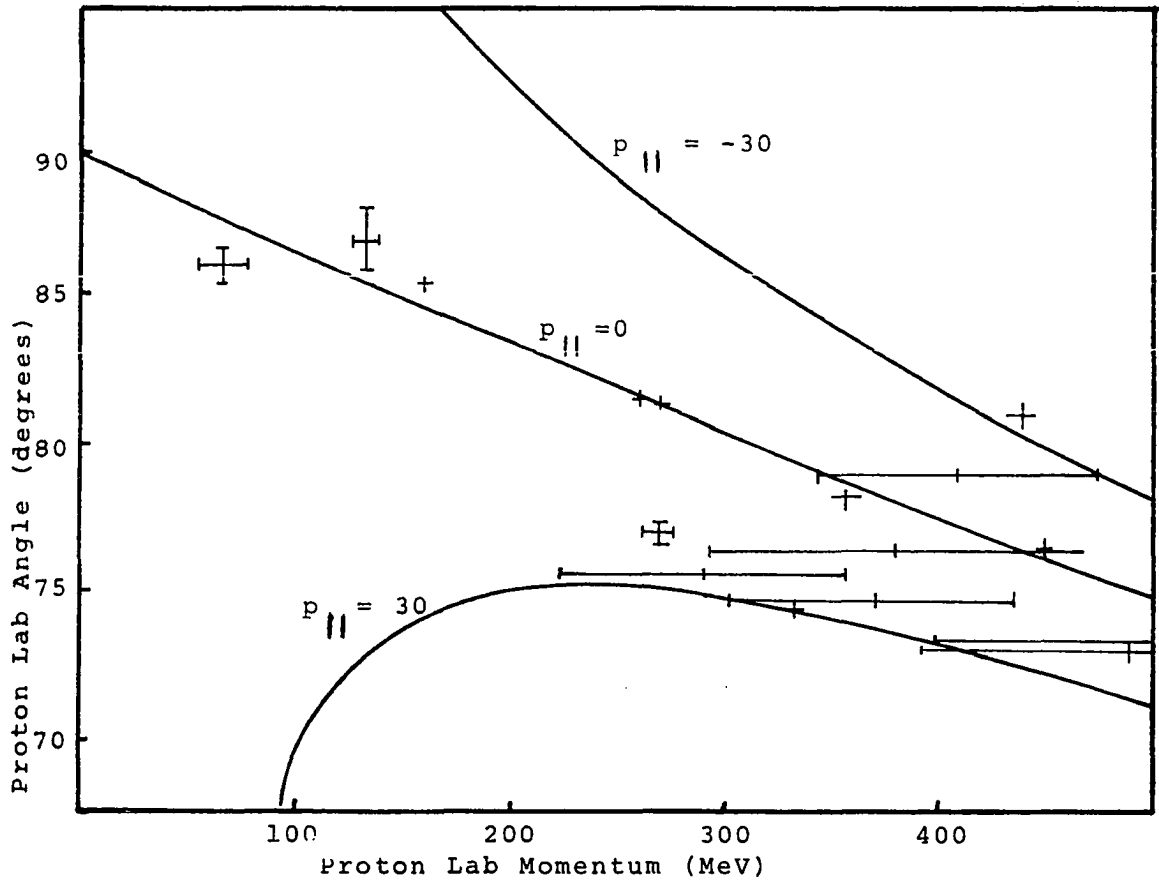


Fig. 8 Momentum vs. Angle Plot for Protons from Elastic π^- -p Events

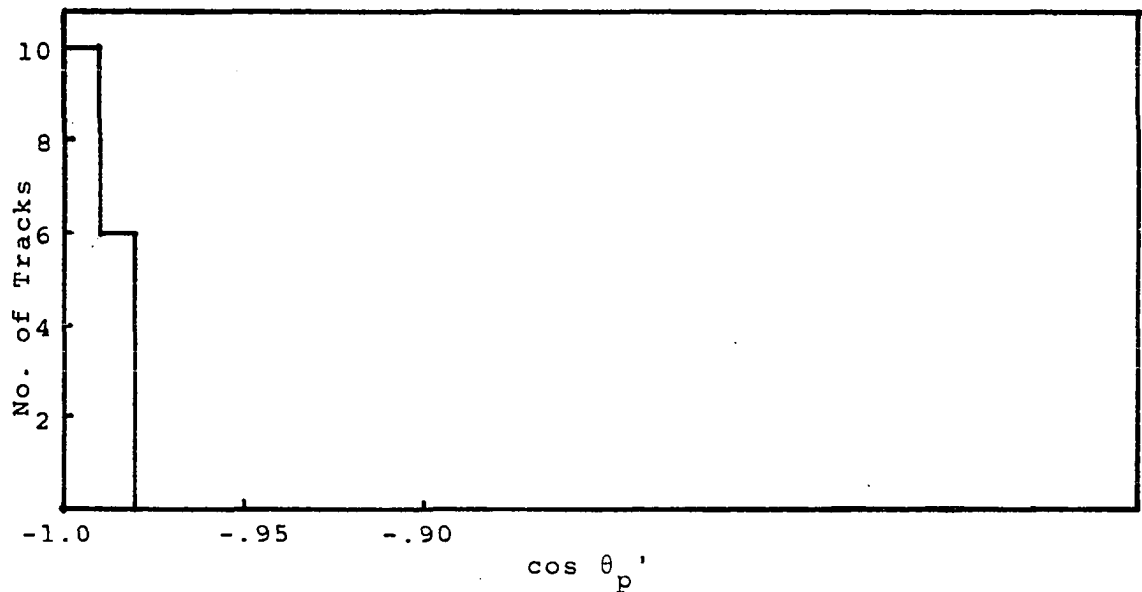


Fig. 9 C.M. Angular Distribution of Protons from Elastic π^- -p Events

given. It is observed that in every case the recoil proton is emitted extremely backward in the C.M. system. This means that the target proton, in the C.M. system, continues in its original direction (backward) after the collision and the collision is a glancing type of collision. This is in agreement with the results of other experiments^(16,17) and the peripheral interpretation of the interaction.

C. Inelastic π^- -N Interactions

The measured data on all these events are given in Appendix C. Table C.1 gives the data on the pion-'proton' interactions and Table C.2 gives the data on pion-'neutron' interactions. The events are arranged according to increasing multiplicity of the charged-pions. Pion tracks are numbered 1,2,3, . . . , and the proton track is indicated by the letter P. The first two figures in the event number refer to the number of the plate in the \mathcal{A} -stack in which the event is located. For each track the values of the momentum, projected angle, and dip angle and their errors are given. Due to the difficulties explained in the previous chapter it was not possible to measure the momenta of all the tracks. For these tracks there are no entries in the first two columns of the tables. The angle measurements have been completed

on all 1742 of these tracks, and momentum measurements have been done on 121 proton tracks and 943 pion tracks. In the following sections this data will be analyzed in some detail. The inelastic interactions will be referred to as π^- -p and π^- -n events.

1-Momentum Distribution of the Recoil Protons

The momentum spectrum of the recoil protons in the lab system is shown in Figure 10. Of the 121 protons measured, 27 are from π^- -n events and 94 are from π^- -p events. The separate distributions for the two different groups of events do not differ from that of Figure 10. All the protons except 3 have a measured momentum of less than 600 MeV. It is possible that the number of protons with higher momenta has been underestimated by the identification technique used in this experiment. As discussed earlier, only particles with greater-than-minimum ionizing tracks were checked as possible proton tracks. Such a proton track has a corresponding momentum of less than 1.6 BeV. However, the low momentum peak is in agreement with the results of other experiments at similar incident energies^(18,19). In reference (19) where the momentum measurement of high energy protons with minimum ionizing tracks were done by δ -ray method, it was found that 87% of the protons had a momentum less than 1.6 BeV. If this holds true in the present experiment, the high momentum

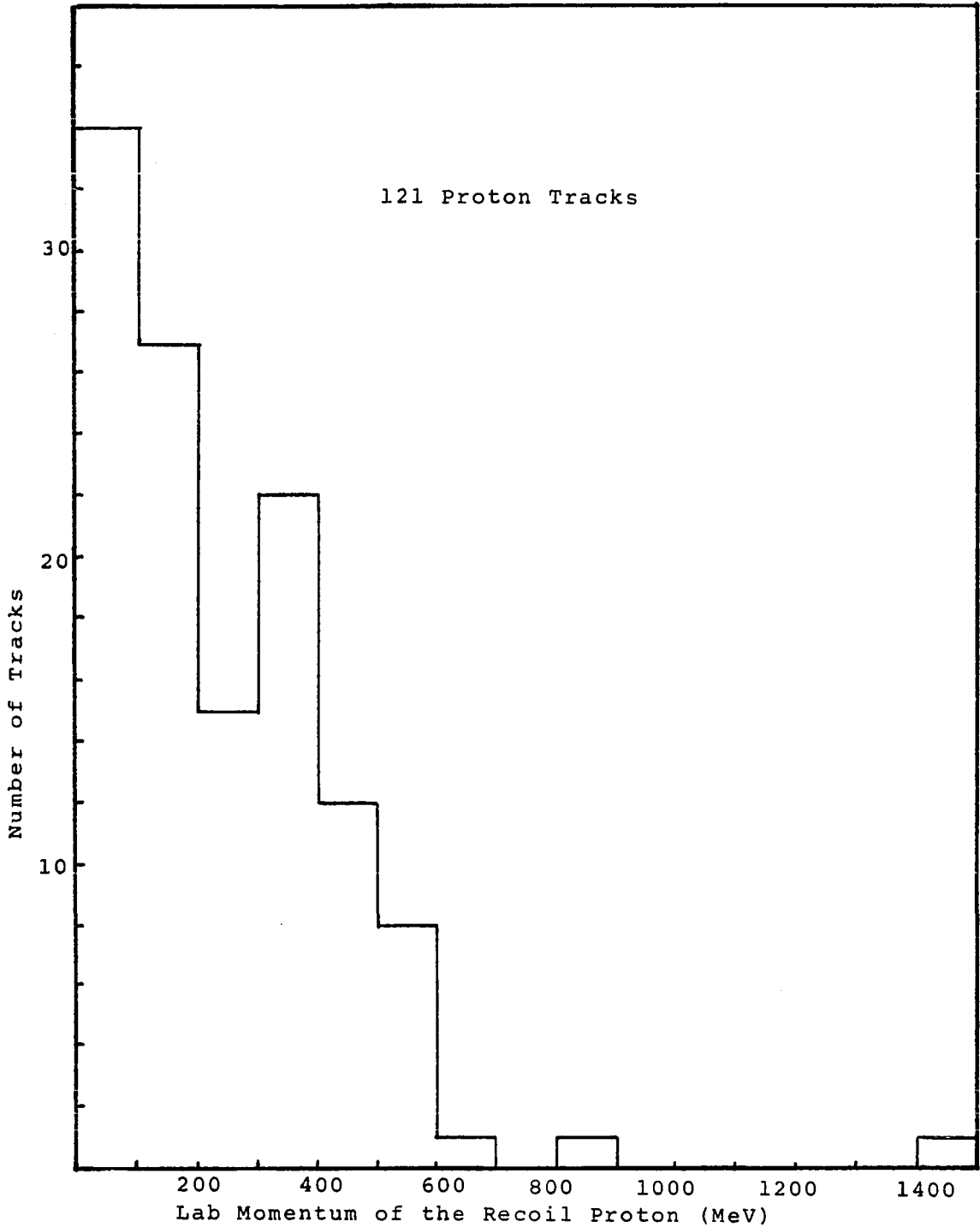


Fig. 10 Recoil Proton Momentum Spectrum

cut-off introduced by not considering the minimum ionizing tracks as possible proton tracks does not significantly affect the shape of the spectrum in Figure 10. The strong maximum at low values in the proton momentum spectrum in the lab system is one of the expected characteristic features of glancing collisions. In fact, the "peripheral" or "glancing" model of Ferrari and Selleri⁽²⁰⁾ predicts a strong maximum at a value of about 400 MeV proton recoil momentum for the process of single-pion production. Since the events used in the spectrum of Figure 10 correspond to processes with many different numbers of pions produced, a quantitative comparison with the predictions of the peripheral model is not possible.

2-Angular Distributions in the C.M. System

The angular distributions of the secondary particles in the C.M. system are of great significance as regards certain aspects of the nature of the interaction. The following equation, which is easily derived from Eqs. 2 and 3, Chapter II, has been used to calculate the C.M. angles of the secondary particles,

$$\tan \theta'_i = \frac{\sin \theta_i}{\gamma_c (\cos \theta_i - \beta_c / \beta_i)}, \quad (42)$$

where for the C.M. velocity a value of $\beta_c = 0.9451$, corresponding to the case of a single nucleon target at rest, has been used.

The recoil protons C.M. angular distribution has a sharp backward peak. All the recoil protons are emitted with cosine of the C.M. angle less than -0.84 . In fact 89% of the protons have $-1.00 \leq \cos \theta'_p < -0.99$. This extreme C.M. backward angular peaking of the recoil protons is another characteristic of peripheral interactions, and is in agreement with the results of other experiments^(21, 22). In reference (21) it is observed that for eight-prong events, the distribution of the protons in the C.M. becomes symmetric. In this experiment only 9 protons from events with $n_s \geq 7$ have been measured and the low statistics does not allow such a conclusion. However, this is partially observed in the distribution of pions as is discussed below.

In Figures 11a and 11b the C.M. angular distribution of the measured pions from all the π^- -p events, and all the π^- -n events, respectively, are shown. First, the similarity of the two distributions suggests the sameness of the nature of pion-nucleon interactions whether the nucleon is a proton or a neutron. Second, the C.M. distribution of the pions is asymmetric with a profound forward peak, and the distribution becomes almost isotropic for $\cos \theta' < 0.4$. This suggests that the distribution can be considered as the superposition of an isotropic part and a forward peak⁽²¹⁾. The ratio of

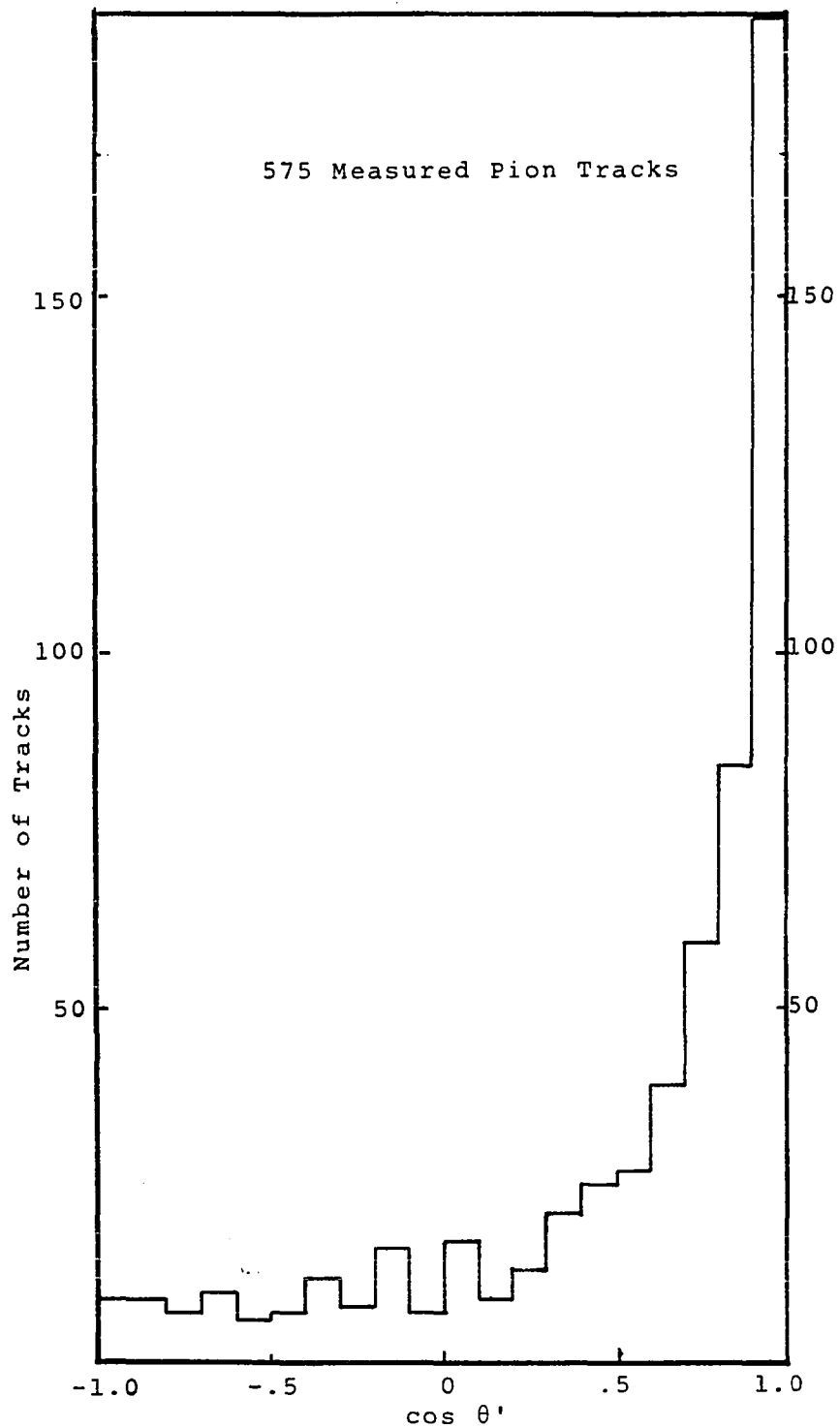


Fig. 11a C.M. Angular Distributions of All the Measured Secondary Pions from Inelastic π^-p Events

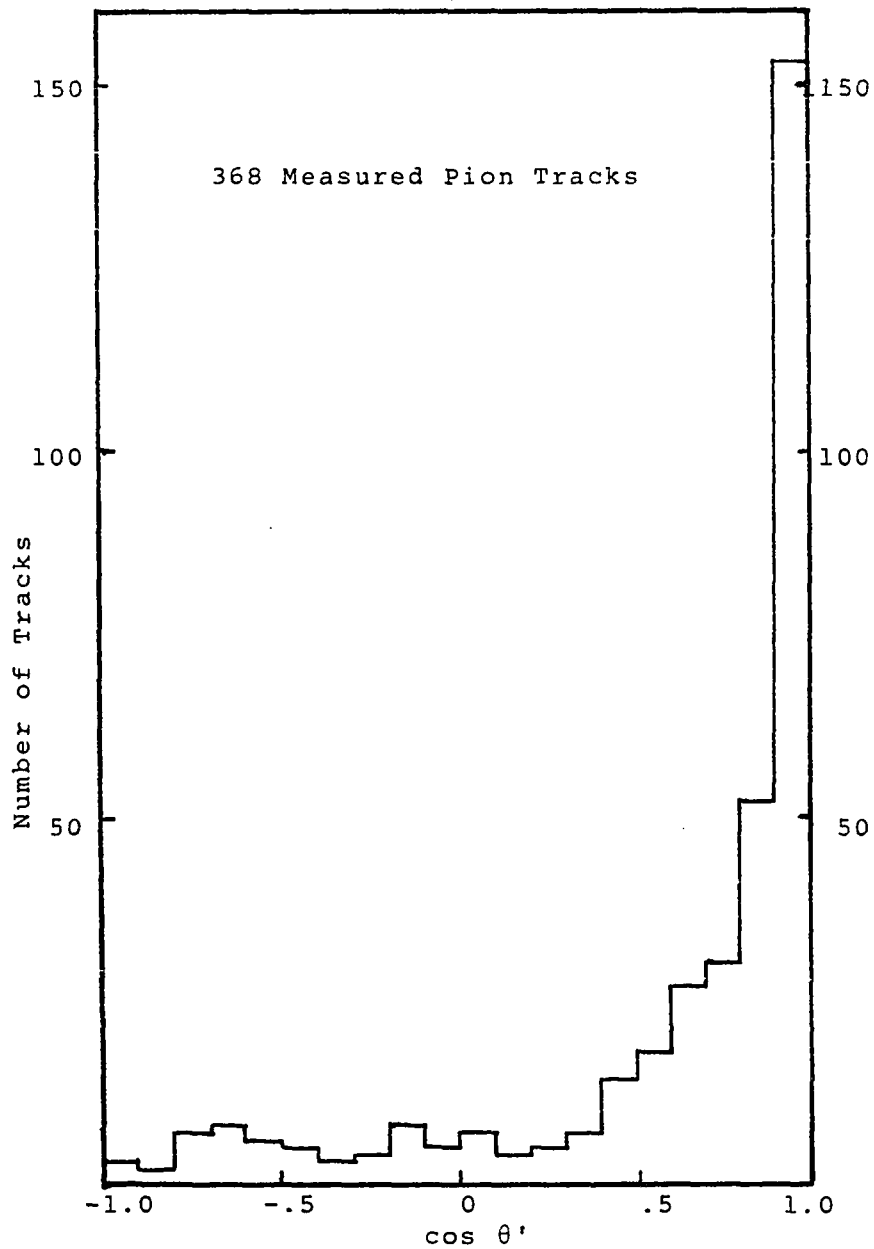


Fig. 11b C.M. Angular Distribution of all the Measured Secondary Pions from Inelastic π^-n Events

the isotropic part to the sum of the two parts can be obtained from the relation

$$\text{ratio} = \frac{2n_B}{n_F + n_B}, \quad (43)$$

where n_B and n_F are the number of backward and forward tracks, respectively. This ratio is 0.32 ± 0.03 for π^- -p, and 0.28 ± 0.04 for π^- -n events.

A rather interesting feature of the C.M. angular distributions is observed by the study of the histograms of Figure 12. Here the C.M. angular distributions of the pions of the π^- -p events with different charged pion multiplicities, n_s , are shown. (The corresponding distributions for the π^- -n events are shown in Figure 13.) For low multiplicity events, $n_s \leq 3$, the pions are emitted extremely asymmetrically and peaked forward. As n_s increases the relative height of the forward peak decreases. Indeed, for events with $n_s \geq 8$, the isotropic part of the distribution is dominant. This is in agreement with the results of other experiments at similar energies^(22,23). A quantitative measure of the change in the shape of the C.M. angular distributions with the shower multiplicity is the ratio defined by Eq. 43. The value of this ratio is $.08 \pm .03$, $.20 \pm .05$, $.56 \pm .10$, and $.58 \pm .10$ for the π^- -p events with $n_s \leq 3$, (4,5), (6,7), ≥ 8 , respectively.

The isotropic angular distribution is one of the predictions of the statistical model which is used to

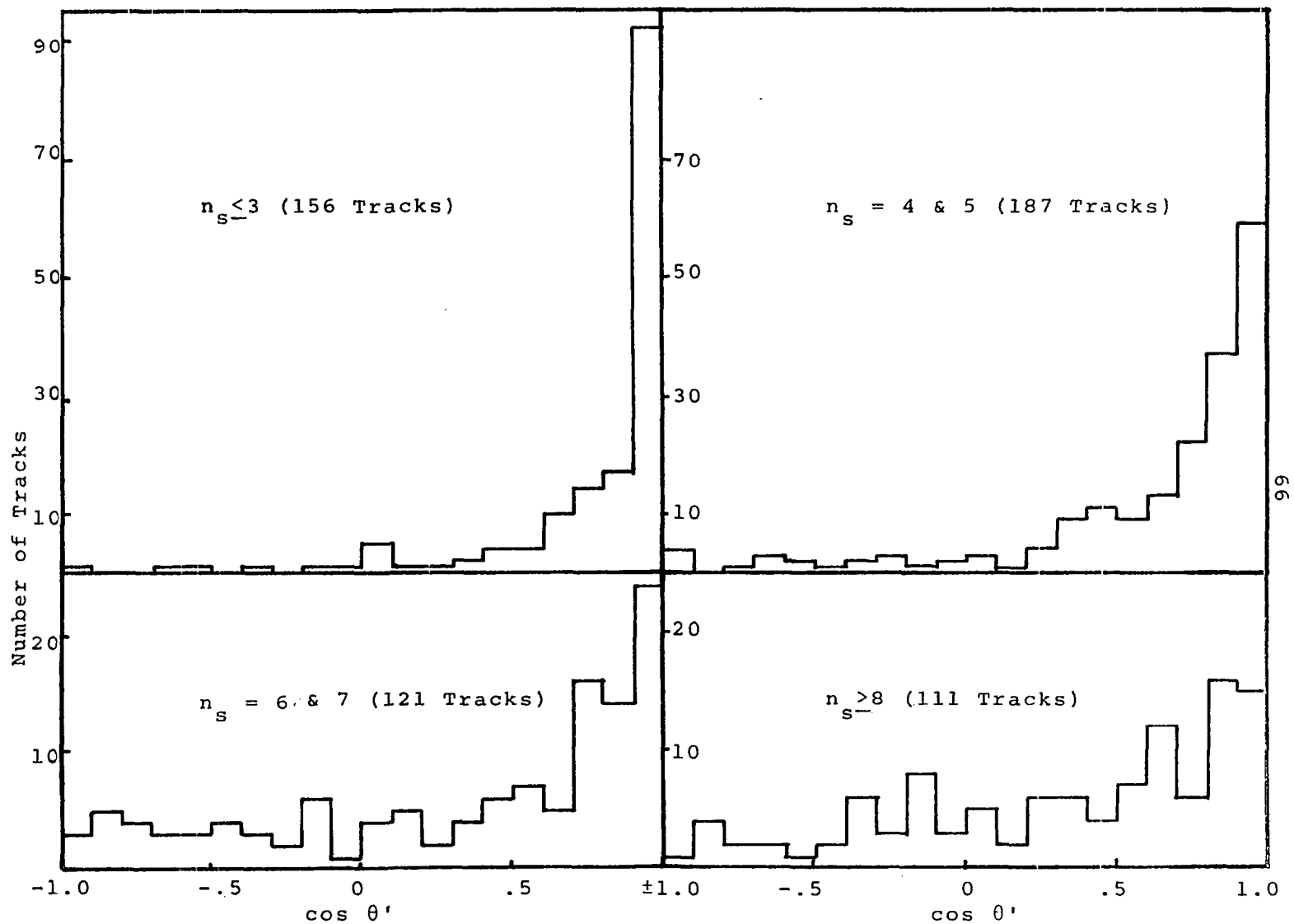


Fig. 12 C.M. Angular Distributions of the Measured Secondary Pions for Different Pion Multiplicities: π^- -p Events

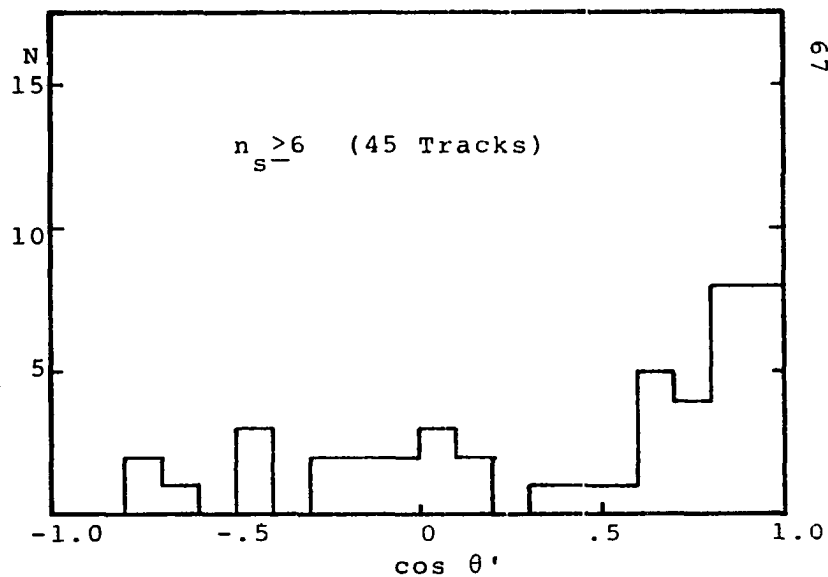
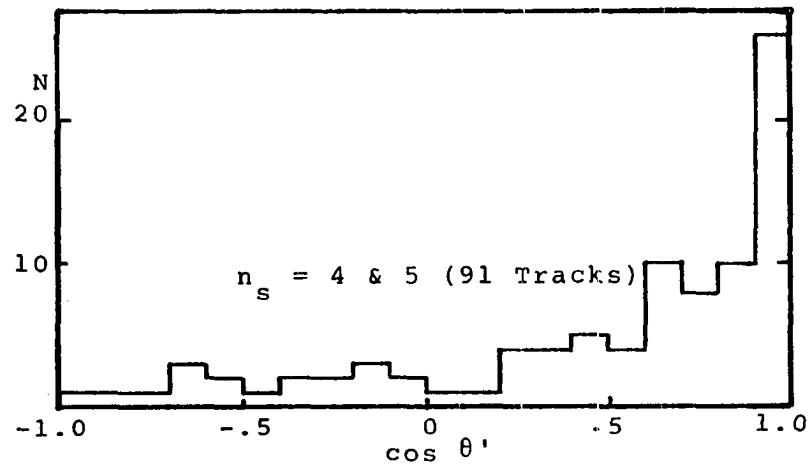
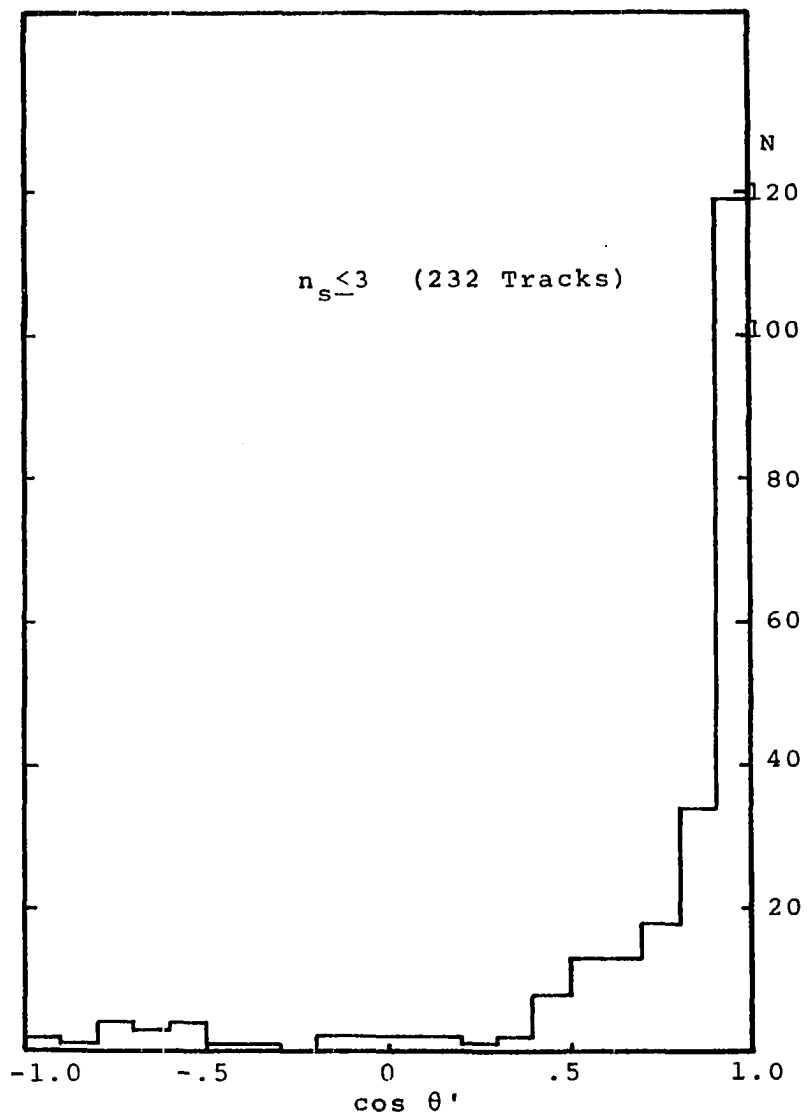


Fig. 13 C. M. Angular Distributions of the Measured Secondary Pions for Different Pion Multiplicities: π^- -n Events

describe the pion-nucleon interactions at high energy. For the case of the Fermi statistical model⁽³⁾, where angular momentum conservation is considered, there must be at least a forward-backward symmetry in the distribution. Statistical processes are related to the small-impact-parameter collisions⁽²⁴⁾, and commonly the expression "central collisions" is used to refer to such collisions to which the statistical model applies. On this basis, the isotropic, or the symmetric, part of the angular distribution can be related to the fraction of events which undergo a central collision. The values of the ratios given by Eq. 43 indicate that for low multiplicities only a very small fraction of the events can be considered as central collisions, whereas for high multiplicity events central collisions can be considered as the dominant mode.

3. Transverse Momentum of Pions

Transverse momentum, p_t , is a quantity of much interest and great significance in high energy interactions. It is defined as the component of the momentum of a secondary particle normal to the direction of the incident particle. From the Lorentz transformation, Eq. 3, this quantity is the same in the lab system as in the C.M. system and is given by

$$p_t = p \sin \theta = p' \sin \theta'.$$

Transverse momentum has become the subject of extensive

experimental study in the past few years. Some of the important features of the transverse momentum which have been observed in various experiments are the following:

i--The distribution of the transverse momentum of the shower particles shows a peak between 100-200 MeV and has a tail for high values of p_t .

ii--The average transverse momentum, $\langle p_t \rangle$, is constant at about 300 MeV over a wide range of the energy of the incident particle^(23,25,26).

iii-- $\langle p_t \rangle$ is independent of the multiplicity of the shower particles^(22,27).

iv-- $\langle p_t \rangle$ increases slowly with the mass of the secondary particle^(18,22).

The shape of the p_t distribution has been studied extensively and many different theoretical curves have been attempted. In the following discussion the p_t distributions for the pions of the present experiment will be presented and some of the theoretical distribution curves will be discussed.

a-Overall p_t -distribution

The average transverse momentum of the pions from elastic events is 315 ± 25 MeV, and due to low statistics its distribution is not given. Figure 14 shows the transverse momentum distribution for secondary pions with measured momenta from the inelastic π^- -p events. Figure

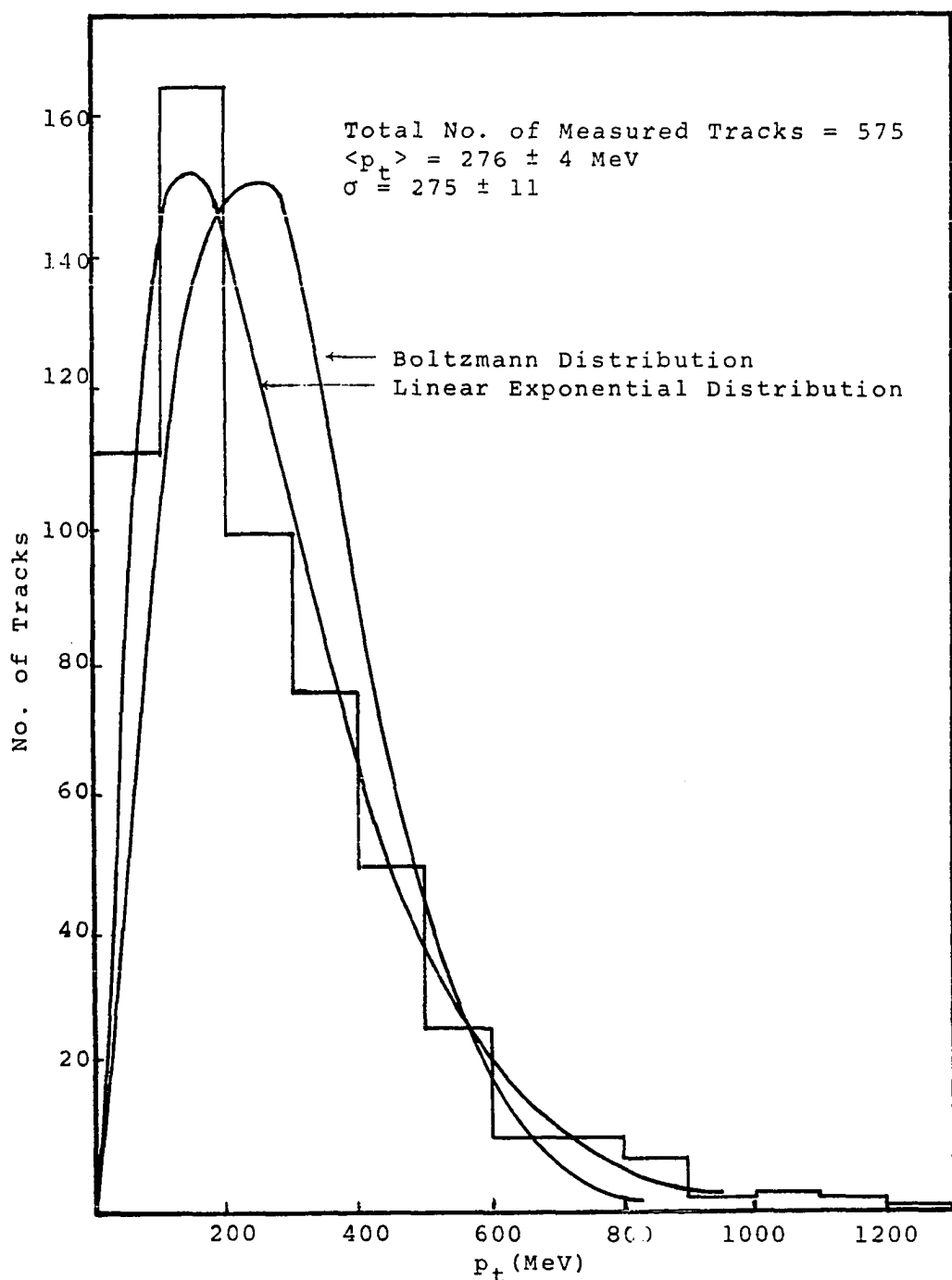


Fig. 14 Overall Transverse Momentum Distribution of the Measured Secondary Pions: π^- -p Events

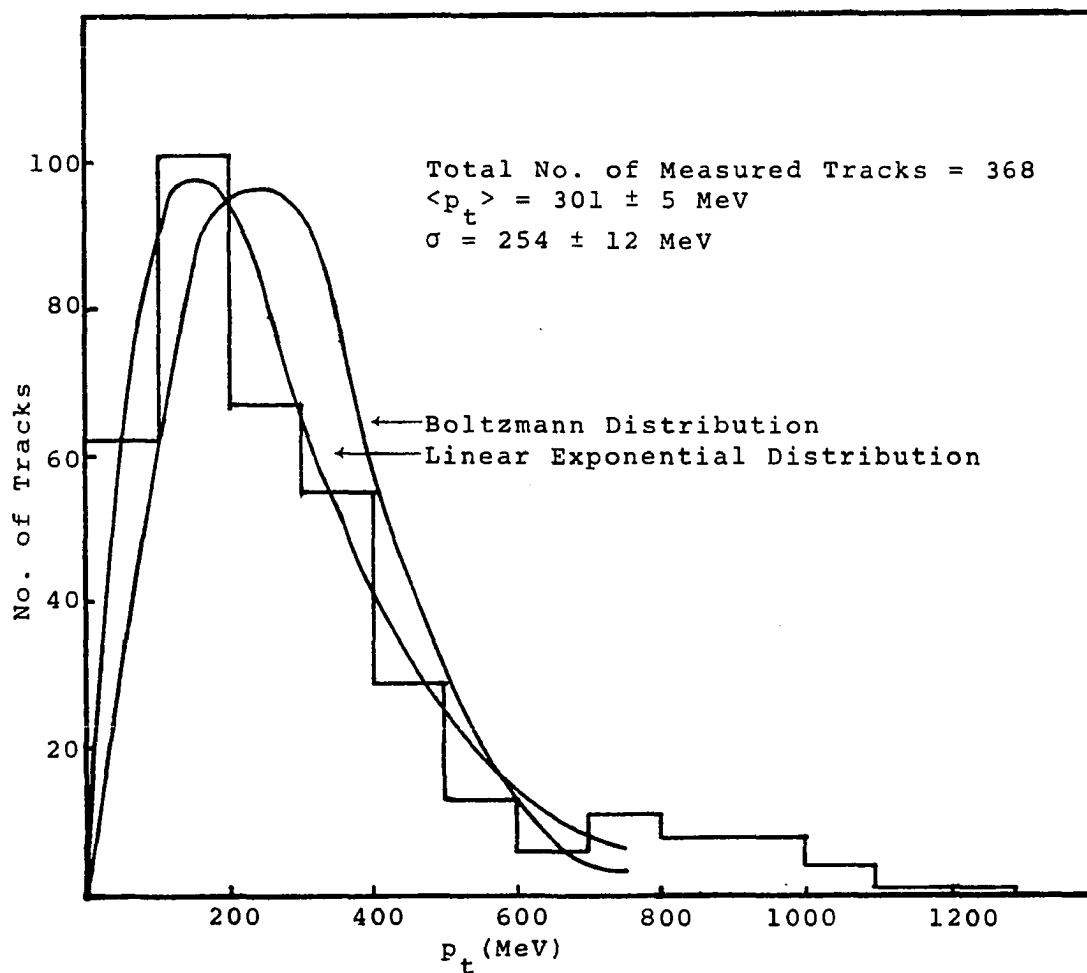


Fig. 15 Overall Transverse Momentum Distribution of the Measured Secondary Pions: π^- -n Events

15 shows the corresponding distribution for the π^- -n events. For both distributions the most probable value of p_t is between 100-200 MeV. The value of $\langle p_t \rangle$ is 276 ± 4 and 301 ± 5 for the π^- -p and π^- -n distributions, respectively, and the corresponding standard deviations, $\sigma = \{\langle p_t^2 \rangle - \langle p_t \rangle^2\}^{1/2}$, for the two distributions are 275 ± 11 and 254 ± 11 . The error in $\langle p_t \rangle$ has been calculated from the error in the angle and momentum of the measured tracks

$$\Delta \langle p_t \rangle = \frac{1}{N} \left\{ \sum_{i=1}^N \{ (\sin \theta_i)^2 (\Delta p_i)^2 + (p_i \cos \theta_i)^2 (\Delta \theta)^2 \} \right\}^{1/2} \quad (44)$$

where N is the number of tracks used in averaging. Both distributions have been fitted to the two following theoretical distribution curves:

1-Boltzmann Distribution--This is given by the following equation

$$f_B(p_t) dp_t = \frac{p_t}{\sigma^2} e^{-p_t^2/2\sigma^2} dp_t.$$

For this distribution the experimental standard deviation has been used for σ and the theoretical fraction of particles in each interval is found by integrating $f_B(p_t) dp_t$ over that interval. Friedlander⁽²⁸⁾ and Aly et al⁽²⁹⁾ arrive at the Boltzmann distribution on the assumption that the secondary particles are emitted symmetrically with respect to the collision axis in the C.M. system. In reference (30) it is rigorously proved that the assump-

tion of axial symmetry, together with the assumption of statistical independence of p_x and p_y , uniquely yield the Boltzmann distribution for p_t .

In addition, Friedlander⁽²⁸⁾ has suggested that for pions a superposition of two Boltzmann distributions involving three parameters to be fixed by the experimental data gives the best fit.

a2-Linear Distribution--Many investigators^(31,32,33) have obtained a best fit for p_t data using the linear exponential distribution function given by the equation

$$f_L(p_t) dp_t = a^2 p_t e^{-ap_t} dp_t,$$

where $1/a$ is a constant given by the most probable value of p_t . The best fit to the data of the present experiment has been obtained with $1/a = 135 \pm 5$ MeV. This is slightly lower than the value used by other investigators^(31,32,33) which has been reported to be between 150-165 MeV.

The linear distribution function seems to fit the data of the present experiment both for the π^- -p and the π^- -n events, which can be seen by a visual inspection of Figures 14 and 15. However the results of a Chi-square goodness of fit test applied to these two distribution functions indicated that the linear distribution function gives a rather poor fit, and the Boltzmann distribution

function gives an even poorer fit. Various other distribution functions and empirical formulae have been proposed to fit the observed p_t distributions. A summary of all these distribution functions can be found in reference 34.

b-Dependence of p_t on θ and n_s

In order to study the dependence of transverse momentum on the laboratory emission angle, θ , of the secondary pions, the data has been divided into four groups according to angle. The distribution of p_t for each of these four groups is shown in Figure 16, for π^- -p events, and Figure 17, for π^- -n events. The eight distributions given in these two figures all resemble the overall p_t distributions given in Figures 14 and 15. It appears that the most probable value of p_t shifts toward higher values with increasing θ and that the peak becomes broader. However, since the low statistics at large angles does not permit a closer comparison of the four distributions only $\langle p_t \rangle$ for each of the distributions is given.

To observe the dependence of $\langle p_t \rangle$ on the pion multiplicity, n_s , the events have been divided into groups with different values of n_s , and $\langle p_t \rangle$ for each group has been calculated. Furthermore, the data for each of these groups has been subdivided into six angular intervals and $\langle p_t \rangle$ has been calculated for each of these intervals. The results of these calculations are given in Table 4. The

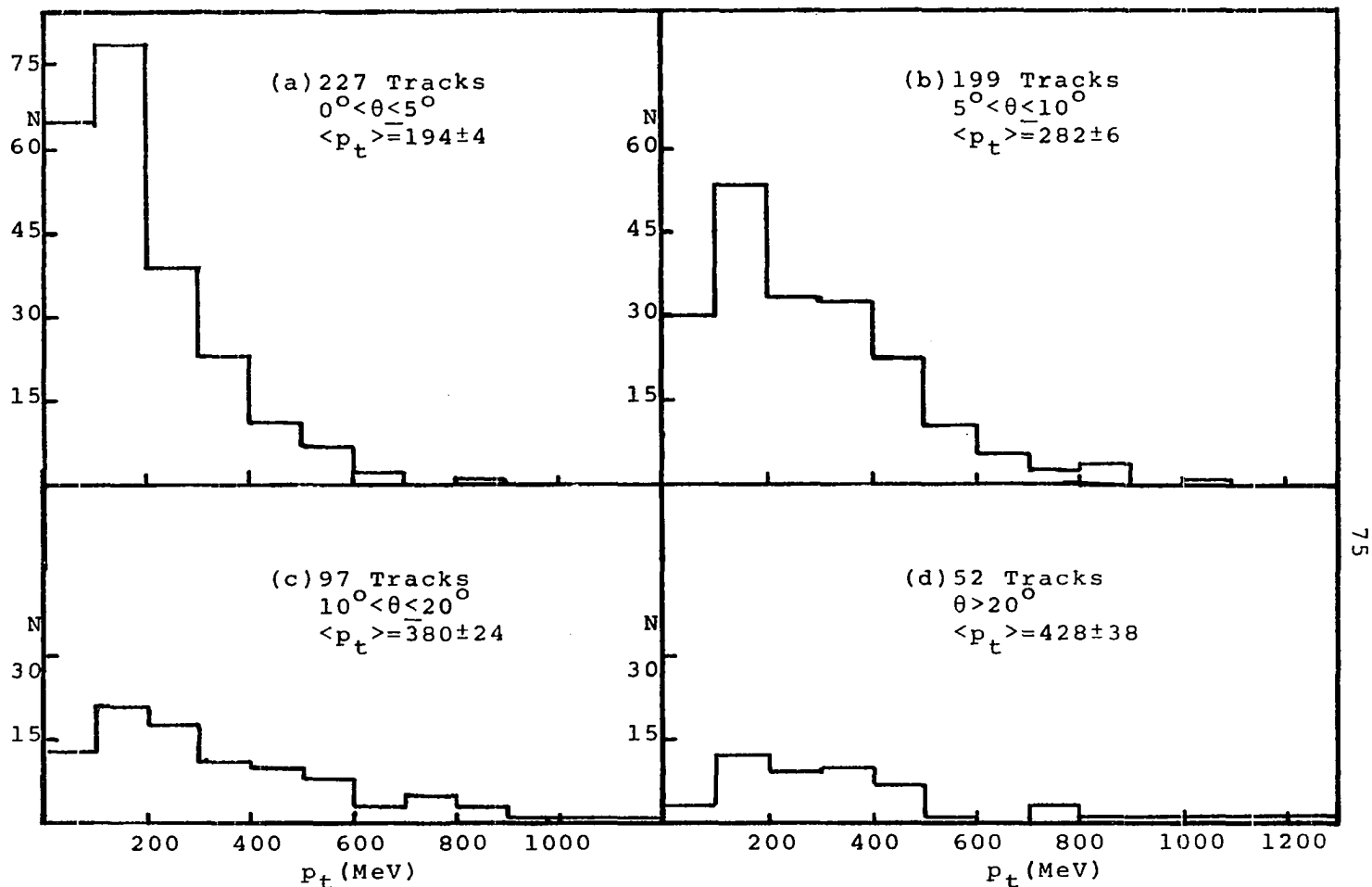


Fig. 16 Transverse Momentum Distributions for
Angular Intervals: π^- -p Events

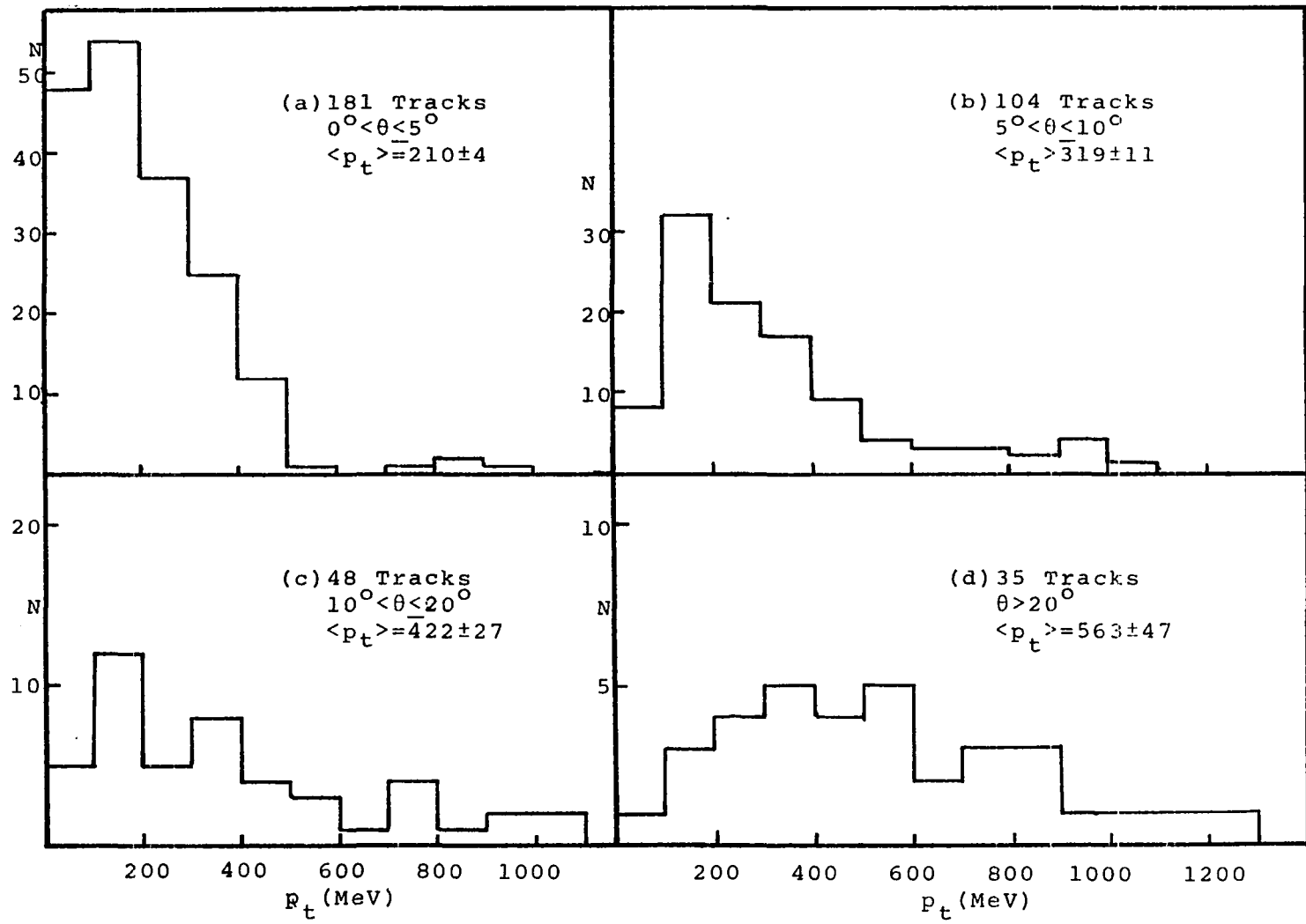


Fig. 17 Transverse Momentum Distributions for Angular Intervals: π^- -n Events

TABLE 4

 DEPENDENCE OF AVERAGE TRANSVERSE
 MOMENTUM ON θ AND n_s

$n_s \backslash \theta$	$0-180^\circ$	$0-5^\circ$	$5^\circ-10^\circ$	$10^\circ-15^\circ$	$15^\circ-20^\circ$	$20^\circ-40^\circ$	$40^\circ-180^\circ$
$\pi^- - p$							
1,2	273±8	225±5	318±8	198±23			
3,4	265±7	198±6	277±9	396±35	625±85	640±111	
5,6	286±8	174±8	282±10	307±28	568±51	298±38	644±59
7,8	298±9	163±7	289±16	200±14	443±40	445±24	719±199
≥ 9	243±15	149±25	218±24	265±27	206±21	454±85	
All	276±4	194±4	282±6	307±15	507±35	420±22	502±53
$\pi^- - n$							
2,3	280±6	219±5	312±14	373±24	540±52	428±56	703±82
4,5	349±13	194±11	345±19	448±74	364±35	657±37	
≥ 6	306±19	128±10	299±37	464±173	450±46	355±30	
All	301±5	210±4	319±11	411±35	425±27	512±26	662±57

values of overall $\langle p_t \rangle$ (second column of the table) show only a small statistical fluctuation, well within error, from the value of 287 ± 4 for the entire set. This is reminiscent of previous observations (22,23,27) which indicate that the overall $\langle p_t \rangle$ is independent of the pion multiplicity. However, for pions with an angle less than 5° (third column of the table), there is a definite dependence of $\langle p_t \rangle$ on n_s ; it decreases steadily with increasing n_s . This fact has not been reported by other investigators who have not made such an analysis. For the angular interval 5° - 10° , $\langle p_t \rangle$ seems to be independent of n_s , and for angles greater than 10° , due to low statistics, the fluctuations of $\langle p_t \rangle$ seem rather sporadic and definite conclusions cannot be drawn. From Table 4 it is also observed that $\langle p_t \rangle$ has a dependence on the angle of emission, it increases with θ up to 15° . Beyond this angle $\langle p_t \rangle$ for all events becomes constant, within statistics. The $\langle p_t \rangle$ for individual groups of events show sporadic fluctuations which is probably a result of low statistics.

c-Dependence of $\langle p_t \rangle$ on C.M. Angle of Emission

The dependence of $\langle p_t \rangle$ on θ' is shown in Figure 18a for π^- -p events, and in Figure 18b for π^- -n events. The two figures are very similar. $\langle p_t \rangle$ increases from a value of about 200 MeV at small angles to a value of about 350 MeV at about 90° beyond which it

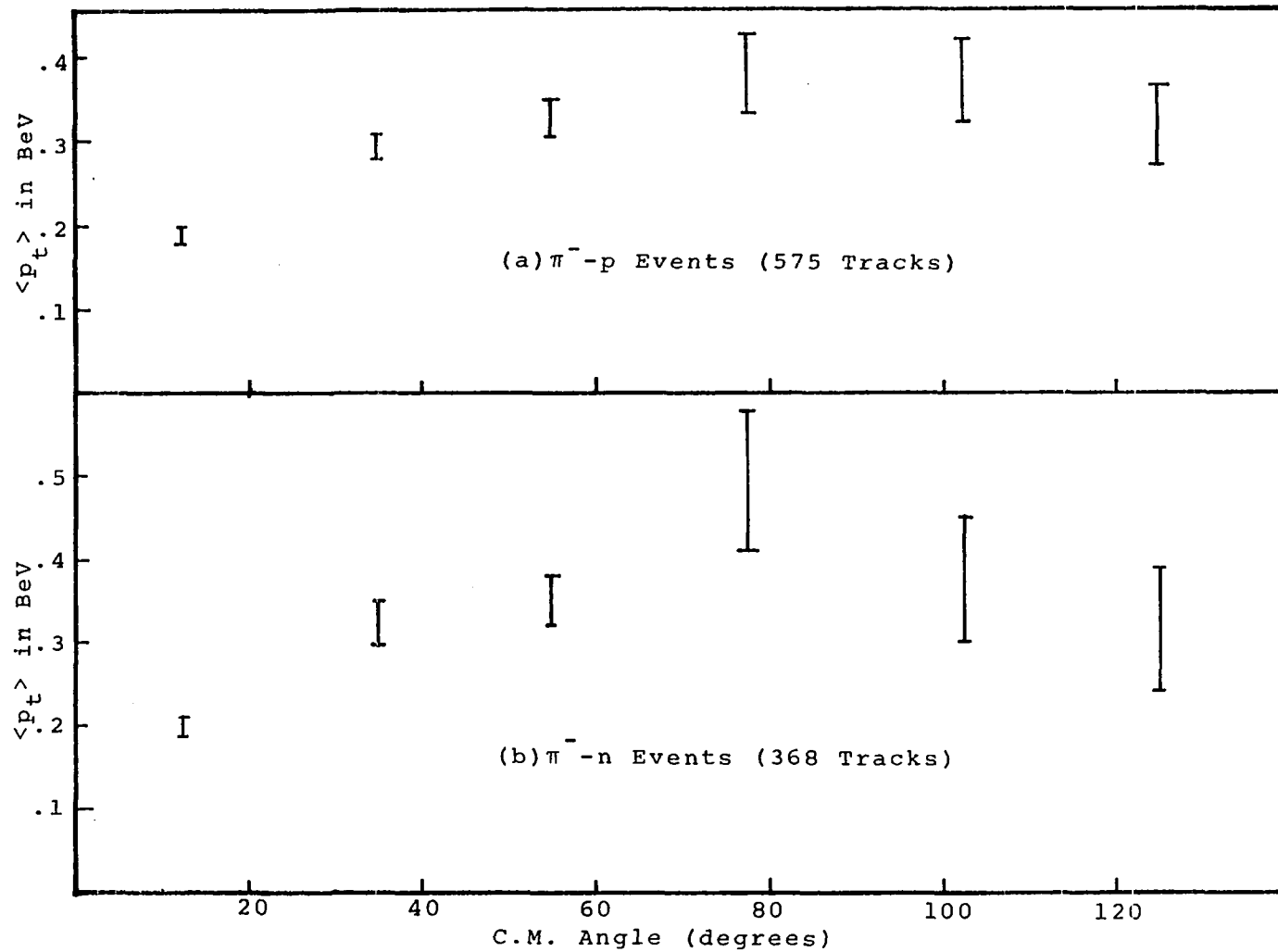


Fig. 18 Average Transverse Momentum vs. C.M. Angle Intervals

seems to decrease which indicates the possibility of symmetry about 90° . These results are in general agreement with the results of other experiments at similar energies (17,22,27). However, the possibility of symmetry about 90° is not reported in these experiments.

4. Target Mass and Effective Target Mass

a-Target Mass

In the interaction of a high energy pion with a target nucleon, assumed to be at rest, one can write the equations for the conservation of energy and momentum as ⁽³⁵⁾

$$\begin{aligned} E_0 + M_{tg} &= \sum E_i, \\ p_0 &= \sum p_i \cos \theta_i \\ 0 &= \sum p_i \sin \theta_i \cos \phi_i \\ 0 &= \sum p_i \sin \theta_i \sin \phi_i \end{aligned} \quad (45)$$

Here M_{tg} is the target mass, E_0 and p_0 are the energy and momentum of the incident particle, E_i and p_i those of the ith secondary particle with angle of emission θ_i , projected angle ϕ_i (with respect to the direction of incident particle). All quantities refer to the lab system and the summation goes over all secondary particles. For the collision of very high energy pions (such as 16.2 BeV) with nucleons, one can neglect $(E_0 - p_0)$ compared to M_{tg} ,

and obtain the following equation by combining the first two equations of Eq. 45.

$$M_{tg} = \sum (E_i - p_i \cos \theta_i). \quad (46)$$

The above equation has been used by many experimentalists (16,18,35,36,37) to represent the target mass in collisions of pions and protons with nucleons (as well as with nuclei). Since the energy of the incident particle does not appear in Eq. 46, it has also been applied for cosmic ray experiments (37,38,39,40) in which the energy of the incident particle is neither easily nor accurately measured. When the energy of the incident particle is known, Eq. 46 can be rewritten in a different form, involving ratios,

$$\begin{aligned} M_{tg} &= \frac{P_0}{\sum p_i \cos \theta_i} \{ \sum (E_i - p_i \cos \theta_i) \} \\ &= p_0 \{ \sum E_i / \sum p_i \cos \theta_i - 1 \}. \end{aligned} \quad (47)$$

The target mass for the events used in the present experiment have been calculated using Eq. 46, but before presenting the results, the assumption of the target being at rest needs to be explored.

If the target is one (or more) of the bound nucleons of an emulsion nucleus with a kinetic energy of T_{tg} , potential energy of U_{tg} , and momentum p_{tg} making an angle θ_{tg} with the incident pion, then the energy and mo-

mentum conservation equations become

$$E_0 + M_{tg} + T_{tg} - U_{tg} = \sum E_i,$$

$$p_0 + p_{tg} \cos \theta_{tg} = \sum p_i \cos \theta_i, \quad (48)$$

where the summation is over all the secondary particles, but it obviously does not include the recoil nucleus since it has not been included in the left side of the equation. Here the small momentum transferred to the recoil nucleus, which is treated as a spectator in the reaction, has been neglected. Combining Eqs. 48, one gets

$$M_{tg} + T_{tg} - U_{tg} - p_{tg} \cos \theta_{tg} = \sum (E_i - p_i \cos \theta_i). \quad (49)$$

If one measures the momentum, energy, and angle of emission of the secondary particles of many pion-nucleus interactions, one can find the distribution of the quantity $\sum (E_i - p_i \cos \theta_i)$ over the events. From Eq. 49 such a distribution will have peaks at the values given by $(M_{tg} + T_{tg} - U_{tg})$ (since the average $\overline{p_{tg} \cos \theta_{tg}} = 0$ for unpolarized nuclei)⁽⁴¹⁾. Thus if the collision is with one, two, or more nucleons, distribution will show the peaks near the values of one, two, etc. nucleon masses.

In calculating the summation in Eq. 46 or 49, one encounters some experimental difficulties. First, there are neutral pions and neutrons among the secondary particles. Second, the momenta of some of the tracks cannot be measured. In order to use Eq. 46, it has been

necessary to assume that (1) the unmeasured particles in each event have the same average $(E-p \cos \theta)$ as the measured particles, (2) the number of neutral pions equals one half the number of charged pions, (3) for events having a multiplicity n_s and no proton track, the neutron has the same $E-p \cos \theta$ as the average of the protons for the events with multiplicity n_s-1 . On the third assumption the possibility of target mass being different for events with greatly different multiplicity has been considered. Although these assumptions seem rather crude for the case of an individual interaction, their application to a group of events seems reasonable so far as the peaks in the distribution are concerned. The distribution of M_{tg} , calculated from Eq. 46 in this fashion, is shown in Figure 19. In Figure 19a and 19b are given the distributions for all π^-p and all π^-n events. Both distributions have a pronounced peak at a value of one nucleon mass. Figure 19c gives the distribution for π^-p events with $n_s > 4$, and Figure 19d that of π^-n events with $n_s > 4$. For these distributions the peak is broader and has been shifted to slightly higher value of M_{tg} . However, they show that the target of the interaction is a single nucleon. This shift in the position of the peak is due to the effect on M_{tg} of assumptions (1) and (2), above, made in the calculation of M_{tg} , which tend to overestimate

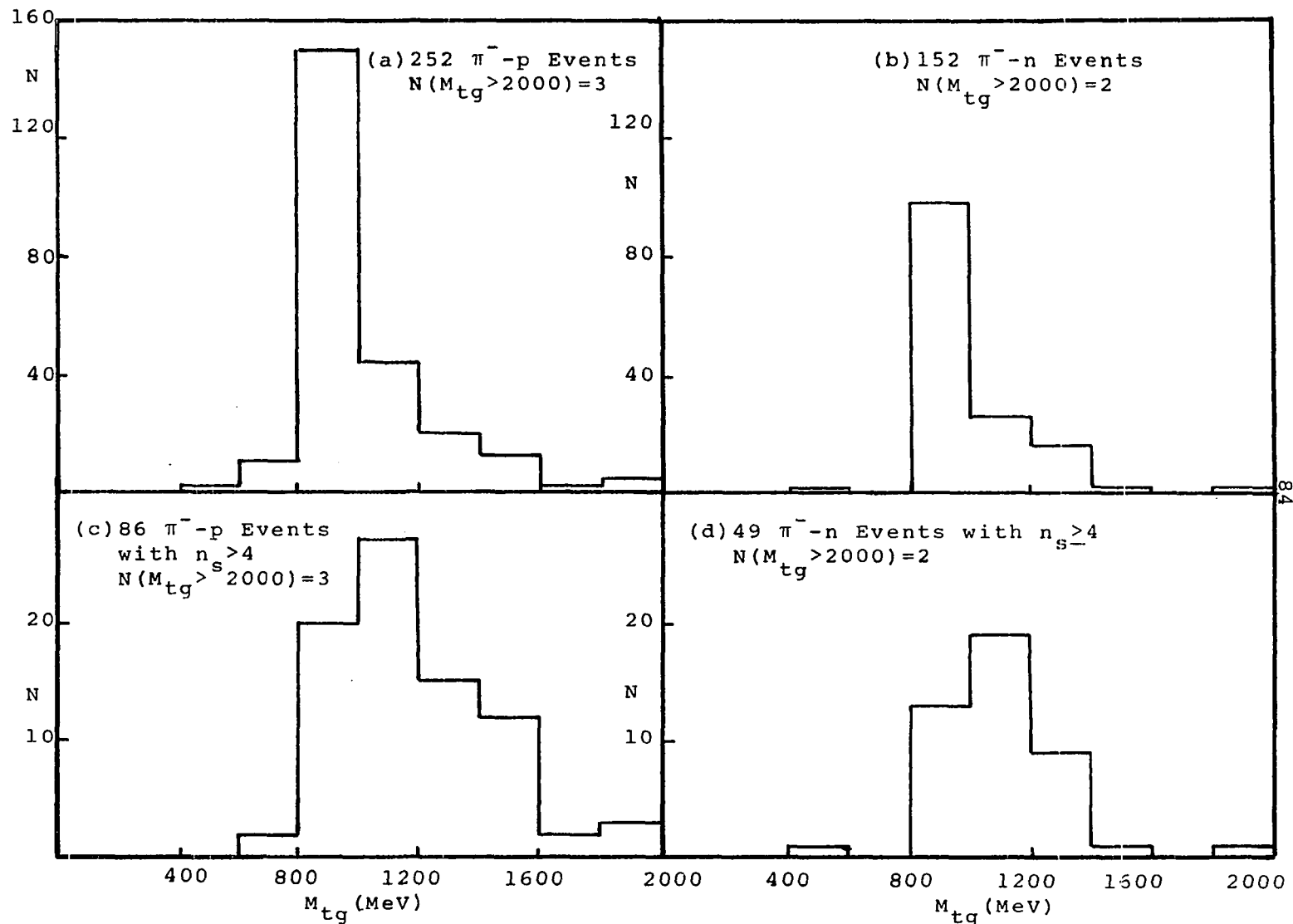


Fig. 19 Target Mass Distributions

M_{tg} for events with high multiplicity. The results of Figure 19 show that the events used in this experiment are indeed interactions with a single nucleon as had been intended by the precautions taken on the selection of the events.

b-Effective Target Mass

In the case of the target being a nucleon, and assumed to be at rest, one can define an effective target mass⁽⁴¹⁾ by leaving out the nucleon from the summation in the Eqs. 46 and 47. That is, the nucleon is being considered as a spectator to the interaction and this is in analogy with Eq. 49 in which the recoil nucleus, considered to be a spectator, was left out of the summation. As in Eq. 49, in which M_{tg} is the mass of that part of the nucleus (the few nucleons) which effectively participate in the interaction, in Eqs. 46 and 47, after leaving out the recoil nucleon, M_{tg} will correspond to the masses of those parts of the target nucleon which effectively participate in the reaction. Therefore the effective target mass, M_{eff} , can be calculated from the following equations

$$M_{eff} = \sum' (E_i - p_i \cos \theta_i), \quad (50)$$

$$\begin{aligned} M_{eff} &= \sum (E_i - p_i \cos \theta_i) - (E_N - p_N \cos \theta_N) \\ &= M_N - E_N + p_N \cos \theta_N, \end{aligned} \quad (51)$$

where \sum indicates sum over all the secondary pions, the subscript N in Eq. 51 refers to the recoil nucleon and the nucleon mass has been used for M_{tg} which is consistent with the results of Figure 19. Eq. 51 has been used for events with an identified and measured proton track, and Eq. 50 along with assumptions (1) and (2) made in calculation of M_{tg} has been used for other events.

The distribution of the effective target mass, calculated in this fashion, is shown in Figure 20. Here the data for π^- -p and π^- -n events have been combined for better statistics, the distribution for each group is very similar to the distributions of Figure 20. For events with low multiplicity, $n_s \leq 4$, the distribution has a pronounced peak at a low value of (50-100) MeV. The average value of M_{eff} is 138 ± 9 MeV, and 96% of the events have an effective target mass of less than $0.5 M_N$. For events with $n_s > 4$ the distribution seems to be rather smeared out over a range of a few hundred MeV. However, 94% of these events have an effective mass of less than $0.7 M_N$, and the average M_{eff} for this group of events is 328 ± 30 MeV. Some experimenters^(18,36) have found that the M_{eff} distribution for such events peaks near the pion mass, and, thus they have interpreted the interactions as peripheral collisions with the pionic cloud of the nucleon. The data of the present experiment does not support such an

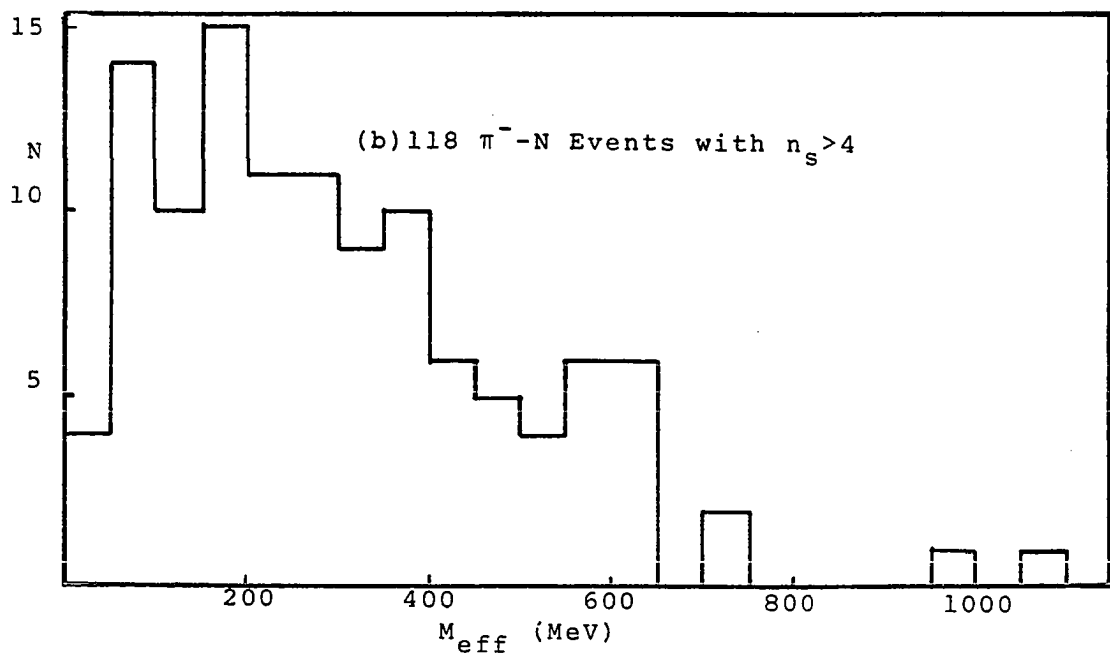
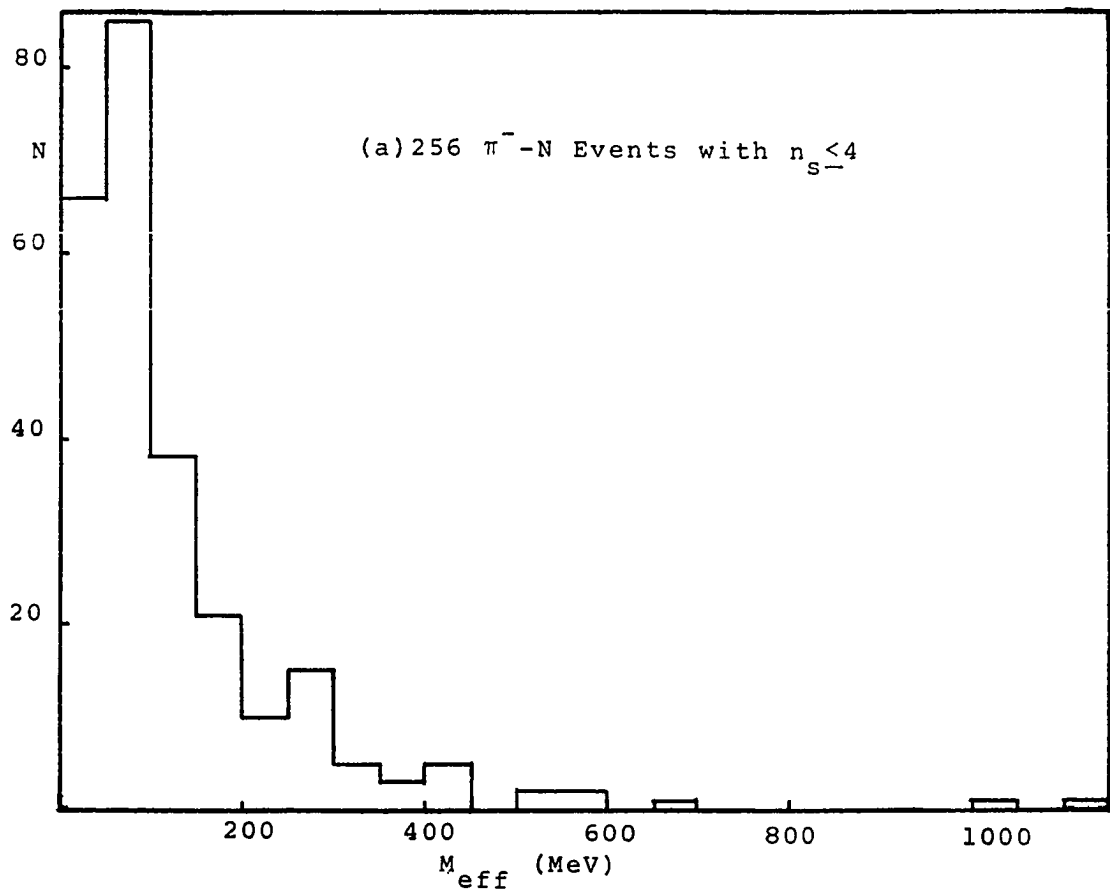


Fig. 20 Effective Target Mass Distributions

interpretation. It suggests, rather, that M_{eff} is different for different events. These results are in general agreement with the experimental results of Gainotti et al.,⁽⁴²⁾ and with the observations of Kaplon and Chen⁽⁴³⁾ who argue that the association of the nucleon effective mass with pion mass is model dependent (one-pion-exchange model) and since other (many-pion-exchange) models are conceivable, the magnitude of M_{eff} probably depends on, among other things, the dynamics of the interaction. In reference (44) the one-pion-exchange model has been applied to the analysis of effective target mass and it is shown that the distribution of M_{eff} depends on the properties of the target nucleon vertex. These authors⁽⁴⁴⁾ consider two exemplary cases, by choosing arbitrary values for the parameters of the target nucleon vertex. In one case they obtain a distribution peaked about one pion mass and in the second case a distribution smeared out between 0 to $0.7 M_N$.

Another method^(17,45) for finding M_{eff} , which has been extensively used, is to find the C.M. Lorentz factor, γ_C , using Castagnoli formula⁽⁴⁶⁾

$$\log \gamma_C = \langle \log \cot \theta \rangle, \quad (52)$$

where the average is taken over the shower particles.

Then using Eq. 4 of Chapter II, γ_C can be related to M_{eff} by the relation

$$\gamma_c = \frac{E_0 + M_{\text{eff}}}{m_\pi^2 + M_{\text{eff}}^2 + 2M_{\text{eff}}E_0}. \quad (53)$$

However, in deriving Castagnoli formula one has to assume that the shower particles are emitted with forward-backward symmetry in the C.M. system. The validity of this assumption cannot be ascertained for the case of pion-nucleon interactions. To the contrary, the measured pions in the present experiment show a marked forward-backward asymmetry in the C.M. system as was shown in Figures 11, 12, and 13. Therefore, the data of this experiment will not be analyzed by the use of the Castagnoli formula.

c-Dependence of Effective Target Mass on Multiplicity

The marked difference between the two distributions of Figure 20, for the two groups of events with $n_s \leq 4$ and $n_s > 4$, encourages one to make a closer examination of the dependence of M_{eff} on n_s . In order to find $\langle M_{\text{eff}} \rangle$ for groups of events with different n_s , Eq. 47 with the summation taken over all the secondary pions can be used. Using \sum' to indicate summation over secondary pions Eq. 47 becomes

$$M_{\text{eff}} = p_0 \left\{ \frac{\sum' E_i}{\sum' p_i \cos \theta_i} - 1 \right\}. \quad (54)$$

Now, if one makes the assumption that M_{eff} , and hence the ratio of the sums in Eq. 54, is a constant for the events

with the same n_s , then $\langle M_{\text{eff}} \rangle$ for that group of events can be found by extending the sums over all the secondary pions of all the events of that group⁽⁴⁷⁾. Furthermore, upon assuming that the neutral pions and the unmeasured charged pions have energy and angle distributions such that the ratio of the sums will be unaffected if the sums are taken over the measured pions only, then M_{eff} can be calculated from Eq. 54 using the measured data. The advantage of using Eq. 54 instead of Eq. 50 is that here one does not have to assume that $n_{\pi^0} = \frac{1}{2}n_s$. This assumption has been questioned by some observers, and in some experiments^(20,48) it has been reported that the ratio of the number of neutral to charged pions depends on n_s and is different than $\frac{1}{2}$.

The results of calculations of $\langle M_{\text{eff}} \rangle$ in the manner described above are shown in Table 5. Here, π^- -p and π^- -n events have been combined and grouped according to the number of charged secondary pions. Also, the target mass, M_{tg} , for each group has been calculated, using this method by including the recoil protons in the sums (Eq. 54) and using factors to allow for the ratios of the number of the measured recoil protons to the total number of secondary nucleons and the number of measured pions to the total number of secondary pions. M_{tg} has been calculated in order to check the validity of this

TABLE 5

n_s	M_{eff} (MeV)	M_{tg} (MeV)
2	174 \pm 39	1185 \pm 72
3	116 \pm 6	877 \pm 38
4	167 \pm 9	902 \pm 45
5	281 \pm 13	961 \pm 46
6	402 \pm 19	1065 \pm 49
7, 8	398 \pm 24	979 \pm 51
≥ 9	540 \pm 35	1179 \pm 71

method of calculating M_{eff} . The last column of Table 5 shows that all groups of events are consistent with having a single nucleon target, and more importantly there is no appreciable dependence of M_{tg} on n_s . However, M_{eff} is larger for events with higher multiplicity. Since M_{eff} is an average over events, its rather large value for events with high n_s indicates that many of these events may have an effective mass close to the nucleon mass, i. e., the entire nucleon is effectively participating in the reaction.

Many investigators^(49,50) have used the constancy of the average transverse momentum to determine momenta for tracks whose momenta could not be measured directly. The above calculations were repeated with inclusion of the tracks with unmeasured momenta, using for each un-

measured track the proper average transverse momentum for the corresponding angular interval and n_s (Table 4). The results of these calculations yielded higher values of M_{eff} , and corresponding values of M_{tg} are not consistent with one nucleon mass which is in contradiction to the results of the previous section (Figure 19). This can be explained by the fact that assigning the value of $\langle p_t \rangle$ of the measured tracks to the unmeasured tracks with large angles of emission, yields large values of momenta for such tracks. These large values of momenta may exceed the kinematical limits of the momenta corresponding to the angles of emission. To obtain the kinematical limits the calculations of Chapter II were repeated for the case of a pion (instead of a nucleon). It was observed that the assignment of $\langle p_t \rangle$ of the measured tracks to the unmeasured ones, in many cases does, indeed, violate these kinematical limitations.

5. Complete Events

a-Missing Mass

Most of the difficulties and uncertainties in the calculation of effective target mass arise from the fact that kinematical data on the events is incomplete due to the existence of neutral particles and the fact that the momenta of some of the tracks could not be measured. This has motivated a search for complete inelastic events; i.e.,

events that data on all of the secondary particles can somehow be determined. These events, for obvious reasons, cannot have more than one neutral particle. As a first technique the missing mass, M_M , for all events having zero or one unmeasured track were calculated using the following equations,

$$M_M^2 = E_M^2 - p_M^2, \quad (55)$$

$$E_M = E_0 + M_N - \sum E_i, \quad (56)$$

$$\vec{p}_M = \vec{p}_0 - \sum \vec{p}_i \quad (57)$$

where the summations are over all the measured tracks. An examination of Eq. 55 shows that for the case of the missing particle being a high energy (~ 1 BeV) π^0 , a small error of 1½% in E_M may introduce a 100% error in M_M , which makes the identification of the missing particle impossible. Considering that the errors in the momenta of the measured pions in this experiment have a range of 5%-50%, one cannot expect to obtain any information from the missing mass analysis*. The values of M_M^2 calculated for the selected group of events of the present experiment ranged from -5 to 29 BeV², and hence the missing mass technique was abandoned.

*That is to say for an individual event. When large statistics are available the missing mass distribution would be peaked at values of M_π or M_N , and the errors would only contribute to the width of the distribution.

b-Kinematical Fitting

From the above analysis it is learned that to successfully find the missing mass, or to identify complete events, the errors in the quantities used in the calculations must be very small. Although the errors in the momenta of the measured pions are large, the errors in angle measurements and proton momenta are satisfactorily small. Therefore, in some cases, by eliminating the momenta of the pions using kinematical relations, one can use the proton momentum and the measured angles to check whether an event is consistent with being a complete π^- -N interaction. Using the energy-momentum conservation equations, one can express the proton momentum in terms of the angles only. Then using the measured values of the angles one can calculate the proton momentum and check against its measured value. Since there are four equations (energy and momentum conservation) one can express proton momentum in terms of the angles for events with a maximum of three pion tracks and no neutral pions. For the case that a π^0 is present (which means three of the kinematical quantities are unknown) there is only one equation left after elimination of the missing quantities. For events with one pion track and a π^0 , after elimination of the three unknown kinematical quantities, the pion-track momentum can be expressed in terms of the proton momentum and the angles. Then the pion-track momen-

tum can be calculated from the proton momentum and the angles and checked against its measured value. Thus, three types of events were checked: (a) events with one pion track and a proton track for the presence of one π^0 , (b) events with two pion tracks and a proton track and (c) events with three pion tracks and a proton track, for the condition of no particles missing. The equations used for this analysis are given in Appendix B.

A total of three events of type (a), one event of type (b) and five events of type (c) were found to be consistent with the requirements of being complete events. These events are described in Table 6. For these events the momentum of the pion for type (a) and the proton for types (b) and (c) as calculated by the method described above, lies within the experimental error of the measured values. For these events the target mass is one nucleon mass, since they are consistent with being complete events of a collision of the incident pion with a nucleon at rest. Therefore, for these events Eq. 51 can be easily used in order to find the effective target mass. M_{eff} for each of these events is given in the last column of Table 6. It is observed that M_{eff} is smaller for events of type (a) and (b), which have two secondary pions, than events of type (c), which have three secondary pions. However, since M_{eff} varies between 40 to 340

TABLE 6

Type	Evt. #	P (MeV) Calc.	P (MeV) Meas.	M_{eff} (MeV)
	310370	5764	5247 \pm 1094	70 \pm 1
a	400042	15564	12213 \pm 3489	40 \pm 2
	400352	14290	11332 \pm 2981	60 \pm 2
b	370068	162	159 \pm 2	73 \pm 1
	240466	389	426 \pm 5	330 \pm 2
	330267	364	300 \pm 80	204 \pm 42
c	400252	163	157 \pm 2	80 \pm 1
	461945	479	423 \pm 70	72 \pm 2
	690014	598	587 \pm 50	341 \pm 17

MeV it is not possible to interpret M_{eff} as a constant of the interaction or to associate it with any physical mass. In order to explore this point further it is necessary to examine the expression for M_{eff} , Eq. 50. Here the recoil nucleon was excluded from the summation, and this was in analogy with the case of collision with one or a few nucleons of a nucleus, where the recoil nucleus is neglected. However, no account was taken of the motion or the binding of the effective target, which would be the analogue of the momentum and potential energy of the nucleons inside the nucleus. Upon fully extending the analogy, and denoting the mass, kinetic and potential energies, momentum and angle of the effective target by

$M_{\text{eff } tg'}$, $T_{\text{eff } tg'}$, $U_{\text{eff } tg'}$, $P_{\text{eff } tg'}$, $\theta_{\text{eff } tg'}$, respectively, then M_{eff} will be given by the following equation, which is the analogue of Eq. 49.

$$M_{\text{eff}} = M_{\text{eff } tg'} + T_{\text{eff } tg'} - U_{\text{eff } tg'} - P_{\text{eff } tg'} \cos \theta_{\text{eff } tg'} \quad (58)$$

From this equation it is clear that M_{eff} cannot be associated with any physical mass, even in the case that $M_{\text{eff } tg}$ is a physical mass. The fact that M_{eff} is not the same for all the events is easily explained by its dependence on $P_{\text{eff } tg}$ and $\theta_{\text{eff } tg}$ which vary from event to event even if $M_{\text{eff } tg}$ were the same. However, when the distribution of M_{eff} over many events is considered in analogy with collisions with nuclei, one expects the distribution to have peaks at the values of $M_{\text{eff } tg'}$ and one expects the peaks to have a width of $\overline{T_{\text{eff } tg'} - U_{\text{eff } tg'}}$, since this quantity can be different for each event. But since $\overline{T_{\text{eff } tg'} - U_{\text{eff } tg'}}$ could be as large (or even much larger than) $M_{\text{eff } tg'}$, the peaks may be so wide that the M_{eff} distribution could appear broad with no apparent peaks.

6. Search for Resonances

High energy interactions have been observed to be accompanied by the production of resonances or particles with a life-time of the order to 10^{-23} sec. (51).

Due to the fast decay of these particles, their identifi-

cation and detection in any process is possible only by a kinematical correlation of the secondary particles. If a number of secondary particles of an interaction are the decay products of a resonant particle, there must exist a kinematical correlation between these particles: the sum of their energies and the sum of their momenta must be equal, respectively, to the energy and momentum of the parent resonant particle, and hence the difference of the squares of these two sums must be the square of the mass of the resonant particle. Using the previous notation, one can write,

$$M_{1,2,3,\dots,m}^2 = \left(\sum_{i=1}^m E_i \right)^2 - \left(\sum_{i=1}^m \vec{p}_i \right)^2, \quad (59)$$

where $M_{1,2,3,\dots,m}$ is called the invariant mass of the m -particle system and is equal to the mass of the resonant particle in the case that the m -particles are its decay products. For a non-resonant interaction with n secondary particles the distribution of any m -particle invariant mass is given by its phase space curve⁽⁵²⁾. If a resonance is produced in the process, then the invariant-mass distribution will show, in addition to the phase space, a peak at the value of the mass of the resonant particle.

For each of the pion-nucleon events measured in this experiment all the possible combinations of the mea-

sured secondary particles have been taken in order to calculate four groups of invariant masses: (1) two-pions, (2) three-pions, (3) pion-proton, (4) pion-pion-proton. The four invariant mass distributions are shown in Figures 21 and 22. These distributions involve events with different numbers of secondary particles (from 3 to 16) and hence the phase space curves for them are not available. In fact phase space calculations get so complicated for large number of secondary particles that no one has obtained the phase space for the cases of more than six particle final states. However, upon general considerations⁽⁵³⁾ one expects the phase space to have a smooth distribution with one maximum at a low value the order of a few times the minimum value of the invariant mass. Any additional peaks can be attributed to the existence of resonant particles. The two distributions of Figure 21 do not show such peaks, which indicates the relative absence of pion resonances in the interactions examined. However, the distributions in Figure 22 show peaks which one might attribute to resonances. The pion-proton invariant mass distribution shows four peaks whose heights are more than one standard error ($\sim\sqrt{N}$) over the background height. When this distribution is plotted using 100 MeV intervals for the invariant mass the height of the four peaks are still more than one standard error above the

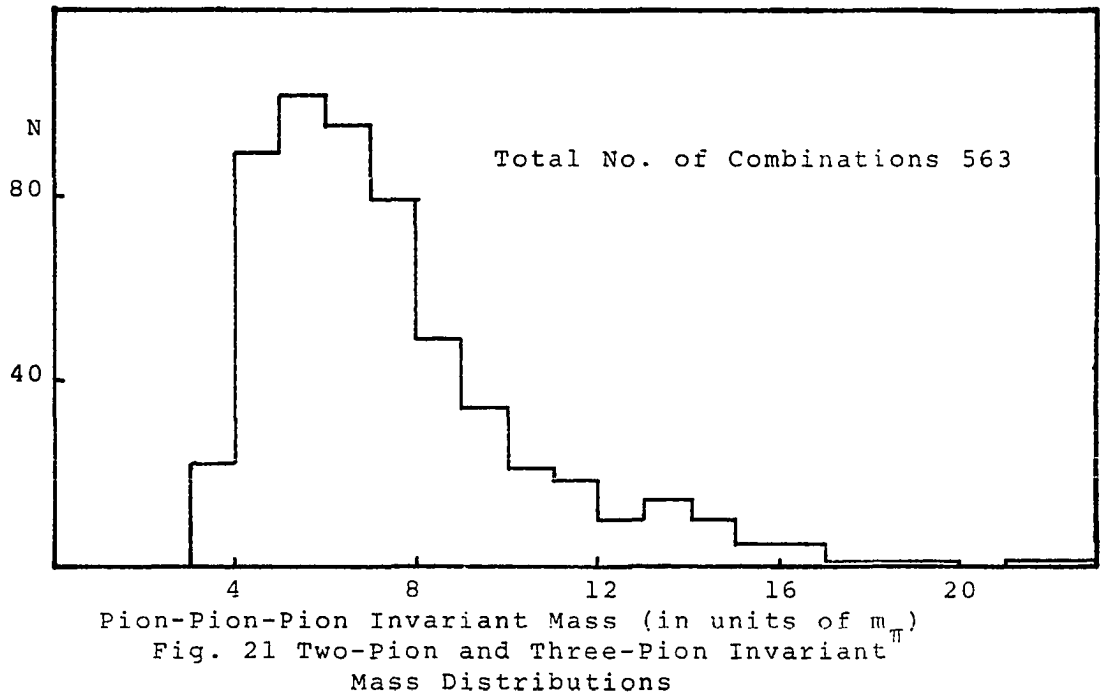
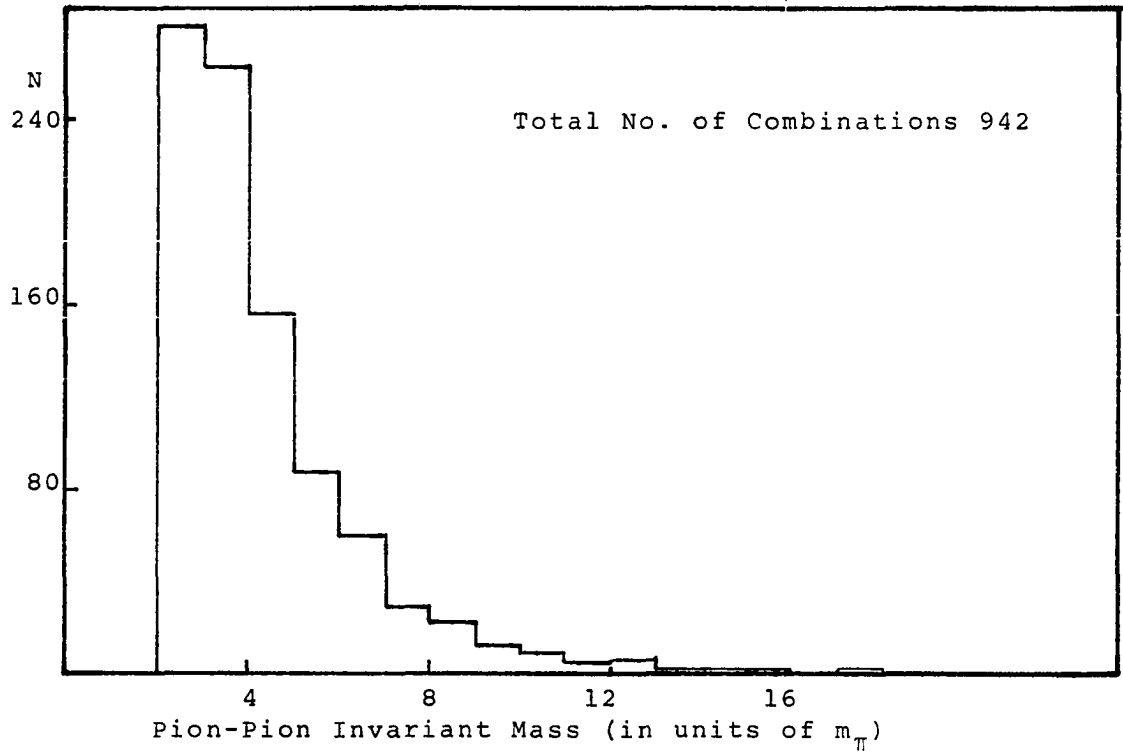


Fig. 21 Two-Pion and Three-Pion Invariant Mass Distributions

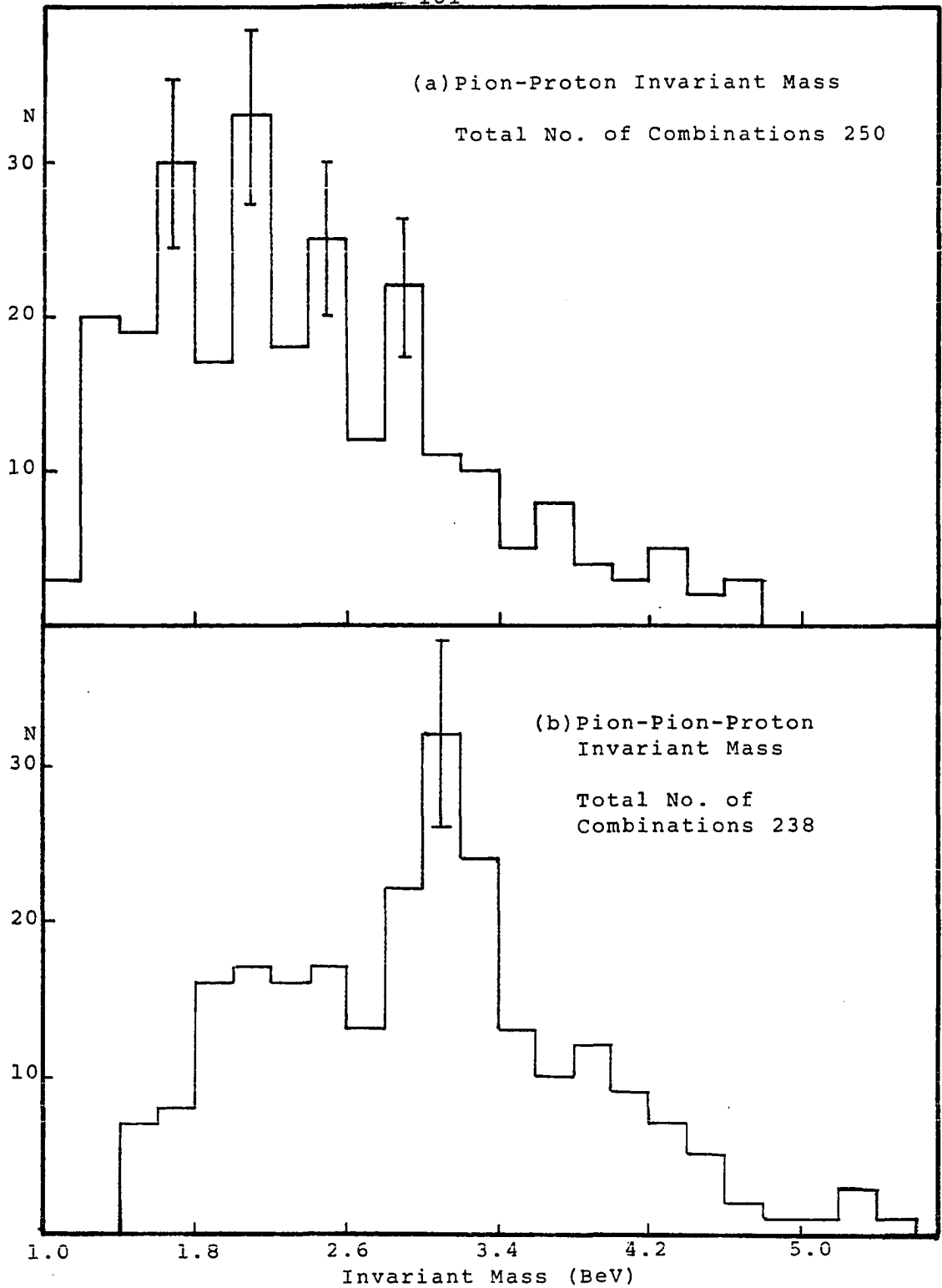


Fig. 22 Pion-Proton and Pion-Pion-Proton Invariant Mass Distributions

background height. The values of the invariant mass at these peaks are 1700, 2100, 2500, and 2900 MeV, all having a width of less than 200 MeV. The cross sections for these resonances are calculated from the estimated number of events which comprise each peak. This number is given by the number of events involved in the entire 250 combinations multiplied by the fraction of the combinations comprising the resonance peak. From this number one calculates the mean free path (using the total length of track scanned) and in turn the cross section. The cross sections for these four peaks (in mb) are $1.0 \pm .3$, $1.4 \pm .4$, $1.2 \pm .3$, $0.9 \pm .3$, respectively. These four peaks have the right mass and width, decay mode (pion, proton), cross section, and probable isotopic spin to match the four known resonances $N(1710)$, $N(2080)$, $\Delta(2420)$, and $\Delta(2850)$ respectively. Data on these and other resonances can be found in reference (54). The pion-pion-proton invariant mass distribution shows a peak with a height of more than twice the standard error over the background height. The invariant mass at this peak (when this distribution is plotted using 300 MeV intervals for the invariant mass the height of the peak is still more than two standard errors above the background height) has a value of 3100 MeV with a width of less than 600 MeV. This peak might be interpreted as the observation of some

charged state of the known resonance $N(3030)$ which has been observed by Citron et al⁽⁵⁵⁾ in the total πp cross section curve. This peak is not observed in the pion-proton invariant mass distribution, however, this is consistent with the interpretation of the peak in the pion-pion-proton invariant mass distribution as the charged state of $N(3030)$. This is because the πN decay modes of $N^\pm(3030)$, and likewise the $\pi\pi N$ decay modes of $N^0(3030)$, are not observables. However, with the interpretation of this peak as $N^\pm(3030)$, one might expect its production to be accompanied with $N^0(3030)$ production which implies the existence of the corresponding peak in pion-proton invariant mass distribution. The absence of this peak in the pion-proton invariant mass distribution allows the possibility of interpreting the peak in the pion-pion-proton invariant mass distribution as a new resonance, $N(3100)$. Due to the very low statistics the determination of most of the properties of this resonance cannot be meaningfully carried out. However, one can attempt to find the partial decay modes for this resonance by inspecting the invariant mass distributions of the decay products of this resonance. In order to do this one must consider all the particles which are involved in the combinations which fall under the peak of the $M_{\pi\pi p}$ distribution; i.e., the 78 combinations with $2800 < M_{\pi\pi p} < 3400$ MeV. About half of these

combinations are due to the resonance and the other half due to the background. Now, in order to inspect the decay products of this resonance, the pion-pion and the pion-proton invariant mass distributions for these 78 combinations are plotted (this yields 78 π - π and 156 π -p invariant masses since for each $M_{\pi\pi p}$ can have one π - π and two π -p combinations). These distributions are shown in Figure 23. Here the $M_{\pi\pi}$ distribution, Figure 23a, does not show any structure other than an expected phase space which indicates that the decay modes of N(3100) do not involve any π - π resonance. But the $M_{\pi p}$ distribution, Figure 23b (solid line), shows peaks in addition to the phase space. To analyze this distribution as regards the decay modes of N(3100) one must first subtract about half of the $M_{\pi p}$'s corresponding to the background which is contained in the 78 $M_{\pi\pi p}$ combinations. To do this the $M_{\pi p}$ distribution for 39 of the $M_{\pi\pi p}$ combinations falling in the adjacent intervals to the peak of $M_{\pi\pi p}$ distribution has been obtained and subtracted from the histogram of Figure 23b. The resulting histogram which will correspond to the decay products of N(3100) only is shown by the dashed lines. One might interpret this histogram as having two peaks at 1500 and 2900 MeV, in addition to the phase space distribution. These peaks correspond to the N(1518) and Δ (2950) resonances respectively. From the

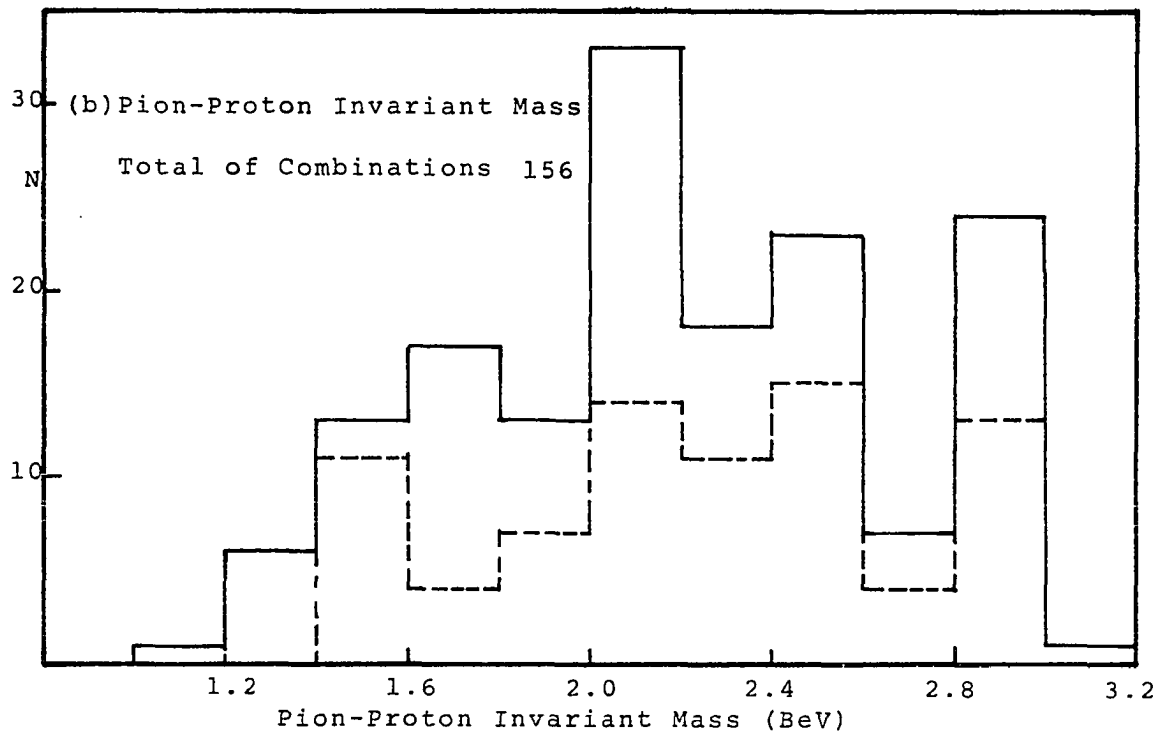
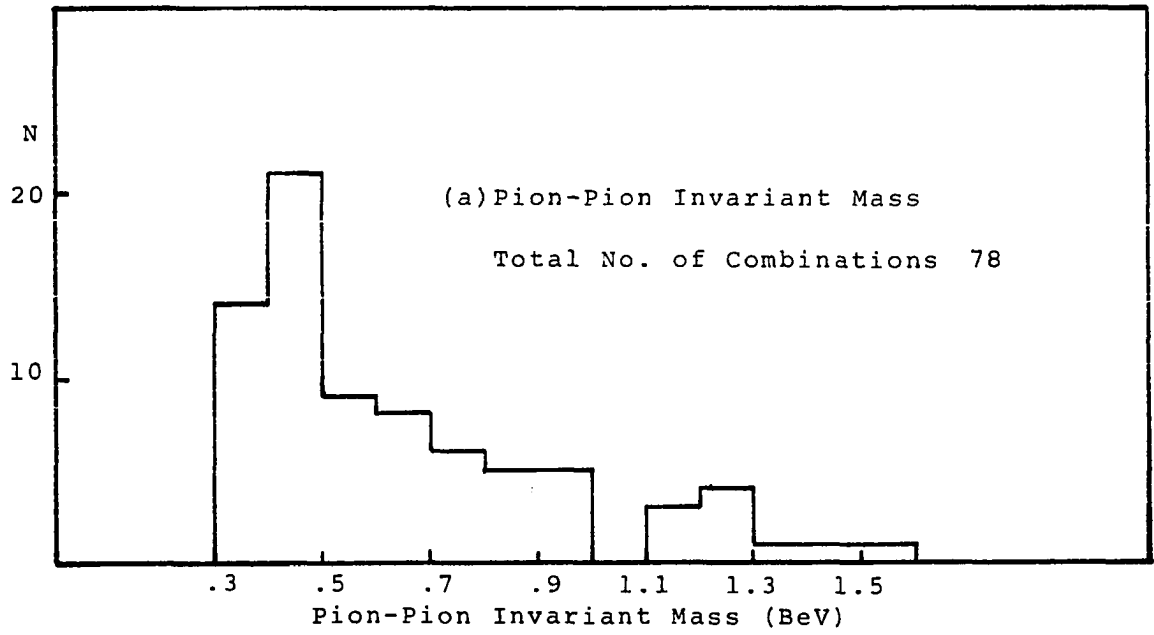


Fig. 23 Invariant Mass Distributions for Combinations with $2800 < M_{\pi\pi p} < 3400$ MeV

ratio of the number of the combinations which comprise these peaks to the number of the combinations which make the background phase space, the partial decay modes for the N(3100) resonance is calculated as follows:

$$\begin{array}{rcl}
 \text{N(3100)} & \rightarrow & \text{N(1518)} + \pi & (10 \pm 3)\% \\
 & & \Delta(2850) + \pi & (11 \pm 4)\% \\
 & & p + \pi + \pi & (79 \pm 10)\%
 \end{array}$$

The cross section for this resonance, N(3100), is 3.3 ± 0.6 mb which was calculated in the manner described before.

Other properties of this resonance cannot be calculated from the data of this experiment.

CHAPTER V

SUMMARY AND CONCLUSIONS

The cross sections for the pion-proton reactions measured in this experiment are 2.9 ± 1.8 , 24.2 ± 2.3 , and $.8 \pm .4$ mb for elastic, inelastic, and charge exchange processes respectively. These results agree with other reported cross sections for these reactions at 16 BeV⁽¹¹⁾. Figure 19 shows that the events analyzed in this experiment are all interactions of the incident pion with a single nucleon of the emulsion nuclei. The mean free path for such collisions is estimated to be $3.2 \pm .2$ meters.

The secondary charged-pion multiplicity distribution for the π^- -p events is in very good agreement with the multiplicity distribution functions suggested by Wang⁽¹²⁾. These multiplicity distribution functions are constructed from the combination of Poisson probability functions with the charge and baryon number conservations incorporated. It is also assumed that neutral pion production is independent of charged pion production,

and that the charged pions are produced in pairs in small regions or "cells" inside the nucleon. The agreement between the present experiment and these multiplicity distribution functions supports the idea of the existence of a number of regions or "cells" inside the nucleon. From Figure 7a it is seen that $46 \pm 5\%$ of the inelastic π^- -p collisions have an outgoing proton and $54 \pm 6\%$ have an outgoing neutron. This indicates that in π^- -p interactions there is equal probability for the outgoing nucleon to be a proton or a neutron. For π^- -n collisions (Figure 7b) however, only $27 \pm 5\%$ of the events have an outgoing proton. This discrepancy is partly due to the experimental inaccuracies such as mistaking the proton tracks for pion tracks, and the fact that π^- -n events are more likely to be collisions with a nucleus than π^- -p events. However this low proportion of secondary protons, 27%, can be mostly attributed to the existence of the huge peak in Figure 7a, events with a secondary neutron and three charged secondary pions. In order to explain this peak by a multiplicity distribution function one has to take into account the possibility of peripheral interactions at low multiplicities, and hence consider g-parity⁽⁵⁶⁾ conservation for the pions in addition to charge and baryon number conservation. The g-parity conservation requires that in a meson-meson inter-

action (likewise in the meson vertex of the peripheral interaction of pions with nucleons) the product of the g-parity of incoming mesons must be equal to that of the outgoing mesons.

The average transverse momentum of the measured secondary charged pions, $\langle p_t \rangle$, in this experiment is 315 ± 25 , 276 ± 4 , and 301 ± 5 MeV for elastic π^- -p, inelastic π^- -p, and π^- -n events, respectively. These figures are in good agreement with most of the previous observations (20) carried out at different incident energies, and indicate the constancy of $\langle p_t \rangle$ over a wide range of incident energy. The distributions of the transverse momenta, Figures 14 and 15, are better fitted by a linear exponential function than by the Boltzmann distribution function. The poor fit of the Boltzmann distribution function indicates that for the pion-nucleon interactions the C.M. axial symmetry may not hold and p_x and p_y may not be independent of each other. The one parameter of the linear exponential function, which gives the best fit, is $1/a = 135 \pm 5$ MeV. Despite the rather good visual fit of the distributions by the linear exponential function, a Chi-square goodness of fit test yielded a very low confidence level for this fit, and a much lower confidence level for the Boltzmann distribution function. In reference 57 the transverse momentum distributions of secondary pions from

pion-nucleus interactions and the data of this experiment have been fitted with many other distribution functions, and it is found that none of them give a better fit than the linear exponential distribution function. The overall $\langle p_t \rangle$ of the measured pions is found to be independent of the pion multiplicity. However, for secondary pions in the $0-5^\circ$ angular interval $\langle p_t \rangle$ appears to depend on the multiplicity, n_s , shown in the third column of Table 4. This dependence can be approximated by an empirical formula of the general form:

$$\langle p_t \rangle = Ae^{-\alpha \langle n_s \rangle} \quad (60)$$

where A, and α are constants and $\langle n_s \rangle$ is the average charged-pion multiplicity for each group of events. The values of $\langle p_t \rangle$ for the $0-5^\circ$ angular interval of the π^- -p interactions are reproduced by Eq. 60 with a choice of $A = 240$ MeV, and $\alpha = .055$. This choice of constants also gives the correct value for the overall $\langle p_t \rangle$ of all the π^- -p events ($\langle n_s \rangle = 4$). The dependence of $\langle p_t \rangle$ on the lab angle of emission, θ , is found to be in general agreement with previous observations (slight increase of $\langle p_t \rangle$ with θ), but due to very low statistics at large angles no conclusions can be obtained on this dependence. However, on the dependence of $\langle p_t \rangle$ on C.M. angle of emission, Figure 18 suggests a symmetry about 90° with the maximum of $\langle p_t \rangle$ occurring at this angle.

The C.M. angular distribution of the measured secondary pions shows an extreme forward peaking, and the degree of this asymmetry depends on the pion multiplicity. The C.M. angular distribution becomes more symmetric with increasing multiplicity. The target mass distributions in Figure 19 indicate that the events analyzed in this experiment satisfy the criterion for being interactions of incident pions with single nucleons. Furthermore they show that the formulae developed by Birger and Smorodin⁽³⁴⁾ provide an excellent method for the determination of the target mass. The concept of effective target mass, defined for the collision with a single nucleon, in analogy to collisions with nuclei, by neglecting the recoil nucleon, is found to be useful in the analysis of the interactions. The distributions of the effective target mass; M_{eff} , for the two groups of events with $n_s \leq 4$ and $n_s > 4$, Figure 20, show a marked difference. The events with low multiplicity show a large peak at a low value of about 75 MeV for M_{eff} , whereas the M_{eff} for the high multiplicity events has a rather broad distribution. The average value of M_{eff} is 138 ± 9 MeV for the low multiplicity and 328 ± 30 MeV for the high multiplicity events. These differences between the two groups of events suggest the possibility that a different mechanism might be responsible for the interactions with

high multiplicity than that for the interactions with low multiplicity. Table 5 shows a rather steady increase of $\langle M_{\text{eff}} \rangle$ with n_s . The large values of $\langle M_{\text{eff}} \rangle$ indicate that for the interactions with high multiplicity the nucleon is more effectively participating in the interaction. Based on the results of Table 5 and Figures 12 and 13 it is observed that central collisions, which could be characterized by a symmetric C.M. angular distribution of the secondary pions and a large value of the effective target mass of the interaction, become dominant for the interactions with a high pion multiplicity. For interactions with low pion multiplicity peripheral collisions, which may be characterized by an asymmetric (with a forward peak) C.M. angular distribution of the secondary pions and a low value of the effective target mass, may be predominant. From the percentage of the symmetric part of the C.M. angular distributions, Eq. 43, and Figure 11, it is concluded that $30 \pm 2\%$ of the inelastic pion-nucleon interactions of the present experiment can be considered as central collisions. This is in good agreement with the observed result of 25 - 30% at 10 BeV/c⁽¹⁹⁾.

From a comparison of Figures 11a and 11b, and Figures 12 and 13, and Figures 14 and 15, and Figures 16 and 17 one can observe the close similarity between the characteristics of the pion-proton and the pion-neutron

interactions examined here. This similarity is so close that for each distribution the resultant distribution obtained by combining the π -p and the π -n events is not appreciably different from the distributions for the separate groups. Due to the indistinguishability of positive and negative pions in emulsion, a comparison between the characteristics of different charge states for pions cannot be carried out. However the similarity of the results obtained for M_{eff} by the two Eqs. 50 and 54 (in using Eq. 50 symmetry of neutral and charged pions is assumed but not in Eq. 54) is consistent with the symmetry of the neutral and charged pions, and with average neutral pion multiplicity being one-half that of the charged pions.

From the study of the invariant mass distributions, Figures 21 and 22, it is inferred that inelastic pion-nucleon interactions at 16.2 BeV are accompanied by baryon resonance production processes. About 15 - 20% of the interactions examined in this experiment proceed via the production of a baryon resonance. The production of meson resonances could not be detected by the invariant mass distributions. This can be attributed to the fact that since mass of most of the known meson resonances fall in the range of background peak of the invariant mass distributions, Figure 21, it is not possible to identify the resonance peaks without a knowledge of

the absolute height of the background.

The peak of π - π -p invariant mass distribution at 3100 MeV might be interpreted as the charged state of the known resonance N(3030), which had previously been observed in π^\pm -p scattering cross sections⁽⁵⁵⁾, or as a new resonance. The large value of 600 MeV of the width of this peak yields a life time of $\sim 10^{-24}$ sec for this resonant particle. Although the statistics of this experiment are not enough to establish this resonant particle, its partial decay modes have been estimated and its production cross section has been calculated to be $3.3 \pm .6$ mb.

As all other similar experiments carried out in nuclear emulsion, this experiment suffers from low statistics compared to the similar experiments carried out in bubble chambers. However, the amount of data used in the present experiment is more than that used in most of the previous experiments in emulsion. Multiple Coulomb scattering measurements have the highest error in this experiment. The development of the new formalism for the noise eliminations, Appendix A, has been aimed at reducing this error. The angle measurements in this experiment, and in emulsion in general, have been very accurate with relative error generally less than $\frac{1}{2}\%$.

APPENDIX A

NOISE ELIMINATION IN MULTIPLE COULOMB SCATTERING

The following is a derivation of Eq. 34 used in Chapter III. Since the idea used here is based on the noise elimination technique developed by Barkas, his notations will be used throughout the derivation.

Each measured value y_k can be written as the sum of a true value y_k^t and a noise term δ_k (which lumps together all erroneous effects). Then the k th second difference is given by

$$D_k = (y_{k+2} - y_{k+1}) - (y_{k+1} - y_k) = (y_k^t - 2y_{k+1}^t + y_{k+2}^t) + (\delta_k - 2\delta_{k+1} + \delta_{k+2}) \quad (\text{A-1})$$

where y_k^t and δ_ℓ^t are statistically independent variables for all k and ℓ . Writing $D_k^t = y_k^t - 2y_{k+1}^t + y_{k+2}^t$, then in

Barkas' notation $\Delta_t^2 = \langle (D_k^t)^2 \rangle$ is the mean square noise-corrected second difference and $D_k^t = \psi_{k+1} + \psi_k + x_{k+1} - x_k$,

where he shows the following to hold true for ψ_k and x_k :

$$\begin{aligned} \langle \psi_k \rangle &= \langle x_k \rangle = 0 \\ \langle x_k \psi_\ell \rangle &= \langle x_k \delta_\ell \rangle = \langle \psi_k \delta_\ell \rangle = 0 \text{ for all } k \text{ and } \ell \\ \langle \psi_k \psi_\ell \rangle &= \langle x_k x_\ell \rangle = 0 \text{ for } k \neq \ell \\ \langle \psi_k^2 \rangle &= 3 \langle x_k^2 \rangle = 3/8 \Delta_t^2. \end{aligned} \quad (\text{A-2})$$

In this notation for the measured second difference, D_k , one obtains

$$D_k = \psi_{k+1} + \psi_k + x_{k+1} - x_k + \delta_k - 2\delta_{k+1} + \delta_{k+2}, \quad (\text{A-3})$$

from which the average second difference products can be calculated with the use of Eq. A-2. One gets,

$$\langle D_k^2 \rangle = \Delta_t^2 + 6\langle \delta_k^2 \rangle - 8\langle \delta_k \delta_{k+1} \rangle + 2\langle \delta_k \delta_{k+2} \rangle, \quad (\text{A-4})$$

$$\langle D_k D_{k+1} \rangle = \frac{1}{4}\Delta_t^2 - 4\langle \delta_k^2 \rangle + 7\langle \delta_k \delta_{k+1} \rangle - 4\langle \delta_k \delta_{k+2} \rangle + \langle \delta_k \delta_{k+3} \rangle. \quad (\text{A-5})$$

Assuming that δ_k and δ_l are statistically independent variables ($\langle \delta_k \delta_l \rangle = \langle \delta_k \rangle \langle \delta_l \rangle = \langle \delta_k \rangle^2$) and also assuming that $\langle \delta_k \rangle = 0$, Barkas eliminates $\langle \delta_k^2 \rangle$ term between Eqs. A-4 and A-5 and obtains an equation for Δ_t^2 in terms of the measured average second difference products. Burwell⁽¹¹⁾ has given physical arguments on the possibilities of δ_k and δ_{k+1} not being independent and $\langle \delta_k \rangle \neq 0$. Then relaxing somewhat the assumptions made by Barkas, Burwell obtains a new equation for Δ_t^2 . Burwell has also suggested the possibility of further relaxation of the assumption.

In this work no assumption is made on the nature of noise, i.e.; in general $\langle \delta_k \rangle \neq 0$ and $\langle \delta_k \delta_{k+l} \rangle \neq \langle \delta_k \rangle \langle \delta_{k+l} \rangle$. An argument for relaxing of these assumptions is given below. Now, the higher order average second difference products are written using Eq. A-3 along with Eq. A-2.

$$\langle D_k D_{k+2} \rangle = \langle \delta_k^2 \rangle - 4\langle \delta_k \delta_{k+1} \rangle + 6\langle \delta_k \delta_{k+2} \rangle - 4\langle \delta_k \delta_{k+3} \rangle + \langle \delta_k \delta_{k+4} \rangle$$

$$\begin{aligned}
\langle D_k D_{k+3} \rangle &= \langle \delta_k \delta_{k+1} \rangle - 4 \langle \delta_k \delta_{k+2} \rangle + 6 \langle \delta_k \delta_{k+3} \rangle - 4 \langle \delta_k \delta_{k+4} \rangle + \langle \delta_k \delta_{k+5} \rangle \\
&\vdots \\
\langle D_k D_{k+l} \rangle &= \langle \delta_k \delta_{k+l-2} \rangle - 4 \langle \delta_k \delta_{k+l-1} \rangle + 6 \langle \delta_k \delta_{k+l} \rangle - 4 \langle \delta_k \delta_{k+l+1} \rangle \\
&\quad + \langle \delta_k \delta_{k+l+2} \rangle.
\end{aligned}
\tag{A-6}$$

From Eqs. A-6 it is seen that if one assumes $\langle \delta_k \delta_{k+l} \rangle = \langle \delta_k \rangle^2$ for $l \geq a$ (with a being any integer, $a \geq 1$) then, even without assuming $\langle \delta_k \rangle = 0$, one must have $\langle D_k D_{k+l} \rangle = 0$ for $l \geq a+2$. It was experimentally found, with the equipment used in this experiment, that $\langle D_k D_{k+l} \rangle \neq 0$ in general for all possible values of l . It was also found that $\langle D_k D_{k+l} \rangle$ values ($l \geq 2$), being comparable to the value of $\langle D_k D_{k+1} \rangle$, do not average to zero, nor do they fluctuate about zero. All this shows that in general $\langle D_k D_{k+l} \rangle$ is not zero which in turn violates the assumption that $\langle \delta_k \delta_{k+l} \rangle = \langle \delta_k \rangle^2$. This experimental evidence has been the motivation and the main argument for relaxing all of the assumptions made by Barkas. Therefore, in the following derivation we will retain all terms related to the noise (i.e. $\langle \delta_k \delta_{k+l} \rangle$, $l = 0, 1, 2, \dots$) and treat them as unknowns.

Now, the first $N+1$ (N is an arbitrary large number) equations of A-6 can be written in the matrix form

(except the first) in the first row will vanish. Also, since the diagonal terms of the determinant have values of one, after renaming the indices, the result will yield

$$\langle \delta_k \delta_{k+l} \rangle = \sum_{n=2}^{N-2-l} 1/6 (n^3 - n) \langle D_k D_{k+l+n} \rangle + \sum_{n=N-1}^{N+2} 1/6 (n^3 - n) x_n. \quad (\text{A-11})$$

Equation A-11 can now be used to write the $\langle \delta_k \delta_{k+l} \rangle$ terms in Eqs. A-4 and A-5 in terms of the mean second-difference products and the x's. After some simplification and algebraic manipulation Eqs. A-4 and A-5 respectively yield

$$\Delta_t^2 = \langle D_k^2 \rangle - 2 \sum_{n=1}^{N-2} (n^2 - 1) \langle D_k D_{k+n} \rangle - 2 \sum_{n=N-1}^{N+2} (n^2 - 1) x_n, \quad (\text{A-12})$$

$$\Delta_t^2 = 4 \sum_{n=1}^{N-2} n^2 \langle D_k D_{k+n} \rangle + 4 \sum_{n=N-1}^{N+2} n^2 x_n. \quad (\text{A-13})$$

If one uses the approximation $(N-1)^2 \approx N^2 \approx (N+1)^2 \approx (N+2)^2$ then it is possible to eliminate the x's between the above two equations. This is because the x's will then occur in

$\sum_{n=N-1}^{N+2} x_n$ form only which can be eliminated as a single unknown.

After eliminating x's one obtains a single equation giving Δ_t^2 in terms of the measured quantities

$\langle D_k D_{k+n} \rangle$:

$$\Delta_t^2 \approx 2/3 \left\{ \langle D_k^2 \rangle + 2 \sum_{n=1}^{N-2} \left(1 - \frac{n}{N}\right) \frac{1}{N^2} \langle D_k D_{k+n} \rangle \right\} / \left(1 - \frac{1}{3N^2}\right). \quad (\text{A-14})$$

The approximation used here is obviously valid if N is taken to be a sufficiently large number. However, N is limited by the number, N , of measured second differences, $N \leq N+1$, and N due to experimental impracticality could be as low as 10 for certain tracks. However, even in such cases, since the x_n terms are only a small contribution to Δ_t^2 (Eq. A-12 and A-13), the inaccuracy of the approximation on x_n 's should not make the final result for Δ_t^2 (Eq. A-14) unreliable. Allowing a minimum value of $N = 8$, $N = 9$, and assuming the x_n 's to be of the same order of magnitude as the $\langle D_k D_{k+n} \rangle$'s in Eq. A-13, then the error introduced in Δ_t^2 by the approximation $(N-1)^2 \approx N^2 \approx (N+1)^2 \approx (N+2)^2$ is estimated to be less than 10%. The expected error is, however, much less than the 10% which was estimated for the most adverse case.

Other Formulae

Other methods and formulae for noise elimination were tried which gave results less consistent than Eq. A-14. In the following pages these methods and formulae are briefly outlined:

1-Barkas' Equations: With the assumption of statistical independence of δ_k and δ_l for all values of $k \neq l$, and the assumption that $\langle \delta_k \rangle = 0$, all terms of the form $\langle \delta_k \delta_{k+l} \rangle$, for $l \neq 0$, drop out of the Eqs. A-4 and

A-5. Similar equations for the mean third difference products can also be written. By using any two of such equations, $\langle \delta_k^2 \rangle$ can be eliminated and an equation for Δ_t^2 in terms of mean second and third difference, D and T , products can be obtained. A few such equations which were tried in this experiment are the following:

$$\begin{aligned}\Delta_t^2 &= 8/11\{\langle D_k^2 \rangle + 3/2\langle D_k D_{k+1} \rangle\} \\ &= 4/11\{5\langle D_k^2 \rangle - 3/2\langle T_k^2 \rangle\} \\ &= \{\langle D_k^2 \rangle - 6\langle D_k D_{k+2} \rangle\}\end{aligned}$$

Burwell⁽¹¹⁾ has shown that these equations are not all independent.

2-Burwell's Equation: The error terms δ_k are expressed in terms of a new parameter θ_k through the relation $\theta_k = \frac{\delta_{k+1} - \delta_k}{t}$ and then it is assumed that $\langle \theta_k \theta_{k+l} \rangle = \langle \theta_k \rangle \langle \theta_{k+l} \rangle$ for $l \geq 2$. Using $\langle D_k D_{k+2} \rangle$ -equation along with equations A-4 and A-5 then the error terms are eliminated and one gets,

$$\Delta_t^2 = 2/3\{\langle D_k^2 \rangle + 2\{\langle D_k D_{k+1} \rangle + \langle D_k D_{k+2} \rangle\}\}. \quad (\text{A-16})$$

This equation can also be obtained directly from equations A-4, A-5, and first equation of A-6 by assuming $\langle \delta_k \delta_{k+l} \rangle = \langle \delta_k \rangle \langle \delta_{k+l} \rangle$ for $l \geq 1$, but $\langle \delta_k \rangle \neq 0$. Another equation for

Δ_t^2 which was also tried is obtained similarly by assuming $\langle \delta_k \delta_{k+l} \rangle = \langle \delta_k \rangle^2$ for $l \geq 2$, but $\langle \delta_k \rangle \neq 0$. This gives

$$\Delta_t^2 = 2/3 \{ \langle D_k^2 \rangle + 2 \{ \langle D_k D_{k+1} \rangle + \langle D_k D_{k+2} \rangle + \langle D_k D_{k+3} \rangle \} \} \quad (A-17)$$

Although Burwell's equation, Eq. A-16, generally gave more satisfactory results than any of the Barkas' equations, Eq. A-15, Eq. A-17 generally did not yield more satisfactory results than Eq. A-16. The assumption on the error terms is further relaxed by assuming $\langle \delta_k \delta_{k+l} \rangle = \langle \delta_k \rangle^2$, for $l \geq N$ only, where N is a large number. Now by taking all equations A-6 together with A-4 and A-5 all the error terms are eliminated and one gets

$$\Delta_t^2 = 2/3 \{ \langle D_k^2 \rangle + 2 \sum_{\ell=1}^{N+1} \langle D_k D_{k+\ell} \rangle \}. \quad (A-18)$$

In using Eq. A-18 it was experimentally observed that the result was highly dependent on the choice of N . This can easily be seen by the fact that since $\langle D_k D_{k+\ell} \rangle$ terms can be negative as well as positive, for large values of N the sum in Eq. A-18 is usually of the same order of magnitude as $\langle D_k D_{k+N} \rangle$, which is non-vanishing and is experimentally observed to have the same order of magnitude as $\langle D_k D_{k+N} \rangle$ for small values of N . Therefore inclusion of $\langle D_k D_{k+N+2} \rangle$ in the summation of Eq. A-18 would appreciably affect the sum, and hence the value of Δ_t^2 . This rather serious difficulty makes the validity of Eq. A-18

which is a generalization of Burwell's equation, rather questionable. In turn, the validity of Burwell's and Barkas' equations, which are all special cases of Eq. A-18, become doubtful.

A comparison between Eq. A-14, which was derived with no assumption regarding the error terms, and Eq. A-18 shows that the factor $(1 - \frac{n^2}{N^2})$ in Eq. A-14 is the desirable factor which removes the difficulty with Eq. A-18 discussed above.

3-Variable Cell Length: If one uses a cell length m times the unit cell t to calculate second differences, $D_{k,m} \equiv Y_k - 2Y_{k+m} + Y_{k+2m}$, then the mean value of the square of two such second differences are

$$\langle D_{k,m}^2 \rangle = m^3 \Delta^2 + 6 \langle \delta_k^2 \rangle - 8 \langle \delta_k \delta_{k+m} \rangle + 2 \langle \delta_k \delta_{k+2m} \rangle \quad (\text{A-19})$$

$$\langle D_{k,n}^2 \rangle = n^3 \Delta^2 + 6 \langle \delta_k^2 \rangle - 8 \langle \delta_k \delta_{k+n} \rangle + 2 \langle \delta_k \delta_{k+2n} \rangle.$$

Upon assuming $\langle \delta_k \delta_\ell \rangle = \langle \delta_k \rangle^2$ for $k \neq \ell$, then the above two equations can be combined to obtain a new equation for Δ^2 ,

$$\Delta^2 = \frac{\langle D_{k,m}^2 \rangle - \langle D_{k,n}^2 \rangle}{m^3 - n^3}. \quad (\text{A-20})$$

In calculating $p\beta$ using the above equation, due to cell length dependence of the scattering factor, since the two averages are calculated over different cell lengths,

one must make an appropriate correction. One correction which was used is to replace the exponents of m and n by 3.13, as suggested by Widgoff⁽⁵⁸⁾. A different correction which was tried was to use the average value of the scattering factor over the interval $nt \rightarrow mt$.

This method, Eq. A-20, was tried and as a test of its consistency m and n were varied over the entire range of their values. The different values of $p\beta$ calculated for each set of data showed systematic trends in both m and n , instead of a statistical fluctuation. However, since these systematic trends generally varied randomly from one set of data to the next, attempts at correcting them were not fruitful. But when the assumption made in derivation of A-20 was deleted, the resulting equation yielded experimental results identical to that of A-14 which shows generally very little or no systematic trend.

APPENDIX B

EQUATIONS USED TO CHECK COMPLETE EVENTS

Three different types of events are considered for which equations are derived to check for the completeness of the events using the angle measurements and proton momentum.

Type a: Events with a proton track and one pion track and an assumed neutral pion (denoted by the subscript m). The energy-momentum equations for this case are

$$\begin{aligned}
 p_m \sin \delta_m + p_\pi \sin \delta_\pi + p_p \sin \delta_p &= 0, \\
 p_m \cos \delta_m \sin \phi_m + p_\pi \cos \delta_\pi \sin \phi_\pi + p_p \cos \delta_p \sin \phi_p &= 0 \\
 p_m \cos \delta_m \cos \phi_m + p_\pi \cos \delta_\pi \cos \phi_\pi + p_p \cos \delta_p \cos \phi_p &= p_0, \\
 \sqrt{p_m^2 + m^2} + \sqrt{p_\pi^2 + m^2} + \sqrt{p_p^2 + M^2} &= E_0 + M,
 \end{aligned}
 \tag{B-1}$$

where the angles are defined by Figure 3 (Chapter III) and p_0 , E_0 are the incident momentum and energy. Using the first three of these equations, δ_m and ϕ_m can be eliminated and p_m written in terms of the other quantities. Then p_m is inserted in the fourth equation which yields a quadratic equation for p_π in terms of the measured angles and p_p . The solution of this quadratic equation for p_π is given by

$$p_\pi = (-a_1 \pm \sqrt{a_1^2 - 4a_0a_2}) / 2a_2$$

where

$$a_0 = B^2 - m^2 (p_p^2 + p_0^2 - 2p_0 p_p \cos \delta_p \cos \phi_p) - m^4$$

$$a_1 = -2AB - 2Am^2$$

$$a_2 = A^2 - 2B - p_p^2 - p_0^2 + 2p_0 p_p \cos \delta_p \cos \phi_p - 2m^2$$

(B-2)

$$A = p_p \cos \delta_\pi \cos \delta_p \cos (\phi_\pi - \phi_p) + p_p \sin \delta_\pi \sin \delta_p$$

$$- p_0 \cos \delta_\pi \cos \phi_\pi$$

$$B = p_0 p_p \cos \delta_p \cos \phi_p - (\sqrt{p_p^2 + m^2} - M)(p_0 + M) - m^2.$$

Type b: Events with a proton track and two pion tracks (denoted by the subscripts 1 and 2). The momentum equations for this case are

$$p_1 \sin \delta_1 + p_2 \sin \delta_2 + p_p \sin \delta_p = 0$$

$$p_1 \cos \delta_1 \sin \phi_1 + p_2 \cos \delta_2 \sin \phi_2 + p_p \cos \delta_p \sin \phi_p = 0$$

(B-3)

$$p_1 \cos \delta_1 \cos \phi_1 + p_2 \cos \delta_2 \cos \phi_2 + p_p \cos \delta_p \cos \phi_p = p_0,$$

The fourth equation is not needed since the two pion momenta (p_1 and p_2) alone need to be eliminated. Eliminating p_1 and p_2 leaves one equation which is used to express p_p in terms of the angles alone. The resulting equation is

$$p_p = \frac{Ap_0}{\cot \delta_1 \cot \delta_2 \sin \delta_p \sin (\phi_1 - \phi_2) + \cos \delta_p (A \cos \phi_p + B \sin \phi_p)}$$

where

$$\begin{aligned}
 A &= \cot \delta_2 \sin \phi_2 - \cot \delta_1 \sin \phi_1, \\
 B &= \cot \delta_1 \cos \phi_1 - \cot \delta_2 \cos \phi_2.
 \end{aligned}
 \tag{B-4}$$

Type c: Events with a proton track and three pion tracks (denoted by the subscripts 1,2,3). The energy-momentum equations for this case are

$$\begin{aligned}
 p_p \sin \delta_p + \sum_{i=1}^3 p_i \sin \delta_i &= 0 \\
 p_p \cos \delta_p \sin \phi_p + \sum_{i=1}^3 p_i \cos \delta_i \sin \phi_i &= 0 \\
 p_p \cos \delta_p \cos \phi_p + \sum_{i=1}^3 p_i \cos \delta_i \cos \phi_i &= P_0 \\
 \sqrt{p_p^2 + M^2} + \sum_{i=1}^3 \sqrt{p_i^2 + m^2} &= E_0 + M
 \end{aligned}
 \tag{B-5}$$

The first three equations are used to express p_1 , p_2 , and p_3 in terms of p_p and the angles. This yields

$$p_1 = -\left\{ A \sin \delta_3 + \frac{AE_{13}}{E_{12}} \sin \delta_2 + p_p (\sin \delta_p + B \sin \delta_3 + C \sin \delta_2) \right\} / \sin \delta_1$$

$$p_2 = (AE_{31} + p_p E_{p1} + p_p BE_{31}) / E_{12}
 \tag{B-6}$$

$$p_3 = A + Bp_p$$

where A, B, C and E_{ij} and F_{ij} are given by

$$A = \frac{p_0 E_{12} \sin \delta_1}{E_{13} F_{12} - E_{12} F_{13}}$$

$$B = \frac{-(E_{p1}F_{12} + E_{12}F_{1p})}{E_{12}F_{13} - E_{13}F_{12}}$$

$$C = (E_{p1} + E_{31}B) / E_{12} \quad (B-7)$$

$$E_{ij} = \cos \delta_i \sin \phi_i \sin \delta_j - \cos \delta_j \sin \phi_j \sin \delta_i$$

$$F_{ij} = \cos \delta_i \cos \phi_i \sin \delta_j - \cos \delta_j \cos \phi_j \sin \delta_i.$$

When equations B-6 are substituted in the fourth equation of B-5, the result expresses p_p in terms of angles alone, which enables one to calculate p_p and check against its measured value.

APPENDIX C

DATA ON INELASTIC π^- -N INTERACTIONS

TABLE C1

DATA ON INELASTIC π^- -p EVENTS

EVENT	TRK	P(MEV)	ϕ ($^\circ$)	δ ($^\circ$)	θ ($^\circ$)
150038	I P	3326 \pm 559	7.4 \pm 0.1 -50.0 \pm 0.1	6.1 \pm 0.4 -54.9 \pm 0.1	9.6 \pm 0.3 68.3 \pm 0.1
150101	I P	15679 \pm 1663	1.3 \pm 0.1 -75.8 \pm 0.1	1.5 \pm 0.4 -24.1 \pm 0.3	2.0 \pm 0.3 77.1 \pm 0.1
183017	I P	7365 \pm 97i 116 \pm 1	0.7 \pm 0.1 18.5 \pm 0.1	-1.9 \pm 0.4 -24.5 \pm 0.3	2.0 \pm 0.4 30.4 \pm 0.2
183057	I P	5627 \pm 501 195 \pm 2	1.6 \pm 0.1 17.3 \pm 0.1	1.0 \pm 0.4 -59.1 \pm 0.1	1.9 \pm 0.2 60.6 \pm 0.1
190056	I P	9443 \pm 1471 172 \pm 2	2.7 \pm 0.1 0.9 \pm 0.1	-1.2 \pm 0.4 75.9 \pm 0.1	3.0 \pm 0.2 75.9 \pm 0.1
190242	I P	5471 \pm 1123 369 \pm 4	0.1 \pm 0.1 8.8 \pm 0.1	-2.7 \pm 0.4 19.4 \pm 0.3	2.7 \pm 0.4 21.2 \pm 0.3
221575	I P	6791 \pm 2045 416 \pm 104	1.9 \pm 0.1 -60.7 \pm 0.1	0.0 \pm 0.0 -22.9 \pm 0.3	1.9 \pm 0.1 63.2 \pm 0.1
240456	I P	11661 \pm 5538	1.7 \pm 0.1 -76.6 \pm 0.1	0.0 \pm 0.0 0.0 \pm 0.0	1.7 \pm 0.1 76.6 \pm 0.1
300291	I P	9391 \pm 1912 100 \pm 1	-0.6 \pm 0.1 56.8 \pm 0.1	0.0 \pm 0.0 -11.3 \pm 0.4	0.6 \pm 0.1 57.5 \pm 0.1
310370	I P	5247 \pm 1094 85 \pm 1	6.2 \pm 0.1 8.0 \pm 0.1	3.4 \pm 0.4 -28.8 \pm 0.3	7.1 \pm 0.2 29.8 \pm 0.3
330031	I P	6640 \pm 872 21 \pm 1	1.4 \pm 0.1 72.8 \pm 2.0	0.0 \pm 0.0 32.6 \pm 13.0	1.4 \pm 0.1 75.6 \pm 2.7
330397	I P	10481 \pm 1834 351 \pm 4	-0.7 \pm 0.1 43.2 \pm 0.1	0.0 \pm 0.0 -39.1 \pm 0.2	0.7 \pm 0.1 55.5 \pm 0.1
370098	I P	1348 \pm 276 455 \pm 100	-3.0 \pm 0.1 44.0 \pm 0.1	-4.9 \pm 0.4 -44.9 \pm 0.2	5.7 \pm 0.3 59.4 \pm 0.1
370358	I P	2715 \pm 95i 25 \pm 1	1.2 \pm 0.1 -67.5 \pm 1.0	1.5 \pm 0.4 -35.4 \pm 8.1	1.9 \pm 0.3 71.8 \pm 2.0
370545	I P	533 \pm 6	5.6 \pm 0.1 -61.0 \pm 0.1	-11.7 \pm 0.4 -12.1 \pm 0.4	13.0 \pm 0.4 61.7 \pm 0.1
380009	I P	8775 \pm 1108	-1.8 \pm 0.1 70.8 \pm 0.1	0.2 \pm 0.2 -12.8 \pm 0.3	1.8 \pm 0.1 71.3 \pm 0.1

EVENT	TRK	P(MEV)	$\phi(^{\circ})$	$\delta(^{\circ})$	$\theta(^{\circ})$
380160	I	5829± 515	0.9±0.1	0.1± 0.1	0.9± 0.1
	P	91± 1	33.0±0.1	0.2± 0.2	33.0± 0.1
400042	I	12213±3489	0.8±0.1	0.0± 0.0	0.8± 0.1
	P	68± 1	-50.3±0.1	-8.9± 2.4	50.9± 0.3
400118	I	7310± 956	-0.6±0.1	-1.2± 0.4	1.3± 0.4
	P	24± 1	78.0±3.0	0.1± 0.1	78.0± 3.0
400273	I	4531±3029	-1.1±0.1	0.0± 0.0	1.1± 0.1
	P	73± 1	-16.4±0.1	-30.5± 0.9	34.3± 0.8
400352	I	11332±2981	1.5±0.1	-1.7± 0.4	2.3± 0.3
	P	316± 3	-59.7±0.1	45.4± 0.2	69.3± 0.1
400391	I	9107±1528	0.6±0.1	0.0± 0.0	0.6± 0.1
	P	19± 1	-76.0±2.0	0.1± 0.1	76.0± 2.0
400395	I	1178± 423	-0.7±0.1	0.0± 0.0	0.7± 0.1
	P	214± 2	47.3±0.1	-58.4± 0.1	69.2± 0.1
461416	I	2674±1136	2.0±0.1	3.2± 0.4	3.8± 0.3
	P		62.4±0.1	2.7± 0.4	62.4± 0.1
461932	I	9570± 687	0.5±0.1	0.0± 0.0	0.5± 0.1
	P	324± 2	-59.5±0.1	-43.9± 0.2	68.5± 0.1
461953	I	5622± 866	-0.7±0.1	1.9± 0.4	2.0± 0.4
	P	33± 1	68.7±1.5	-35.4± 8.1	72.8± 2.1
461969	I		-4.8±0.1	0.0± 0.0	4.8± 0.1
	P	370± 45	36.3±0.1	19.0± 0.3	40.4± 0.1
760125	I		-12.4±0.1	17.1± 0.5	21.0± 0.4
	P	358± 5	8.7±0.1	-44.7± 0.3	45.4± 0.3
760035	I	3310± 907	-1.4±0.1	0.0± 0.0	1.4± 0.1
	P	229± 3	-6.5±0.1	70.8± 0.3	70.9± 0.3
780136	I	3053± 393	6.6±0.1	1.0± 0.3	6.7± 0.1
	P	206± 3	-15.8±0.1	-19.5± 1.4	24.9± 1.1
183045	I	2360± 340	-2.6±0.1	1.4± 0.4	3.0± 0.2
	2	1024± 214	6.3±0.1	-3.4± 0.4	7.2± 0.2
183068	I		-40.8±0.1	23.0± 0.3	45.8± 0.1
	2	425± 42	5.9±0.1	5.4± 0.4	8.0± 0.3

EVENT	TRK	P (MEV)	ϕ (°)	δ (°)	θ (°)
183192	1		-6.8 ± 0.1	-9.8 ± 0.4	11.9 ± 0.3
	2	6505 ± 974	-1.1 ± 0.1	0.0 ± 0.0	1.1 ± 0.1
190120	1	2482 ± 1191	-5.5 ± 0.1	3.2 ± 0.4	6.4 ± 0.2
	2	6310 ± 2450	18.6 ± 0.1	0.0 ± 0.0	18.6 ± 0.1
221850	1	2890 ± 326	-6.3 ± 0.1	1.2 ± 0.4	6.4 ± 0.1
	2	7471 ± 4257	-0.4 ± 0.1	3.4 ± 0.4	3.4 ± 0.4
240515	1	2687 ± 240	0.2 ± 0.1	4.0 ± 0.4	4.0 ± 0.4
	2		-55.7 ± 0.1	45.2 ± 0.2	66.6 ± 0.1
310365	1		-19.7 ± 0.1	-32.0 ± 0.3	37.0 ± 0.3
	2	1786 ± 216	-7.9 ± 0.1	2.7 ± 0.4	8.3 ± 0.2
310392	1	10866 ± 934	5.0 ± 0.1	-1.8 ± 0.4	5.3 ± 0.2
	2	3699 ± 280	-8.8 ± 0.1	1.3 ± 0.4	8.9 ± 0.1
330256	1	1166 ± 179	-3.2 ± 0.1	-2.4 ± 0.4	4.0 ± 0.3
	2	7416 ± 757	1.0 ± 0.1	0.0 ± 0.0	1.0 ± 0.1
330374	1	10899 ± 2545	2.5 ± 0.1	0.0 ± 0.0	2.5 ± 0.1
	2		40.4 ± 0.1	-41.7 ± 0.2	55.3 ± 0.1
350584	1	2289 ± 299	2.1 ± 0.1	0.0 ± 0.0	2.1 ± 0.1
	2	11173 ± 3171	-2.4 ± 0.1	-1.5 ± 0.4	2.8 ± 0.2
351286	1	7569 ± 2494	2.8 ± 0.1	0.1 ± 0.1	2.8 ± 0.1
	2		-34.5 ± 0.1	-10.5 ± 0.4	35.9 ± 0.1
351300	1	477 ± 87	8.2 ± 0.1	5.1 ± 0.4	9.6 ± 0.2
	2	1660 ± 364	-2.8 ± 0.1	-4.0 ± 0.4	4.9 ± 0.3
370034	1		-59.2 ± 0.1	-13.7 ± 0.3	60.2 ± 0.1
	2	4564 ± 674	2.0 ± 0.1	0.0 ± 0.0	2.0 ± 0.1
370216	1	288 ± 48	-1.3 ± 0.1	1.4 ± 0.4	1.9 ± 0.3
	2		9.7 ± 0.1	0.0 ± 0.0	9.7 ± 0.1
370334	1	9793 ± 1215	-3.1 ± 0.1	1.4 ± 0.4	3.4 ± 0.2
	2	846 ± 90	3.1 ± 0.1	-8.3 ± 0.4	8.9 ± 0.4
370372	1	659 ± 118	-1.6 ± 0.1	-1.3 ± 0.4	2.1 ± 0.3
	2		70.7 ± 0.1	20.3 ± 0.3	71.9 ± 0.1
380037	1	2743 ± 153	2.0 ± 0.1	-2.3 ± 0.4	3.0 ± 0.3
	2	947 ± 119	6.3 ± 0.1	2.3 ± 0.4	6.7 ± 0.2

EVENT	TRK	P(MEV)	$\phi(^{\circ})$	$\delta(^{\circ})$	$\theta(^{\circ})$
380040	1	3917 \pm 459	-6.0 \pm 0.1	-3.8 \pm 0.4	7.1 \pm 0.2
	2	10234 \pm 2136	2.0 \pm 0.1	0.0 \pm 0.0	2.0 \pm 0.1
380102	1	406 \pm 40	-9.4 \pm 0.1	-10.4 \pm 0.4	14.0 \pm 0.3
	2		18.6 \pm 0.1	18.7 \pm 0.3	26.1 \pm 0.2
380320	1		-10.8 \pm 0.1	16.1 \pm 0.3	19.3 \pm 0.3
	2		-5.2 \pm 0.1	-13.8 \pm 0.4	14.7 \pm 0.4
400033	1	5506 \pm 804	-1.2 \pm 0.1	0.1 \pm 0.1	1.2 \pm 0.1
	2		66.1 \pm 0.1	-23.9 \pm 0.3	68.3 \pm 0.1
400056	1		-64.4 \pm 0.1	-12.2 \pm 0.4	65.0 \pm 0.1
	2	13725 \pm 2642	3.3 \pm 0.1	1.6 \pm 0.4	3.7 \pm 0.2
400173	1	11582 \pm 1983	2.2 \pm 0.1	1.4 \pm 0.4	2.6 \pm 0.2
	2	3726 \pm 1229	3.2 \pm 0.1	-4.9 \pm 0.4	5.9 \pm 0.3
410018	1	6002 \pm 694	0.1 \pm 0.1	0.0 \pm 0.0	0.1 \pm 0.1
	2	521 \pm 145	-2.3 \pm 0.1	1.1 \pm 0.3	2.5 \pm 0.2
443495	1	5151 \pm 1433	0.8 \pm 0.1	2.0 \pm 0.4	2.2 \pm 0.4
	2	1953 \pm 314	-2.9 \pm 0.1	-6.2 \pm 0.4	6.8 \pm 0.4
461942	1		-8.1 \pm 0.1	18.1 \pm 0.3	19.8 \pm 0.3
	2	5374 \pm 591	-0.4 \pm 0.1	-2.3 \pm 0.4	2.3 \pm 0.4
481081	1	2436 \pm 137	-0.5 \pm 0.1	1.3 \pm 0.4	1.4 \pm 0.4
	2	10638 \pm 4402	-1.9 \pm 0.1	0.9 \pm 0.4	2.1 \pm 0.2
481133	1	2073 \pm 642	11.3 \pm 0.1	-4.1 \pm 0.4	12.0 \pm 0.2
	2	694 \pm 202	1.1 \pm 0.1	-5.1 \pm 0.4	5.2 \pm 0.4
690058	1	2793 \pm 440	-5.5 \pm 0.1	2.0 \pm 0.6	5.9 \pm 0.2
	2	2943 \pm 669	2.0 \pm 0.1	3.6 \pm 0.6	4.1 \pm 0.5
760042	1	304 \pm 119	8.0 \pm 0.1	9.6 \pm 0.3	12.5 \pm 0.2
	2		-117.6 \pm 0.1	-42.1 \pm 0.8	110.1 \pm 0.3
182926	1	4400 \pm 451	-5.4 \pm 0.1	-0.8 \pm 0.4	5.5 \pm 0.1
	2	2990 \pm 534	-4.0 \pm 0.1	0.0 \pm 0.0	4.0 \pm 0.1
	3	6745 \pm 384	2.2 \pm 0.1	1.0 \pm 0.4	2.4 \pm 0.2
	P	477 \pm 4	31.2 \pm 0.1	4.4 \pm 0.4	31.5 \pm 0.1
183035	1	6286 \pm 1292	-4.8 \pm 0.1	0.7 \pm 0.4	4.9 \pm 0.1
	2	8502 \pm 1404	-0.6 \pm 0.1	-0.9 \pm 0.4	1.1 \pm 0.3
	3	1954 \pm 573	3.2 \pm 0.1	4.5 \pm 0.4	5.5 \pm 0.3

EVENT	TRK	P (MEV)	$\phi(^{\circ})$	$\delta(^{\circ})$	$\theta(^{\circ})$
	P	320 \pm 50	55.3 \pm 0.1	-54.7 \pm 0.1	70.8 \pm 0.1
183148	1		-54.5 \pm 0.1	-48.3 \pm 0.2	67.3 \pm 0.1
	2	4717 \pm 265	-2.6 \pm 0.1	1.0 \pm 0.4	2.8 \pm 0.2
	3		0.4 \pm 0.1	5.3 \pm 0.4	5.3 \pm 0.4
	P	101 \pm 1	82.9 \pm 0.1	-6.6 \pm 0.5	82.9 \pm 0.1
190107	1		-108.6 \pm 0.1	-37.9 \pm 0.2	104.6 \pm 0.1
	2	2163 \pm 462	-6.4 \pm 0.1	-3.9 \pm 0.4	7.5 \pm 0.2
	3	1393 \pm 53	10.9 \pm 0.1	0.5 \pm 0.4	10.9 \pm 0.1
	P	199 \pm 2	4.8 \pm 0.1	9.7 \pm 0.4	10.8 \pm 0.4
190216	1	851 \pm 222	-14.6 \pm 0.1	1.5 \pm 0.4	14.7 \pm 0.1
	2	11551 \pm 5956	-0.6 \pm 0.1	1.1 \pm 0.4	1.3 \pm 0.4
	3	8216 \pm 1567	1.8 \pm 0.1	2.1 \pm 0.4	2.8 \pm 0.3
	P	81 \pm 1	49.1 \pm 0.1	67.4 \pm 0.2	75.4 \pm 0.1
240466	1	3898 \pm 555	1.8 \pm 0.1	1.4 \pm 0.4	2.3 \pm 0.3
	2	1358 \pm 322	2.1 \pm 0.1	-5.5 \pm 0.4	5.9 \pm 0.4
	3		-45.6 \pm 0.1	-8.9 \pm 0.4	46.3 \pm 0.1
	P	426 \pm 5	8.0 \pm 0.1	0.0 \pm 0.0	8.0 \pm 0.1
240510	1	3546 \pm 290	0.8 \pm 0.1	-2.3 \pm 0.4	2.4 \pm 0.4
	2	3825 \pm 226	-0.6 \pm 0.1	0.0 \pm 0.0	0.6 \pm 0.1
	3	5109 \pm 719	-0.2 \pm 0.1	0.0 \pm 0.0	0.2 \pm 0.1
	P		66.7 \pm 0.1	81.7 \pm 0.0	86.7 \pm 0.0
300252	1	2610 \pm 340	19.1 \pm 0.1	2.8 \pm 0.4	19.3 \pm 0.1
	2		0.2 \pm 0.1	-11.3 \pm 0.4	11.3 \pm 0.4
	3	9139 \pm 2600	-0.7 \pm 0.1	0.0 \pm 0.0	0.7 \pm 0.1
	P	86 \pm 1	3.4 \pm 0.1	-55.9 \pm 0.3	56.0 \pm 0.3
330267	1	4558 \pm 1429	-4.9 \pm 0.1	0.8 \pm 0.4	5.0 \pm 0.1
	2	2279 \pm 460	13.2 \pm 0.1	0.0 \pm 0.0	13.2 \pm 0.1
	3		6.9 \pm 0.1	18.1 \pm 0.3	19.3 \pm 0.3
	P	300 \pm 80	-0.7 \pm 0.1	-33.2 \pm 0.3	33.2 \pm 0.3
351190	1	1543 \pm 539	-2.3 \pm 0.1	-3.2 \pm 0.4	3.9 \pm 0.3
	2		6.1 \pm 0.1	-8.3 \pm 0.4	10.3 \pm 0.3
	3		24.0 \pm 0.1	-7.0 \pm 0.4	24.9 \pm 0.1
	P	360 \pm 250	38.8 \pm 0.1	27.4 \pm 0.3	46.2 \pm 0.2
370026	1	1588 \pm 582	-4.9 \pm 0.1	6.2 \pm 0.4	7.9 \pm 0.3
	2	7547 \pm 1633	0.0 \pm 0.1	-3.2 \pm 0.4	3.2 \pm 0.4
	3	7144 \pm 525	0.8 \pm 0.1	1.2 \pm 0.4	1.4 \pm 0.3
	P	315 \pm 4	1.8 \pm 0.1	-72.7 \pm 0.1	72.7 \pm 0.1

EVENT	TRK	P (MEV)	ϕ (°)	δ (°)	θ (°)
370308	1		-47.9 ± 0.1	-10.6 ± 0.4	48.8 ± 0.1
	2		-1.9 ± 0.1	-15.1 ± 0.3	15.2 ± 0.3
	3		38.7 ± 0.1	18.9 ± 0.3	42.4 ± 0.1
	P	87 ± 1	22.8 ± 0.1	32.2 ± 0.9	38.7 ± 0.7
370398	1		-23.0 ± 0.1	40.9 ± 0.2	45.9 ± 0.2
	2		-1.4 ± 0.1	14.1 ± 0.3	14.2 ± 0.3
	3	6904 ± 842	0.4 ± 0.1	0.0 ± 0.0	0.4 ± 0.1
	P	142 ± 1	-80.8 ± 0.1	-4.9 ± 0.4	80.8 ± 0.1
370545	1	3665 ± 715	-2.1 ± 0.1	-2.4 ± 0.4	3.2 ± 0.3
	2		-0.8 ± 0.1	-16.0 ± 0.3	16.0 ± 0.3
	3	4915 ± 847	1.9 ± 0.1	3.4 ± 0.4	3.9 ± 0.4
	P	206 ± 2	-47.2 ± 0.1	67.0 ± 0.1	74.6 ± 0.1
380070	1		-19.2 ± 0.1	8.5 ± 0.4	20.9 ± 0.2
	2		-0.7 ± 0.1	13.5 ± 0.3	13.5 ± 0.3
	3	6595 ± 1860	2.2 ± 0.1	-3.6 ± 0.4	4.2 ± 0.3
	P		76.4 ± 0.1	-44.9 ± 0.2	80.4 ± 0.1
380095	1	2730 ± 215	-7.6 ± 0.1	1.0 ± 0.4	7.7 ± 0.1
	2	6430 ± 1027	3.2 ± 0.1	0.0 ± 0.0	3.2 ± 0.1
	3	3134 ± 1116	13.9 ± 0.1	-2.0 ± 0.4	14.0 ± 0.1
	P	26 ± 1	31.0 ± 1.0	0.3 ± 0.3	31.0 ± 1.0
380177	1	3403 ± 777	-1.5 ± 0.1	0.0 ± 0.0	1.5 ± 0.1
	2		5.5 ± 0.1	-3.5 ± 0.4	6.5 ± 0.2
	3		29.9 ± 0.1	-17.6 ± 0.4	34.3 ± 0.2
	P	22 ± 1	52.0 ± 3.0	0.1 ± 0.1	52.0 ± 3.0
380348	1		-12.3 ± 0.1	-23.5 ± 0.3	26.4 ± 0.3
	2	2851 ± 351	0.6 ± 0.1	-4.2 ± 0.4	4.2 ± 0.4
	3		5.4 ± 0.1	3.4 ± 0.4	6.4 ± 0.2
	P	101 ± 1	-42.5 ± 0.1	29.4 ± 0.4	50.0 ± 0.2
392065	1		-21.1 ± 0.1	-40.1 ± 0.2	44.5 ± 0.2
	2	3795 ± 381	-0.9 ± 0.1	-0.8 ± 0.4	1.2 ± 0.3
	3		4.9 ± 0.1	21.2 ± 0.3	21.7 ± 0.3
	P	27 ± 1	-50.0 ± 5.3	-16.9 ± 8.4	52.0 ± 5.3
392116	1	728 ± 59	-7.1 ± 0.1	4.7 ± 0.4	8.5 ± 0.2
	2	1799 ± 399	-0.7 ± 0.1	0.0 ± 0.0	0.7 ± 0.1
	3	4026 ± 335	0.3 ± 0.1	-0.6 ± 0.4	0.7 ± 0.4
	P	16 ± 1	63.8 ± 0.8	0.6 ± 0.6	63.8 ± 0.8
400060	1		-18.3 ± 0.1	3.2 ± 0.4	18.6 ± 0.1
	2		1.5 ± 0.1	-15.3 ± 0.3	15.4 ± 0.3

EVENT	TRK	P (MEV)	$\phi(^{\circ})$	$\delta(^{\circ})$	$\theta(^{\circ})$
	3	1354 \pm 84	5.4 \pm 0.1	0.0 \pm 0.0	5.4 \pm 0.1
	P	72 \pm 1	72.4 \pm 0.1	45.4 \pm 0.9	77.7 \pm 0.2
400166	1	1872 \pm 393	-8.4 \pm 0.1	3.1 \pm 0.4	8.9 \pm 0.2
	2	1912 \pm 272	-0.6 \pm 0.1	-2.6 \pm 0.4	2.7 \pm 0.4
	3	2785 \pm 748	11.6 \pm 0.1	-3.6 \pm 0.4	12.1 \pm 0.2
	P	32 \pm 1	-6.0 \pm 1.0	0.1 \pm 0.1	6.0 \pm 1.0
400232	1		-4.1 \pm 0.1	12.4 \pm 0.3	13.0 \pm 0.3
	2	4557 \pm 569	0.8 \pm 0.1	-3.2 \pm 0.4	3.3 \pm 0.4
	3	3255 \pm 574	4.2 \pm 0.1	-5.5 \pm 0.4	6.9 \pm 0.3
	P	440 \pm 50	25.1 \pm 0.1	-6.2 \pm 0.4	25.8 \pm 0.1
400252	1	5574 \pm 571	-5.6 \pm 0.1	-3.6 \pm 0.4	6.7 \pm 0.2
	2	10070 \pm 2057	0.3 \pm 0.1	0.1 \pm 0.1	0.3 \pm 0.1
	3		6.8 \pm 0.1	6.2 \pm 0.4	9.2 \pm 0.3
	P	157 \pm 2	53.4 \pm 0.1	6.7 \pm 0.7	53.7 \pm 0.1
400262	1	1257 \pm 179	-7.0 \pm 0.1	-2.9 \pm 0.4	7.6 \pm 0.2
	2	1842 \pm 181	3.4 \pm 0.1	1.2 \pm 0.4	3.6 \pm 0.2
	3	325 \pm 80	7.2 \pm 0.1	2.6 \pm 0.4	7.7 \pm 0.2
	P	400 \pm 260	-44.3 \pm 0.1	50.9 \pm 0.1	63.2 \pm 0.1
400388	1		-11.2 \pm 0.1	17.7 \pm 0.3	20.8 \pm 0.3
	2	3467 \pm 805	-2.5 \pm 0.1	-4.3 \pm 0.4	5.0 \pm 0.3
	3		15.5 \pm 0.1	-13.0 \pm 0.3	20.1 \pm 0.2
	P	107 \pm 1	82.5 \pm 0.1	10.4 \pm 0.8	82.6 \pm 0.1
410035	1	3383 \pm 469	-0.9 \pm 0.1	-1.7 \pm 0.3	1.9 \pm 0.3
	2		-2.1 \pm 0.1	-6.3 \pm 0.3	6.6 \pm 0.3
	3		-64.0 \pm 0.1	35.3 \pm 0.2	69.0 \pm 0.1
	P	396 \pm 4	49.4 \pm 0.1	0.0 \pm 0.0	49.4 \pm 0.1
410036	1	2114 \pm 360	3.5 \pm 0.1	0.6 \pm 0.3	3.6 \pm 0.1
	2	6162 \pm 694	1.0 \pm 0.1	-0.9 \pm 0.3	1.3 \pm 0.2
	3	5212 \pm 754	-5.1 \pm 0.1	-1.8 \pm 0.3	5.4 \pm 0.1
	P	174 \pm 2	73.0 \pm 0.1	-10.5 \pm 0.6	73.3 \pm 0.1
420003	1		-7.9 \pm 0.1	-14.0 \pm 0.3	16.0 \pm 0.3
	2	7012 \pm 2599	-0.1 \pm 0.1	0.0 \pm 0.0	0.1 \pm 0.1
	3	1327 \pm 162	-7.2 \pm 0.1	-1.5 \pm 0.3	7.4 \pm 0.1
	P	574 \pm 6	2.6 \pm 0.1	-2.2 \pm 0.3	3.4 \pm 0.2
443379	1	2697 \pm 496	-9.0 \pm 0.1	1.4 \pm 0.4	9.1 \pm 0.1
	2		9.2 \pm 0.1	-13.1 \pm 0.3	16.0 \pm 0.3
	3		16.3 \pm 0.1	21.3 \pm 0.3	26.6 \pm 0.2
	P	556 \pm 10	13.3 \pm 0.1	-13.1 \pm 0.3	18.6 \pm 0.2

EVENT	TRK	P (MEV)	ϕ ($^{\circ}$)	δ ($^{\circ}$)	θ ($^{\circ}$)
461453	1		-8.7 ± 0.1	-10.0 ± 0.4	13.2 ± 0.3
	2	1094 ± 207	-5.6 ± 0.1	3.7 ± 0.4	6.7 ± 0.2
	3	1949 ± 218	2.9 ± 0.1	0.2 ± 0.2	2.9 ± 0.1
	P	156 ± 2	70.2 ± 0.1	18.5 ± 0.7	71.3 ± 0.1
461945	1	460 ± 36	-2.0 ± 0.1	8.3 ± 0.4	8.5 ± 0.4
	2	1248 ± 102	-1.2 ± 0.1	3.7 ± 0.4	3.9 ± 0.4
	3	3807 ± 1763	1.5 ± 0.1	-1.4 ± 0.4	2.1 ± 0.3
	P	423 ± 70	21.2 ± 0.1	-65.5 ± 0.2	67.3 ± 0.2
461997	1		-14.5 ± 0.1	10.9 ± 0.4	18.1 ± 0.2
	2	3101 ± 540	-2.4 ± 0.1	-2.9 ± 0.4	3.8 ± 0.3
	3	4755 ± 360	2.5 ± 0.1	0.0 ± 0.0	2.5 ± 0.1
	P		57.6 ± 0.1	72.2 ± 0.0	80.6 ± 0.0
480828	1		0.7 ± 0.1	-7.9 ± 0.4	7.9 ± 0.4
	2		-1.1 ± 0.1	-2.9 ± 0.4	3.1 ± 0.4
	3	5404 ± 854	-13.9 ± 0.1	11.1 ± 0.3	17.7 ± 0.2
	P	369 ± 4	-47.0 ± 0.1	15.1 ± 0.3	48.8 ± 0.1
480892	1	1343 ± 231	16.4 ± 0.1	-2.6 ± 0.4	16.6 ± 0.1
	2	2854 ± 226	5.3 ± 0.1	0.0 ± 0.0	5.3 ± 0.1
	3	3795 ± 1197	0.1 ± 0.1	0.1 ± 0.1	0.1 ± 0.1
	P	387 ± 4	-49.2 ± 0.1	12.8 ± 0.3	50.4 ± 0.1
513288	1		-30.8 ± 0.1	-54.6 ± 0.1	60.2 ± 0.1
	2	4353 ± 385	-1.5 ± 0.1	-1.4 ± 0.4	2.1 ± 0.3
	3	2659 ± 1126	0.4 ± 0.1	3.7 ± 0.4	3.7 ± 0.4
	P	870 ± 610	-16.3 ± 0.1	25.5 ± 0.3	30.0 ± 0.3
690014	1	7502 ± 1964	-0.6 ± 0.1	-2.6 ± 0.6	2.7 ± 0.6
	2	1506 ± 276	7.5 ± 0.1	2.0 ± 0.6	7.8 ± 0.2
	3	1795 ± 691	7.8 ± 0.1	6.0 ± 0.6	9.8 ± 0.4
	P	587 ± 50	-21.4 ± 0.1	21.1 ± 0.5	29.7 ± 0.3
780107	1		-0.2 ± 0.1	-11.1 ± 0.3	11.1 ± 0.3
	2		-6.3 ± 0.1	-14.7 ± 0.3	16.0 ± 0.3
	3	5572 ± 1969	-9.9 ± 0.1	-2.1 ± 0.3	10.1 ± 0.1
	P	111 ± 2	53.9 ± 0.1	25.2 ± 1.2	57.8 ± 0.4
780112	1	6002 ± 1133	1.9 ± 0.1	1.7 ± 0.3	2.5 ± 0.2
	2	3323 ± 649	-0.1 ± 0.1	1.5 ± 0.3	1.5 ± 0.3
	3		-12.8 ± 0.1	-22.0 ± 0.3	25.3 ± 0.3
	P	27 ± 1	-5.9 ± 0.1	-36.2 ± 0.4	36.6 ± 0.4
780140	1	4482 ± 2078	11.3 ± 0.1	7.4 ± 0.3	13.5 ± 0.2
	2		-3.5 ± 0.1	25.9 ± 0.2	26.1 ± 0.2

EVENT	TRK	P (MEV)		$\phi(^{\circ})$	$\delta(^{\circ})$	$\theta(^{\circ})$
	3			30.2 ± 0.1	77.1 ± 0.2	78.9 ± 0.2
	P	$25 \pm$	1	53.6 ± 0.1	0.0 ± 0.0	53.6 ± 0.1
780143	1	$3023 \pm$	515	1.5 ± 0.1	0.0 ± 0.0	1.5 ± 0.1
	2	$5312 \pm$	609	3.4 ± 0.1	1.6 ± 0.6	3.8 ± 0.3
	3			36.7 ± 0.1	-12.5 ± 0.6	38.5 ± 0.2
	P	$85 \pm$	1	61.5 ± 0.1	-10.9 ± 2.9	62.1 ± 0.3
850006	1	5452 ± 2019		-4.9 ± 0.1	-2.0 ± 0.3	5.3 ± 0.1
	2	2464 ± 1227		-1.8 ± 0.1	1.8 ± 0.3	2.5 ± 0.2
	3	1337 ± 611		-5.1 ± 0.1	-5.4 ± 0.3	7.4 ± 0.2
	P	$376 \pm$	4	11.1 ± 0.1	-7.3 ± 0.3	13.3 ± 0.2
990045	1			4.0 ± 0.1	14.6 ± 0.3	15.1 ± 0.3
	2	5392 ± 1044		3.0 ± 0.1	-4.1 ± 0.3	5.1 ± 0.2
	3			-27.1 ± 0.1	33.2 ± 0.4	41.8 ± 0.3
	P	$233 \pm$	3	7.1 ± 0.1	-63.3 ± 0.3	63.5 ± 0.3
150058	1			33.5 ± 0.1	34.4 ± 0.2	46.5 ± 0.1
	2	4274 ± 441		6.5 ± 0.1	-1.9 ± 0.4	6.8 ± 0.1
	3	5716 ± 1089		-8.0 ± 0.1	3.4 ± 0.4	8.7 ± 0.2
	4			165.9 ± 0.1	9.4 ± 0.4	163.1 ± 0.2
182955	1			-32.5 ± 0.1	-16.9 ± 0.3	36.2 ± 0.2
	2	966 ± 62		-5.6 ± 0.1	-1.2 ± 0.4	5.7 ± 0.1
	3	2610 ± 198		-0.1 ± 0.1	0.6 ± 0.4	0.6 ± 0.4
	4			58.7 ± 0.1	11.1 ± 0.4	59.3 ± 0.1
182984	1	6131 ± 567		-1.3 ± 0.1	0.0 ± 0.0	1.3 ± 0.1
	2	3973 ± 714		-0.9 ± 0.1	-4.8 ± 0.4	4.9 ± 0.4
	3	2492 ± 268		2.8 ± 0.1	-1.2 ± 0.4	3.0 ± 0.2
	4			57.4 ± 0.1	47.0 ± 0.2	68.4 ± 0.1
183036	1	834 ± 242		-7.2 ± 0.1	-6.8 ± 0.4	9.9 ± 0.3
	2	3245 ± 900		-3.0 ± 0.1	3.4 ± 0.4	4.5 ± 0.3
	3	4351 ± 866		0.9 ± 0.1	0.0 ± 0.0	0.9 ± 0.1
	4			-1.4 ± 0.1	20.3 ± 0.3	20.3 ± 0.3
183046	1			-9.0 ± 0.1	-22.3 ± 0.3	24.0 ± 0.3
	2	929 ± 446		-4.3 ± 0.1	3.3 ± 0.4	5.4 ± 0.3
	3	2590 ± 429		4.8 ± 0.1	1.2 ± 0.4	4.9 ± 0.1
	4	787 ± 197		37.1 ± 0.1	-7.4 ± 0.4	37.7 ± 0.1
183164	1			-59.7 ± 0.1	13.4 ± 0.3	60.6 ± 0.1
	2	3410 ± 2500		1.0 ± 0.1	-1.8 ± 0.4	2.1 ± 0.4
	3			1.3 ± 0.1	-5.5 ± 0.4	5.7 ± 0.4
	4			-1.0 ± 0.1	33.5 ± 0.3	33.5 ± 0.3

EVENT	TRK	P(MEV)	$\phi(^{\circ})$	$\delta(^{\circ})$	$\theta(^{\circ})$
190041	1		-36.3 ± 0.1	-10.9 ± 0.4	37.7 ± 0.1
	2	2421 ± 566	-4.5 ± 0.1	5.4 ± 0.4	7.0 ± 0.3
	3	1681 ± 204	4.5 ± 0.1	-1.4 ± 0.4	4.7 ± 0.2
	4	2075 ± 740	7.8 ± 0.1	-4.5 ± 0.4	9.0 ± 0.2
190076	1	4191 ± 449	-8.4 ± 0.1	1.7 ± 0.4	8.6 ± 0.1
	2		12.0 ± 0.1	20.8 ± 0.3	23.9 ± 0.3
	3		31.0 ± 0.1	55.4 ± 0.1	60.9 ± 0.1
	4		42.7 ± 0.1	-26.6 ± 0.3	48.9 ± 0.2
221565	1	1512 ± 1394	-13.1 ± 0.1	-12.8 ± 0.3	18.2 ± 0.2
	2	890 ± 114	-10.0 ± 0.1	6.5 ± 0.4	11.9 ± 0.2
	3	4569 ± 394	-3.5 ± 0.1	0.0 ± 0.0	3.5 ± 0.1
	4	4491 ± 741	4.0 ± 0.1	-5.0 ± 0.4	6.4 ± 0.3
221642	1	794 ± 184	-24.5 ± 0.1	3.3 ± 0.4	24.7 ± 0.1
	2	13970 ± 7771	-2.5 ± 0.1	0.0 ± 0.0	2.5 ± 0.1
	3		-0.5 ± 0.1	15.7 ± 0.3	15.7 ± 0.3
	4		58.4 ± 0.1	-44.5 ± 0.2	68.1 ± 0.1
221663	1	1466 ± 666	-7.0 ± 0.1	-3.8 ± 0.4	8.0 ± 0.2
	2	2500 ± 975	-2.8 ± 0.1	6.4 ± 0.4	7.0 ± 0.4
	3	6321 ± 843	-0.3 ± 0.1	2.7 ± 0.4	2.7 ± 0.4
	4		48.6 ± 0.1	-32.9 ± 0.3	56.3 ± 0.2
221681	1	2193 ± 156	-5.3 ± 0.1	0.0 ± 0.0	5.3 ± 0.1
	2	6559 ± 638	2.1 ± 0.1	0.1 ± 0.1	2.1 ± 0.1
	3		3.3 ± 0.1	-12.1 ± 0.4	12.5 ± 0.4
	4	1155 ± 481	5.6 ± 0.1	-7.8 ± 0.4	9.6 ± 0.3
221825	1	8598 ± 1577	-0.1 ± 0.1	1.9 ± 0.4	1.9 ± 0.4
	2	712 ± 105	3.2 ± 0.1	2.8 ± 0.4	4.3 ± 0.3
	3		13.8 ± 0.1	52.6 ± 0.1	53.9 ± 0.1
	4	1415 ± 477	-2.8 ± 0.1	-12.1 ± 0.4	12.4 ± 0.4
221874	1	4631 ± 1266	-5.9 ± 0.1	0.0 ± 0.0	5.9 ± 0.1
	2	1561 ± 488	-3.7 ± 0.1	-4.0 ± 0.4	5.4 ± 0.3
	3		30.6 ± 0.1	-10.6 ± 0.4	32.2 ± 0.2
	4		-27.8 ± 0.1	-19.9 ± 0.3	33.7 ± 0.2
221883	1		-15.0 ± 0.1	3.4 ± 0.4	15.4 ± 0.1
	2		-11.7 ± 0.1	6.5 ± 0.4	13.4 ± 0.2
	3		-0.6 ± 0.1	0.0 ± 0.0	0.6 ± 0.1
	4	1893 ± 132	4.1 ± 0.1	-3.3 ± 0.4	5.3 ± 0.3
262590	1		-13.2 ± 0.1	0.4 ± 0.4	13.2 ± 0.1
	2	1962 ± 390	-3.9 ± 0.1	3.2 ± 0.4	5.0 ± 0.3

EVENT	TRK	P (MEV)	$\phi(^{\circ})$	$\delta(^{\circ})$	$\theta(^{\circ})$
	3	6653±1020	-3.1±0.1	0.0± 0.0	3.1± 0.1
	4		3.3±0.1	-10.2± 0.4	10.7± 0.4
262636	1		-11.9±0.1	-6.8± 0.4	13.7± 0.2
	2	8064±1264	-2.0±0.1	3.3± 0.4	3.9± 0.3
	3	3020± 472	6.7±0.1	0.0± 0.0	6.7± 0.1
	4		125.9±0.1	-26.3± 0.3	121.7± 0.1
310380	1	5057± 891	2.3±0.1	-1.5± 0.4	2.7± 0.2
	2	2372±1518	1.3±0.1	4.8± 0.4	5.0± 0.4
	3		-2.9±0.1	13.3± 0.3	13.6± 0.3
	4		-45.8±0.1	-32.7± 0.3	54.1± 0.2
330009	1		-0.7±0.1	30.7± 0.3	30.7± 0.3
	2	1210± 350	3.8±0.1	0.0± 0.0	3.8± 0.1
	3	5272±1500	5.3±0.1	0.0± 0.0	5.3± 0.1
	4		7.0±0.1	-2.7± 0.4	7.5± 0.2
330071	1	1850± 272	-7.4±0.1	2.5± 0.4	7.8± 0.2
	2	1896± 87	-1.2±0.1	0.7± 0.4	1.4± 0.2
	3		1.6±0.1	17.8± 0.3	17.9± 0.3
	4	1180± 227	12.4±0.1	-1.2± 0.4	12.5± 0.1
330141	1	2721± 748	-0.9±0.1	-3.6± 0.4	3.7± 0.4
	2	3562± 493	10.1±0.1	-2.0± 0.4	10.3± 0.1
	3	2904± 399	13.8±0.1	0.0± 0.0	13.8± 0.1
	4		-26.2±0.1	-8.6± 0.4	27.5± 0.1
330202	1		-22.9±0.1	26.3± 0.3	34.3± 0.2
	2		-3.4±0.1	22.0± 0.3	22.2± 0.3
	3	3477± 706	3.6±0.1	6.4± 0.4	7.3± 0.4
	4	3365± 990	24.9±0.1	-1.3± 0.4	24.9± 0.1
350606	1	795± 97	24.0±0.1	0.0± 0.0	24.0± 0.1
	2		19.5±0.1	8.0± 0.4	21.0± 0.2
	3	4958± 283	4.4±0.1	-2.3± 0.4	5.0± 0.2
	4	1156± 186	-2.5±0.1	-9.3± 0.4	9.6± 0.4
350694	1		-30.9±0.1	-8.2± 0.4	31.9± 0.1
	2	9695±2605	-2.6±0.1	0.1± 0.1	2.6± 0.1
	3	326± 34	7.2±0.1	4.7± 0.4	8.6± 0.2
	4		64.1±0.1	45.0± 0.2	72.0± 0.1
351262	1	1292± 239	9.9±0.1	-5.8± 0.4	11.5± 0.2
	2	2185± 531	2.8±0.1	4.1± 0.4	5.0± 0.3
	3	3365± 297	-3.5±0.1	-1.1± 0.4	3.7± 0.2
	4		-9.9±0.1	14.2± 0.3	17.3± 0.3

EVENT	TRK	P (MEV)	ϕ ($^{\circ}$)	δ ($^{\circ}$)	θ ($^{\circ}$)
370326	1	1430 \pm 127	-0.4 \pm 0.1	-5.1 \pm 0.4	5.1 \pm 0.4
	2		0.9 \pm 0.1	7.5 \pm 0.4	7.6 \pm 0.4
	3	1690 \pm 220	0.9 \pm 0.1	-6.3 \pm 0.4	6.4 \pm 0.4
	4		4.1 \pm 0.1	13.6 \pm 0.3	14.2 \pm 0.3
370492	1		-63.8 \pm 0.1	-18.1 \pm 0.3	65.2 \pm 0.1
	2	873 \pm 131	1.9 \pm 0.1	7.5 \pm 0.4	7.7 \pm 0.4
	3		3.3 \pm 0.1	10.2 \pm 0.4	10.7 \pm 0.4
	4		29.3 \pm 0.1	-43.1 \pm 0.2	50.4 \pm 0.2
380101	1		-26.0 \pm 0.1	-2.9 \pm 0.4	26.1 \pm 0.1
	2		-1.8 \pm 0.1	-9.9 \pm 0.4	10.1 \pm 0.4
	3	2337 \pm 305	1.9 \pm 0.1	4.8 \pm 0.4	5.2 \pm 0.4
	4		11.2 \pm 0.1	14.9 \pm 0.3	18.6 \pm 0.2
380157	1		-1.5 \pm 0.1	-3.1 \pm 0.4	3.4 \pm 0.4
	2		0.8 \pm 0.1	16.8 \pm 0.3	16.8 \pm 0.3
	3		2.3 \pm 0.1	-5.1 \pm 0.4	5.6 \pm 0.4
	4		17.8 \pm 0.1	-27.0 \pm 0.3	32.0 \pm 0.3
380266	1	1448 \pm 550	-9.5 \pm 0.1	7.2 \pm 0.4	11.9 \pm 0.3
	2	4210 \pm 308	1.1 \pm 0.1	1.2 \pm 0.4	1.6 \pm 0.3
	3	2701 \pm 273	3.6 \pm 0.1	-1.6 \pm 0.4	3.9 \pm 0.2
	4		18.4 \pm 0.1	-13.5 \pm 0.3	22.7 \pm 0.2
380318	1		-16.2 \pm 0.1	12.6 \pm 0.3	20.4 \pm 0.2
	2	4340 \pm 703	-4.0 \pm 0.1	3.7 \pm 0.4	5.4 \pm 0.3
	3	1167 \pm 91	2.4 \pm 0.1	4.9 \pm 0.4	5.5 \pm 0.4
	4		11.5 \pm 0.1	21.4 \pm 0.3	24.2 \pm 0.3
392026	1	638 \pm 64	-2.0 \pm 0.1	7.8 \pm 0.4	8.1 \pm 0.4
	2	2454 \pm 714	0.3 \pm 0.1	0.0 \pm 0.0	0.3 \pm 0.1
	3	2822 \pm 152	3.4 \pm 0.1	0.0 \pm 0.0	3.4 \pm 0.1
	4	74 \pm 1	26.7 \pm 0.1	-57.6 \pm 0.1	61.4 \pm 0.1
392042	1		-12.3 \pm 0.1	1.9 \pm 0.4	12.4 \pm 0.1
	2		-10.9 \pm 0.1	3.8 \pm 0.4	11.5 \pm 0.2
	3	2330 \pm 133	-3.1 \pm 0.1	-1.2 \pm 0.4	3.3 \pm 0.2
	4	1355 \pm 119	4.2 \pm 0.1	-4.6 \pm 0.4	6.2 \pm 0.3
392191	1	1991 \pm 402	-6.6 \pm 0.1	-4.7 \pm 0.4	8.1 \pm 0.2
	2	1491 \pm 304	-3.4 \pm 0.1	5.5 \pm 0.4	6.5 \pm 0.3
	3	2032 \pm 319	-2.8 \pm 0.1	-2.2 \pm 0.4	3.6 \pm 0.3
	4		25.3 \pm 0.1	-26.7 \pm 0.3	36.1 \pm 0.2
392230	1	1720 \pm 238	-10.2 \pm 0.1	-0.9 \pm 0.4	10.2 \pm 0.1
	2	2337 \pm 555	1.0 \pm 0.1	-3.9 \pm 0.4	4.0 \pm 0.4

EVENT	TRK	P (MEV)	ϕ ($^{\circ}$)	δ ($^{\circ}$)	θ ($^{\circ}$)
	3	1952 \pm 345	4.5 \pm 0.1	1.9 \pm 0.4	4.9 \pm 0.2
	4	3700 \pm 1000	5.2 \pm 0.1	6.1 \pm 0.4	8.0 \pm 0.3
400032	1	1177 \pm 149	-15.0 \pm 0.1	5.7 \pm 0.4	16.0 \pm 0.2
	2	3922 \pm 631	-3.9 \pm 0.1	0.1 \pm 0.1	3.9 \pm 0.1
	3	2620 \pm 316	1.8 \pm 0.1	5.2 \pm 0.4	5.5 \pm 0.4
	4		66.8 \pm 0.1	12.5 \pm 0.3	67.4 \pm 0.1
400092	1		-10.8 \pm 0.1	19.6 \pm 0.3	22.3 \pm 0.3
	2		-10.3 \pm 0.1	-3.3 \pm 0.4	10.8 \pm 0.2
	3		-1.4 \pm 0.1	20.5 \pm 0.3	20.5 \pm 0.3
	4		4.9 \pm 0.1	-9.6 \pm 0.4	10.8 \pm 0.4
400133	1	5736 \pm 1010	-4.0 \pm 0.1	0.9 \pm 0.4	4.1 \pm 0.1
	2	3195 \pm 343	2.8 \pm 0.1	1.3 \pm 0.4	3.1 \pm 0.2
	3		53.9 \pm 0.1	-6.8 \pm 0.4	54.2 \pm 0.1
	4		128.8 \pm 0.1	-34.2 \pm 0.3	121.2 \pm 0.1
400146	1	685 \pm 33	-8.6 \pm 0.1	1.3 \pm 0.4	8.7 \pm 0.1
	2	966 \pm 61	-1.9 \pm 0.1	-2.0 \pm 0.4	2.8 \pm 0.3
	3	4444 \pm 304	-0.4 \pm 0.1	0.0 \pm 0.0	0.4 \pm 0.1
	4		17.7 \pm 0.1	19.2 \pm 0.3	25.9 \pm 0.2
400153	1		-20.9 \pm 0.1	-12.8 \pm 0.3	24.4 \pm 0.2
	2		-20.3 \pm 0.1	17.6 \pm 0.3	26.6 \pm 0.2
	3	8467 \pm 2278	5.5 \pm 0.1	2.2 \pm 0.4	5.9 \pm 0.2
	4		41.9 \pm 0.1	-29.7 \pm 0.3	49.7 \pm 0.2
400197	1		-12.1 \pm 0.1	-11.0 \pm 0.4	16.3 \pm 0.3
	2	5213 \pm 4124	-3.7 \pm 0.1	0.0 \pm 0.0	3.7 \pm 0.1
	3	905 \pm 174	11.8 \pm 0.1	-5.8 \pm 0.4	13.1 \pm 0.2
	4		23.8 \pm 0.1	17.3 \pm 0.3	29.1 \pm 0.2
400263	1	2389 \pm 208	-9.0 \pm 0.1	-1.9 \pm 0.4	9.2 \pm 0.1
	2	3818 \pm 595	1.8 \pm 0.1	3.8 \pm 0.4	4.2 \pm 0.4
	3	1074 \pm 201	4.0 \pm 0.1	3.6 \pm 0.4	5.4 \pm 0.3
	4		35.3 \pm 0.1	-18.5 \pm 0.3	39.3 \pm 0.2
410038	1		28.7 \pm 0.1	-8.9 \pm 0.3	29.9 \pm 0.1
	2	2813 \pm 405	-2.4 \pm 0.1	-1.4 \pm 0.3	2.8 \pm 0.2
	3		-3.4 \pm 0.1	11.9 \pm 0.3	12.4 \pm 0.3
	4		-12.7 \pm 0.1	-11.1 \pm 0.3	16.8 \pm 0.2
443488	1		-9.9 \pm 0.1	13.3 \pm 0.3	16.5 \pm 0.2
	2	2580 \pm 323	1.5 \pm 0.1	0.0 \pm 0.0	1.5 \pm 0.1
	3		5.7 \pm 0.1	-30.8 \pm 0.3	31.3 \pm 0.3
	4		13.9 \pm 0.1	31.2 \pm 0.3	33.9 \pm 0.3

EVENT	TRK	P(MEV)	$\phi(^{\circ})$	$\delta(^{\circ})$	$\theta(^{\circ})$
443513	1		-29.1 ± 0.1	-22.0 ± 0.3	35.9 ± 0.2
	2		-26.9 ± 0.1	-45.1 ± 0.2	51.0 ± 0.2
	3		-5.2 ± 0.1	7.8 ± 0.4	9.4 ± 0.3
	4	1282 ± 96	12.3 ± 0.1	0.0 ± 0.0	12.3 ± 0.1
443520	1		-15.1 ± 0.1	0.0 ± 0.0	15.1 ± 0.1
	2	329 ± 28	-11.8 ± 0.1	-2.3 ± 0.4	12.0 ± 0.1
	3	2740 ± 404	-2.7 ± 0.1	-2.5 ± 0.4	3.7 ± 0.3
	4		32.7 ± 0.1	8.9 ± 0.4	33.8 ± 0.1
461399	1		-5.2 ± 0.1	-2.6 ± 0.4	5.8 ± 0.2
	2		-0.9 ± 0.1	-7.5 ± 0.4	7.6 ± 0.4
	3	517 ± 29	0.5 ± 0.1	7.2 ± 0.4	7.2 ± 0.4
	4	6548 ± 855	2.9 ± 0.1	0.0 ± 0.0	2.9 ± 0.1
461410	1	164 ± 15	-2.5 ± 0.1	-1.9 ± 0.4	3.1 ± 0.3
	2	3561 ± 337	3.0 ± 0.1	1.8 ± 0.4	3.5 ± 0.2
	3	3720 ± 1539	5.5 ± 0.1	-2.8 ± 0.4	6.2 ± 0.2
	4		7.7 ± 0.1	15.2 ± 0.3	17.0 ± 0.3
461911	1	1307 ± 390	-8.8 ± 0.1	-3.0 ± 0.4	9.3 ± 0.2
	2	100 ± 7	-4.2 ± 0.1	12.4 ± 0.4	13.1 ± 0.4
	3	4258 ± 610	6.0 ± 0.1	1.5 ± 0.4	6.2 ± 0.1
	4	566 ± 35	7.5 ± 0.1	1.5 ± 0.4	7.6 ± 0.1
461957	1	5524 ± 540	-0.1 ± 0.1	2.0 ± 0.4	2.0 ± 0.4
	2	7059 ± 1770	3.1 ± 0.1	-2.3 ± 0.4	3.9 ± 0.3
	3		6.2 ± 0.1	-15.3 ± 0.3	16.5 ± 0.3
	4		-39.7 ± 0.1	16.6 ± 0.4	42.5 ± 0.2
461987	1		-2.9 ± 0.1	6.7 ± 0.4	7.3 ± 0.4
	2	1562 ± 285	-0.4 ± 0.1	0.1 ± 0.1	0.4 ± 0.1
	3		3.7 ± 0.1	-40.6 ± 0.2	40.7 ± 0.2
	4		6.1 ± 0.1	1.5 ± 0.4	6.3 ± 0.1
481110	1		3.3 ± 0.1	-6.5 ± 0.4	7.3 ± 0.4
	2	4590 ± 617	-2.2 ± 0.1	0.2 ± 0.2	2.2 ± 0.1
	3	1600 ± 870	-17.0 ± 0.1	6.5 ± 0.4	18.2 ± 0.2
	4		-24.0 ± 0.1	-26.0 ± 0.3	34.8 ± 0.2
481132	1	1943 ± 222	-4.3 ± 0.1	2.4 ± 0.4	4.9 ± 0.2
	2	1227 ± 173	-10.7 ± 0.1	1.1 ± 0.4	10.8 ± 0.1
	3		-15.1 ± 0.1	-5.4 ± 0.4	16.0 ± 0.2
	4		-38.0 ± 0.1	-15.5 ± 0.3	40.6 ± 0.1
481148	1		-41.8 ± 0.1	15.7 ± 0.3	44.1 ± 0.1
	2	4786 ± 617	-4.1 ± 0.1	0.0 ± 0.0	4.1 ± 0.1

EVENT	TRK	P (MEV)	$\phi (^{\circ})$	$\delta (^{\circ})$	$\theta (P)$
	3	2169 \pm 100	0.5 \pm 0.1	-1.0 \pm 0.4	1.1 \pm 0.4
	4		35.6 \pm 0.1	18.8 \pm 0.3	39.7 \pm 0.2
480820	1		-23.5 \pm 0.1	-14.2 \pm 0.4	27.2 \pm 0.2
	2		-6.2 \pm 0.1	-8.6 \pm 0.4	10.6 \pm 0.3
	3		-5.6 \pm 0.1	-8.6 \pm 0.4	10.3 \pm 0.3
	4		-2.4 \pm 0.1	25.5 \pm 0.3	25.6 \pm 0.3
560057	1		12.8 \pm 0.1	-7.7 \pm 0.3	14.9 \pm 0.2
	2	1815 \pm 433	2.2 \pm 0.1	-0.6 \pm 0.3	2.3 \pm 0.1
	3		-4.0 \pm 0.1	20.3 \pm 0.3	20.7 \pm 0.3
	4		-27.1 \pm 0.1	-4.4 \pm 0.6	27.4 \pm 0.1
690002	1		-8.2 \pm 0.1	-4.8 \pm 0.6	9.5 \pm 0.3
	2		-7.0 \pm 0.1	-8.4 \pm 0.6	10.9 \pm 0.5
	3		7.0 \pm 0.1	-7.0 \pm 0.6	9.9 \pm 0.4
	4		35.9 \pm 0.1	-18.3 \pm 0.6	39.7 \pm 0.3
690064	1		-2.7 \pm 0.1	4.2 \pm 0.6	5.0 \pm 0.5
	2		18.8 \pm 0.1	-21.1 \pm 0.5	28.0 \pm 0.4
	3		175.9 \pm 0.1	-23.7 \pm 0.5	156.0 \pm 0.5
	4		-16.2 \pm 0.1	-44.3 \pm 0.3	46.6 \pm 0.3
760091	1		-27.7 \pm 0.1	-9.5 \pm 0.6	29.2 \pm 0.2
	2	3732 \pm 894	1.2 \pm 0.1	2.0 \pm 0.6	2.3 \pm 0.5
	3	386 \pm 150	41.4 \pm 0.1	-4.2 \pm 0.6	41.6 \pm 0.1
	4		-20.1 \pm 0.1	-26.2 \pm 0.5	32.6 \pm 0.4
760109	1		-19.4 \pm 0.1	34.5 \pm 0.4	39.0 \pm 0.3
	2	1019 \pm 147	5.1 \pm 0.1	0.0 \pm 0.0	5.1 \pm 0.1
	3	580 \pm 147	19.3 \pm 0.1	-1.5 \pm 0.6	19.4 \pm 0.1
	4		116.5 \pm 0.1	-8.7 \pm 0.6	116.2 \pm 0.1
780138	1	3463 \pm 559	3.6 \pm 0.1	-1.6 \pm 0.3	3.9 \pm 0.2
	2	2304 \pm 849	3.0 \pm 0.1	3.6 \pm 0.3	4.7 \pm 0.2
	3	7601 \pm 2689	2.3 \pm 0.1	-4.1 \pm 0.3	4.7 \pm 0.3
	4		-45.2 \pm 0.1	34.6 \pm 0.2	54.5 \pm 0.1
850052	1		24.9 \pm 0.1	-8.4 \pm 0.3	26.2 \pm 0.1
	2	1227 \pm 606	9.1 \pm 0.1	5.8 \pm 0.3	10.8 \pm 0.2
	3	2194 \pm 648	-9.1 \pm 0.1	2.1 \pm 0.3	9.3 \pm 0.1
	4		-47.8 \pm 0.1	-16.3 \pm 0.3	49.9 \pm 0.1
190155	1		-16.9 \pm 0.1	12.2 \pm 0.4	20.7 \pm 0.2
	2	1186 \pm 501	-7.7 \pm 0.1	2.8 \pm 0.4	8.2 \pm 0.2
	3	3282 \pm 809	1.0 \pm 0.1	-6.5 \pm 0.4	6.6 \pm 0.4
	4	1391 \pm 283	6.8 \pm 0.1	-6.5 \pm 0.4	9.4 \pm 0.3

EVENT	TRK	P (MEV)	ϕ (°)	δ (°)	θ (°)
	5	739± 133	29.2±0.1	-4.5± 0.4	29.5± 0.1
	P	1580±1100	-15.4±0.1	5.5± 0.4	16.3± 0.2
190182	1	7300±1266	-4.1±0.1	4.5± 0.4	6.1± 0.3
	2	3694± 291	0.5±0.1	-1.3± 0.4	1.4± 0.4
	3		3.1±0.1	-10.8± 0.4	11.2± 0.4
	4	3091±2044	4.8±0.1	6.5± 0.4	8.1± 0.3
	5		8.2±0.1	-10.9± 0.4	13.6± 0.3
	P	465± 160	36.3±0.1	7.7± 0.4	37.0± 0.1
221712	1	2152± 158	-3.0±0.1	0.0± 0.0	3.0± 0.1
	2	642± 111	-1.3±0.1	-4.7± 0.4	4.9± 0.4
	3	1773± 540	-1.0±0.1	6.2± 0.4	6.3± 0.4
	4	2945± 600	2.9±0.1	5.4± 0.4	6.1± 0.4
	5	3911± 367	6.7±0.1	0.8± 0.4	6.7± 0.1
	P	345± 25	-66.8±0.1	-47.8± 0.2	74.7± 0.1
240451	1	799± 131	7.6±0.1	-9.5± 0.4	12.1± 0.3
	2	5662± 511	4.1±0.1	-1.6± 0.4	4.4± 0.2
	3		0.8±0.1	22.7± 0.3	22.7± 0.3
	4	3483± 487	-5.9±0.1	1.8± 0.4	6.2± 0.2
	5		-85.9±0.1	-11.5± 0.4	86.0± 0.1
	P	360± 4	28.5±0.1	40.1± 0.6	47.8± 0.5
320001	1		-77.2±0.1	17.8± 0.3	77.8± 0.1
	2		-19.1±0.1	-26.7± 0.3	32.4± 0.2
	3	8064±2008	-0.5±0.1	4.0± 0.4	4.0± 0.4
	4	2976±1535	4.1±0.1	-3.3± 0.4	5.3± 0.3
	5		17.0±0.1	-29.7± 0.3	33.8± 0.3
	P	356± 4	-54.1±0.1	-38.7± 0.2	62.8± 0.1
330193	i		-9.7±0.1	11.6± 0.4	15.1± 0.3
	2	3463± 401	-8.4±0.1	-3.5± 0.4	9.1± 0.2
	3	1783± 519	3.3±0.1	-8.8± 0.4	9.4± 0.4
	4	1675± 305	7.4±0.1	-5.3± 0.4	9.1± 0.2
	5		3.3±0.1	44.7± 0.2	44.8± 0.2
	P	19± 1	-59.3±1.5	0.6± 0.6	59.3± 1.5
350642	1	2076± 267	0.0±0.1	-1.9± 0.4	1.9± 0.4
	2		-18.2±0.1	-5.4± 0.4	19.0± 0.1
	3		-20.1±0.1	-5.4± 0.4	20.8± 0.1
	4		178.6±0.1	-1.8± 0.4	177.7± 0.3
	5	2241± 851	16.3±0.1	10.9± 0.4	19.5± 0.2
	P	208± 2	37.6±0.1	15.3± 0.3	40.2± 0.1

EVENT	TRK	P (MEV)	ϕ ($^{\circ}$)	δ ($^{\circ}$)	θ ($^{\circ}$)
351215	1	708 \pm 142	31.0 \pm 0.1	-11.4 \pm 0.4	32.8 \pm 0.2
	2	6001 \pm 1088	2.3 \pm 0.1	-2.4 \pm 0.4	3.3 \pm 0.3
	3		-1.4 \pm 0.1	6.6 \pm 0.4	6.7 \pm 0.4
	4	1388 \pm 488	-5.4 \pm 0.1	2.5 \pm 0.4	5.9 \pm 0.2
	5	2460 \pm 1490	-10.7 \pm 0.1	2.6 \pm 0.4	11.0 \pm 0.1
	P		-67.3 \pm 0.1	-23.5 \pm 0.3	69.3 \pm 0.1
351288	1	1229 \pm 596	4.0 \pm 0.1	-3.4 \pm 0.4	5.2 \pm 0.3
	2	636 \pm 95	3.8 \pm 0.1	6.7 \pm 0.4	7.7 \pm 0.4
	3	1892 \pm 243	2.7 \pm 0.1	2.3 \pm 0.4	3.5 \pm 0.3
	4		-8.5 \pm 0.1	-12.0 \pm 0.4	14.7 \pm 0.3
	5	321 \pm 30	-21.9 \pm 0.1	0.1 \pm 0.1	21.9 \pm 0.1
	P	350 \pm 3	-0.6 \pm 0.1	24.1 \pm 0.3	24.1 \pm 0.3
370190	1	3219 \pm 1029	-6.6 \pm 0.1	-1.2 \pm 0.4	6.7 \pm 0.1
	2	1919 \pm 169	-5.7 \pm 0.1	2.9 \pm 0.4	6.4 \pm 0.2
	3		-1.9 \pm 0.1	-25.0 \pm 0.3	25.1 \pm 0.3
	4		6.5 \pm 0.1	20.4 \pm 0.3	21.4 \pm 0.3
	5		12.4 \pm 0.1	11.7 \pm 0.3	17.0 \pm 0.2
	P	37 \pm 1	-47.0 \pm 0.1	0.2 \pm 0.2	47.0 \pm 0.1
370338	1		-12.7 \pm 0.1	-12.2 \pm 0.4	17.5 \pm 0.3
	2		-3.6 \pm 0.1	-3.7 \pm 0.4	5.2 \pm 0.3
	3	2233 \pm 250	-2.8 \pm 0.1	0.0 \pm 0.0	2.8 \pm 0.1
	4	2189 \pm 253	2.4 \pm 0.1	0.0 \pm 0.0	2.4 \pm 0.1
	5		3.1 \pm 0.1	9.1 \pm 0.4	9.6 \pm 0.4
	P	85 \pm 1	-65.3 \pm 0.1	20.9 \pm 0.7	67.0 \pm 0.1
380036	1	1273 \pm 182	-2.2 \pm 0.1	6.4 \pm 0.4	6.8 \pm 0.4
	2		3.4 \pm 0.1	-6.6 \pm 0.4	7.4 \pm 0.4
	3	474 \pm 103	6.2 \pm 0.1	10.2 \pm 0.4	11.9 \pm 0.3
	4	1003 \pm 123	10.0 \pm 0.1	0.0 \pm 0.0	10.0 \pm 0.1
	5		10.9 \pm 0.1	13.3 \pm 0.3	17.1 \pm 0.2
	P	452 \pm 6	9.4 \pm 0.1	-6.6 \pm 0.4	11.5 \pm 0.2
380105	1		-9.1 \pm 0.1	8.7 \pm 0.4	12.6 \pm 0.3
	2		-7.3 \pm 0.1	10.7 \pm 0.4	12.9 \pm 0.3
	3	1039 \pm 252	-1.1 \pm 0.1	-5.7 \pm 0.4	5.8 \pm 0.4
	4	3005 \pm 432	0.9 \pm 0.1	-3.0 \pm 0.4	3.1 \pm 0.4
	5	2836 \pm 395	5.7 \pm 0.1	2.8 \pm 0.4	6.3 \pm 0.2
	P	103 \pm 1	-23.6 \pm 0.1	33.9 \pm 0.6	40.5 \pm 0.5
392178	1		-24.3 \pm 0.1	42.0 \pm 0.2	47.4 \pm 0.2
	2		-6.4 \pm 0.1	6.2 \pm 0.4	8.9 \pm 0.3
	3	857 \pm 105	-0.7 \pm 0.1	-5.1 \pm 0.4	5.1 \pm 0.4
	4	3022 \pm 478	-0.6 \pm 0.1	-3.6 \pm 0.4	3.6 \pm 0.4

EVENT	TRK	P(MEV)	$\phi(^{\circ})$	$\delta(^{\circ})$	$\theta(^{\circ})$
	5	2667± 203	17.3±0.1	0.0± 0.0	17.3± 0.1
	P	570± 360	-1.2±0.1	5.8± 0.4	5.9± 0.4
400204	1	3550±2184	-1.0±0.1	-3.5± 0.4	3.6± 0.4
	2		2.4±0.1	-18.4± 0.3	18.6± 0.3
	3	2836± 828	6.4±0.1	11.0± 0.4	12.7± 0.3
	4	438± 41	13.3±0.1	3.7± 0.4	13.8± 0.1
	5	4375± 930	14.8±0.1	-4.6± 0.4	15.5± 0.2
	P	131± 1	67.5±0.1	-2.1± 0.6	67.5± 0.1
480886	1		-0.2±0.1	6.1± 0.4	6.1± 0.4
	2		-0.3±0.1	0.1± 0.1	0.3± 0.1
	3		0.1±0.1	0.0± 0.0	0.1± 0.1
	4		5.8±0.1	5.2± 0.4	7.8± 0.3
	5		14.4±0.1	0.0± 0.0	14.4± 0.1
	P	75± 1	-2.0±0.1	28.9± 0.5	29.0± 0.5
480909	1		-42.4±0.1	5.1± 0.4	42.6± 0.1
	2		11.3±0.1	-12.2± 0.4	16.6± 0.3
	3		21.6±0.1	8.1± 0.4	23.0± 0.2
	4		34.7±0.1	-36.6± 0.2	48.7± 0.1
	5		44.1±0.1	28.5± 0.3	50.9± 0.2
	P	278± 3	51.3±0.1	-31.5± 0.3	57.8± 0.1
560053	1		8.5±0.1	18.2± 0.3	20.0± 0.3
	2	1835± 646	3.4±0.1	3.6± 0.3	5.0± 0.2
	3	1287± 325	1.8±0.1	1.6± 0.3	2.4± 0.2
	4		-3.1±0.1	7.6± 0.3	8.2± 0.3
	5	2603± 710	-5.0±0.1	-1.8± 0.3	5.3± 0.1
	P	448± 5	-18.3±0.1	-44.5± 0.3	47.4± 0.3
650015	1		9.8±0.1	-7.8± 0.5	12.5± 0.3
	2		-2.1±0.1	-6.1± 0.5	6.4± 0.5
	3	4462±1091	-5.6±0.1	1.4± 0.3	5.8± 0.1
	4	236± 48	-5.6±0.1	1.4± 0.3	5.8± 0.1
	5	1069± 321	-7.9±0.1	7.2± 0.3	10.7± 0.2
	P	259± 3	46.2±0.1	41.9± 0.3	59.0± 0.2
780010	1	1098± 399	18.2±0.1	-6.8± 0.3	19.4± 0.1
	2		12.2±0.1	-30.4± 0.2	32.5± 0.2
	3	673± 186	8.7±0.1	1.6± 0.3	8.8± 0.1
	4	3982±1174	3.1±0.1	-3.0± 0.3	4.3± 0.2
	5		-38.0±0.1	-15.9± 0.3	40.7± 0.1
	P	24± 1	-40.0±0.1	-1.4± 0.3	40.0± 0.1

EVENT	TRK	P (MEV)	$\phi(^{\circ})$	$\delta(^{\circ})$	$\theta(^{\circ})$
850055	1		176.0 ± 0.1	-30.7 ± 0.2	149.1 ± 0.2
	2		10.1 ± 0.1	-14.7 ± 0.3	17.8 ± 0.3
	3		4.2 ± 0.1	-8.3 ± 0.3	9.3 ± 0.3
	4	641 ± 283	-3.6 ± 0.1	9.5 ± 0.3	10.2 ± 0.3
	5	4262 ± 1968	-10.1 ± 0.1	3.2 ± 0.3	10.6 ± 0.1
	P	29 ± 1	-48.4 ± 0.1	33.0 ± 7.1	56.2 ± 3.1
150061	1		8.9 ± 0.1	14.0 ± 0.3	16.5 ± 0.3
	2	1130 ± 161	6.6 ± 0.1	7.0 ± 0.4	9.6 ± 0.3
	3	4243 ± 495	-1.7 ± 0.1	2.7 ± 0.4	3.2 ± 0.3
	4	840 ± 163	-2.6 ± 0.1	2.7 ± 0.5	3.7 ± 0.4
	5		-9.3 ± 0.1	10.8 ± 0.4	14.2 ± 0.3
	6		-22.8 ± 0.1	-58.8 ± 0.1	61.5 ± 0.1
150105	1		-4.4 ± 0.1	-39.3 ± 0.2	39.5 ± 0.2
	2		-3.3 ± 0.1	6.2 ± 0.4	7.0 ± 0.4
	3	1091 ± 332	-3.0 ± 0.1	7.8 ± 0.4	8.4 ± 0.4
	4		4.1 ± 0.1	-13.6 ± 0.3	14.2 ± 0.3
	5	3970 ± 878	7.1 ± 0.1	6.7 ± 0.4	9.8 ± 0.3
	6		38.8 ± 0.1	-46.4 ± 0.2	57.5 ± 0.1
150118	1		13.8 ± 0.1	18.0 ± 0.3	22.5 ± 0.2
	2	2712 ± 510	10.8 ± 0.1	5.4 ± 0.4	12.1 ± 0.2
	3	1839 ± 213	1.6 ± 0.1	-1.3 ± 0.4	2.1 ± 0.3
	4		-0.8 ± 0.1	-10.1 ± 0.4	10.1 ± 0.4
	5		-1.4 ± 0.1	-15.9 ± 0.3	16.0 ± 0.3
	6		-2.5 ± 0.1	-20.5 ± 0.3	20.6 ± 0.3
150139	1		34.0 ± 0.1	18.7 ± 0.3	38.3 ± 0.2
	2		2.7 ± 0.1	-12.2 ± 0.4	12.5 ± 0.4
	3	6222 ± 533	1.6 ± 0.1	2.9 ± 0.4	3.3 ± 0.4
	4		-9.4 ± 0.1	12.1 ± 0.4	15.3 ± 0.3
	5	1024 ± 56	-11.9 ± 0.1	0.0 ± 0.0	11.9 ± 0.1
	6	294 ± 35	-32.5 ± 0.1	7.2 ± 0.4	33.2 ± 0.1
182973	1		-21.4 ± 0.1	-11.2 ± 0.4	24.0 ± 0.2
	2		-16.3 ± 0.1	-15.4 ± 0.3	22.3 ± 0.2
	3		-0.7 ± 0.1	-17.7 ± 0.3	17.7 ± 0.3
	4	1810 ± 722	2.3 ± 0.1	-4.5 ± 0.4	5.1 ± 0.4
	5	2895 ± 459	10.3 ± 0.1	-4.1 ± 0.4	11.1 ± 0.2
	6		11.3 ± 0.1	-5.9 ± 0.4	12.7 ± 0.2
183093	1		-16.7 ± 0.1	10.4 ± 0.4	19.6 ± 0.2
	2	1829 ± 163	-1.0 ± 0.1	-6.2 ± 0.4	6.3 ± 0.4
	3	1951 ± 119	5.8 ± 0.1	0.0 ± 0.0	5.8 ± 0.1
	4	2553 ± 299	5.9 ± 0.1	-4.5 ± 0.4	7.4 ± 0.3

EVENT	TRK	P(MEV)	$\phi(^{\circ})$	$\delta(^{\circ})$	$\theta(^{\circ})$
	5		44.9 ± 0.1	-23.9 ± 0.3	49.6 ± 0.1
	6		-5.8 ± 0.1	4.0 ± 0.4	7.0 ± 0.2
221641	1	1430 ± 472	-11.4 ± 0.1	-7.4 ± 0.4	13.6 ± 0.2
	2	1866 ± 1026	-3.1 ± 0.1	12.3 ± 0.4	17.7 ± 0.4
	3	762 ± 404	17.9 ± 0.1	-7.9 ± 0.4	19.5 ± 0.2
	4		34.4 ± 0.1	-20.4 ± 0.3	39.3 ± 0.2
	5		63.6 ± 0.1	29.9 ± 0.3	67.3 ± 0.1
	6		3.3 ± 0.1	35.3 ± 0.3	35.4 ± 0.3
221791	1		-31.3 ± 0.1	23.9 ± 0.3	38.6 ± 0.2
	2	7894 ± 1695	-2.0 ± 0.1	0.0 ± 0.0	2.0 ± 0.1
	3	5285 ± 547	3.6 ± 0.1	0.0 ± 0.0	3.6 ± 0.1
	4	541 ± 169	4.1 ± 0.1	-11.2 ± 0.4	11.9 ± 0.4
	5	198 ± 28	18.2 ± 0.1	-11.4 ± 0.4	21.4 ± 0.2
	6	230 ± 18	32.9 ± 0.1	-21.9 ± 0.3	38.8 ± 0.2
282667	1		-6.7 ± 0.1	-3.4 ± 0.4	7.5 ± 0.2
	2	3994 ± 886	-6.3 ± 0.1	-1.6 ± 0.4	6.5 ± 0.1
	3	1969 ± 632	8.4 ± 0.1	0.2 ± 0.2	8.4 ± 0.1
	4	922 ± 107	9.4 ± 0.1	1.3 ± 0.4	9.5 ± 0.1
	5		65.1 ± 0.1	-22.9 ± 0.3	67.2 ± 0.1
	6	290 ± 25	7.7 ± 0.1	8.1 ± 0.4	11.2 ± 0.3
310394	1	3664 ± 1622	2.8 ± 0.1	3.4 ± 0.4	4.4 ± 0.3
	2	2119 ± 344	3.0 ± 0.1	-5.8 ± 0.4	6.5 ± 0.4
	3	1110 ± 324	-1.0 ± 0.1	-9.3 ± 0.4	9.4 ± 0.4
	4	865 ± 208	-1.8 ± 0.1	4.7 ± 0.4	5.0 ± 0.4
	5		-3.7 ± 0.1	-20.0 ± 0.3	20.3 ± 0.3
	6		-17.0 ± 0.1	11.0 ± 0.4	20.2 ± 0.2
320105	1		-15.6 ± 0.1	-8.1 ± 0.4	17.5 ± 0.2
	2		-7.4 ± 0.1	-14.2 ± 0.3	16.0 ± 0.3
	3		-0.6 ± 0.1	-11.0 ± 0.4	11.0 ± 0.4
	4	2057 ± 672	0.1 ± 0.1	-2.3 ± 0.4	2.3 ± 0.4
	5		3.6 ± 0.1	-3.8 ± 0.4	5.2 ± 0.3
	6		10.0 ± 0.1	-10.2 ± 0.4	14.2 ± 0.3
330135	1	193 ± 43	-24.7 ± 0.1	6.0 ± 0.4	25.4 ± 0.1
	2	1359 ± 210	-16.3 ± 0.1	3.9 ± 0.4	16.7 ± 0.1
	3		-4.5 ± 0.1	-11.5 ± 0.4	12.3 ± 0.4
	4	2581 ± 724	-0.2 ± 0.1	4.7 ± 0.4	4.7 ± 0.4
	5	3032 ± 290	6.5 ± 0.1	0.9 ± 0.4	6.6 ± 0.1
	6		26.3 ± 0.1	12.9 ± 0.3	29.1 ± 0.2

EVENT	TRK	P (MEV)	$\phi (^{\circ})$	$\delta (^{\circ})$	$\theta (^{\circ})$
330266	1		-62.7 ± 0.1	-19.3 ± 0.3	64.3 ± 0.1
	2	343 ± 87	-22.9 ± 0.1	-5.6 ± 0.4	23.5 ± 0.1
	3		-12.9 ± 0.1	-22.1 ± 0.3	25.4 ± 0.3
	4	1279 ± 148	-6.2 ± 0.1	1.9 ± 0.4	6.5 ± 0.2
	5		4.9 ± 0.1	21.4 ± 0.3	21.9 ± 0.3
	6	593 ± 60	22.6 ± 0.1	2.6 ± 0.4	22.7 ± 0.1
351207	1	2289 ± 904	-22.2 ± 0.1	-2.4 ± 0.4	22.3 ± 0.1
	2		-14.7 ± 0.1	11.3 ± 0.4	18.5 ± 0.3
	3	4457 ± 930	-3.6 ± 0.1	6.2 ± 0.4	7.2 ± 0.3
	4		6.8 ± 0.1	-12.3 ± 0.3	14.0 ± 0.3
	5		7.0 ± 0.1	39.1 ± 0.2	39.6 ± 0.2
	6		10.5 ± 0.1	20.7 ± 0.3	23.1 ± 0.3
351214	1		-25.4 ± 0.1	8.7 ± 0.4	26.8 ± 0.2
	2		-11.1 ± 0.1	-61.2 ± 0.1	61.8 ± 0.1
	3	2383 ± 191	-7.8 ± 0.1	-1.6 ± 0.4	8.0 ± 0.1
	4	893 ± 90	-5.9 ± 0.1	2.0 ± 0.4	6.2 ± 0.2
	5	3043 ± 122	6.8 ± 0.1	0.0 ± 0.0	6.8 ± 0.1
	6		34.8 ± 0.1	37.1 ± 0.2	49.1 ± 0.1
351240	1		-9.3 ± 0.1	-35.1 ± 0.2	36.2 ± 0.2
	2		-2.2 ± 0.1	-6.1 ± 0.4	6.5 ± 0.4
	3	2948 ± 744	-1.9 ± 0.1	0.0 ± 0.0	1.9 ± 0.1
	4	1872 ± 528	12.1 ± 0.1	5.6 ± 0.4	13.3 ± 0.2
	5		13.7 ± 0.1	-7.7 ± 0.4	15.7 ± 0.2
	6		-59.7 ± 0.1	52.7 ± 0.0	72.2 ± 0.1
351247	1		-9.7 ± 0.1	3.8 ± 0.4	10.4 ± 0.2
	2	2993 ± 589	-7.3 ± 0.1	0.7 ± 0.4	7.3 ± 0.1
	3	2825 ± 1300	-2.4 ± 0.1	-8.6 ± 0.3	8.9 ± 0.3
	4		-2.1 ± 0.1	11.2 ± 0.4	11.4 ± 0.4
	5		0.4 ± 0.1	4.9 ± 0.4	4.9 ± 0.4
	6		38.1 ± 0.1	14.2 ± 0.3	40.3 ± 0.1
351267	1		-48.0 ± 0.1	65.9 ± 0.2	74.1 ± 0.1
	2	428 ± 61	-3.4 ± 0.1	-3.9 ± 0.4	5.2 ± 0.3
	3	6319 ± 542	-2.0 ± 0.1	0.0 ± 0.0	2.0 ± 0.1
	4	1280 ± 332	-1.4 ± 0.1	-9.6 ± 0.4	9.7 ± 0.4
	5		3.5 ± 0.1	-19.5 ± 0.3	19.8 ± 0.3
	6	1861 ± 199	6.4 ± 0.1	-0.4 ± 0.4	6.4 ± 0.1
370084	1	1798 ± 284	-13.9 ± 0.1	-3.6 ± 0.4	14.3 ± 0.1
	2	2511 ± 402	-8.6 ± 0.1	4.6 ± 0.4	9.7 ± 0.2
	3	4796 ± 874	-2.4 ± 0.1	0.0 ± 0.0	2.4 ± 0.1
	4	2560 ± 414	1.7 ± 0.1	1.3 ± 0.4	2.1 ± 0.3

EVENT	TRK	P (MEV)	$\phi(^{\circ})$	$\delta(^{\circ})$	$\theta(^{\circ})$
	5	1587± 374	16.5±0.1	-1.2± 0.4	16.5± 0.1
	6		35.0±0.1	15.9± 0.3	38.0± 0.1
370249	1		-41.4±0.1	-5.5± 0.4	41.7± 0.1
	2		-7.6±0.1	16.7± 0.3	18.3± 0.3
	3		0.0±0.1	-10.8± 0.4	10.8± 0.4
	4		5.4±0.1	-18.8± 0.3	19.5± 0.3
	5	3755±1061	7.1±0.1	6.7± 0.4	9.8± 0.3
	6		9.9±0.1	19.8± 0.3	22.0± 0.3
380049	1		-6.8±0.1	-11.9± 0.4	13.7± 0.3
	2	990± 394	-3.2±0.1	13.6± 0.3	14.0± 0.3
	3	2101± 245	-2.2±0.1	-1.5± 0.4	2.7± 0.2
	4	5756±1084	0.1±0.1	5.1± 0.4	5.1± 0.4
	5	3569± 685	3.5±0.1	4.2± 0.4	5.5± 0.3
	6		5.5±0.1	-5.6± 0.4	7.8± 0.3
380068	1		-49.0±0.1	16.8± 0.3	51.1± 0.1
	2	1426± 194	-2.5±0.1	-2.8± 0.4	3.8± 0.3
	3	1695± 188	1.0±0.1	2.8± 0.4	3.0± 0.4
	4	1526± 212	2.7±0.1	1.5± 0.4	3.1± 0.2
	5		7.8±0.1	9.5± 0.3	12.3± 0.2
	6	247± 14	83.0±0.1	-4.0± 0.4	83.0± 0.1
400071	1	2942± 381	-15.3±0.1	-4.9± 0.4	16.0± 0.2
	2	1753± 393	-2.6±0.1	-9.4± 0.4	9.7± 0.4
	3	2833± 265	-1.9±0.1	-2.7± 0.4	3.3± 0.3
	4	2177± 321	3.3±0.1	-2.3± 0.4	4.0± 0.2
	5	1361± 175	10.5±0.1	0.0± 0.0	10.5± 0.1
	6		18.8±0.1	27.0± 0.3	32.5± 0.2
400282	1		-50.8±0.1	-46.9± 0.2	64.4± 0.1
	2		-9.9±0.1	18.0± 0.3	20.5± 0.3
	3		-2.5±0.1	2.8± 0.4	3.8± 0.3
	4	1985± 290	2.8±0.1	-2.9± 0.4	4.0± 0.3
	5		3.4±0.1	4.9± 0.4	6.0± 0.3
	6		5.7±0.1	8.5± 0.4	10.2± 0.3
400300	1	2632± 351	-41.3±0.1	2.3± 0.4	41.4± 0.1
	2		-10.0±0.1	-10.8± 0.4	14.7± 0.3
	3	388± 76	-4.5±0.1	-6.2± 0.4	7.7± 0.3
	4	4656± 644	-5.0±0.1	1.4± 0.4	5.2± 0.1
	5	3343± 642	6.8±0.1	2.0± 0.4	7.1± 0.1
	6	528± 53	49.1±0.1	1.2± 0.4	49.1± 0.1

EVENT	TRK	P (MEV)	$\phi (^{\circ})$	$\delta (^{\circ})$	$\theta (^{\circ})$
443451	1	226 \pm 23	-120.7 \pm 0.1	5.7 \pm 0.4	120.5 \pm 0.1
	2		-18.6 \pm 0.1	-7.0 \pm 0.4	19.8 \pm 0.2
	3		-9.6 \pm 0.1	28.3 \pm 0.3	29.8 \pm 0.3
	4		-9.6 \pm 0.1	15.8 \pm 0.3	18.4 \pm 0.3
	5	468 \pm 47	20.8 \pm 0.1	11.1 \pm 0.4	23.5 \pm 0.2
	6	1210 \pm 248	23.9 \pm 0.1	3.9 \pm 0.4	24.2 \pm 0.1
443532	1		-4.9 \pm 0.1	13.7 \pm 0.4	14.5 \pm 0.4
	2		-0.5 \pm 0.1	-8.2 \pm 0.4	8.2 \pm 0.4
	3		3.4 \pm 0.1	-6.3 \pm 0.4	7.2 \pm 0.4
	4	501 \pm 45	3.8 \pm 0.1	4.3 \pm 0.4	5.7 \pm 0.3
	5		15.2 \pm 0.1	-21.6 \pm 0.3	26.2 \pm 0.2
	6		25.9 \pm 0.1	41.0 \pm 0.2	47.2 \pm 0.2
461985	1	1913 \pm 950	-22.0 \pm 0.1	5.7 \pm 0.4	22.7 \pm 0.1
	2	451 \pm 47	-16.9 \pm 0.1	2.2 \pm 0.4	17.0 \pm 0.1
	3	256 \pm 9	-11.7 \pm 0.1	0.0 \pm 0.0	11.7 \pm 0.1
	4		6.6 \pm 0.1	-11.7 \pm 0.4	13.4 \pm 0.4
	5	1018 \pm 133	8.8 \pm 0.1	-4.7 \pm 0.4	10.0 \pm 0.2
	6		16.5 \pm 0.1	10.5 \pm 0.4	19.5 \pm 0.2
560019	1	348 \pm 132	13.6 \pm 0.1	-2.5 \pm 0.3	13.8 \pm 0.1
	2		9.8 \pm 0.1	24.0 \pm 0.3	25.8 \pm 0.3
	3		2.9 \pm 0.1	-1.9 \pm 0.3	3.5 \pm 0.2
	4	207 \pm 61	-7.4 \pm 0.1	-5.7 \pm 0.3	9.3 \pm 0.2
	5	500 \pm 134	-22.0 \pm 0.1	-7.7 \pm 0.3	23.2 \pm 0.1
	6		23.4 \pm 0.1	-36.7 \pm 0.2	42.6 \pm 0.2
760054	1		-3.2 \pm 0.1	-12.3 \pm 0.6	12.7 \pm 0.6
	2		0.5 \pm 0.1	9.9 \pm 0.6	9.9 \pm 0.6
	3		0.8 \pm 0.1	-7.2 \pm 0.6	7.2 \pm 0.6
	4	2434 \pm 412	11.1 \pm 0.1	2.7 \pm 0.7	11.4 \pm 0.2
	5		11.9 \pm 0.1	11.8 \pm 0.5	16.7 \pm 0.4
	6		5.3 \pm 0.1	-22.3 \pm 0.5	22.9 \pm 0.5
760154	1		-29.1 \pm 0.1	36.1 \pm 0.4	45.1 \pm 0.3
	2	2314 \pm 422	-3.8 \pm 0.1	2.2 \pm 0.6	4.4 \pm 0.3
	3		-1.0 \pm 0.1	-6.0 \pm 0.6	6.1 \pm 0.6
	4	2384 \pm 277	1.2 \pm 0.1	0.0 \pm 0.0	1.2 \pm 0.1
	5	6372 \pm 1269	7.0 \pm 0.1	0.0 \pm 0.0	7.0 \pm 0.1
	6		-59.4 \pm 0.1	18.3 \pm 0.3	61.1 \pm 0.1
190098	1		-11.2 \pm 0.1	-12.2 \pm 0.3	16.5 \pm 0.2
	2		-10.6 \pm 0.1	15.7 \pm 0.3	18.9 \pm 0.3
	3		-4.0 \pm 0.1	-7.6 \pm 0.4	8.6 \pm 0.4
	4	890 \pm 81	-1.6 \pm 0.1	-1.7 \pm 0.4	2.3 \pm 0.3

EVENT	TRK	P (MEV)	ϕ ($^{\circ}$)	δ ($^{\circ}$)	θ ($^{\circ}$)
190098	5	3296 \pm 428	2.0 \pm 0.1	-2.2 \pm 0.4	3.0 \pm 0.3
	6		9.7 \pm 0.1	19.9 \pm 0.3	22.1 \pm 0.3
	7		13.1 \pm 0.1	17.9 \pm 0.3	22.1 \pm 0.2
	P	115 \pm 1	6.8 \pm 0.1	-40.4 \pm 0.4	40.9 \pm 0.4
221781	1	365 \pm 37	-65.4 \pm 0.1	3.4 \pm 0.4	65.4 \pm 0.1
	2	2678 \pm 371	-18.3 \pm 0.1	-2.0 \pm 0.4	18.4 \pm 0.1
	3	4311 \pm 1730	-1.4 \pm 0.1	0.0 \pm 0.0	1.4 \pm 0.1
	4		6.3 \pm 0.1	18.2 \pm 0.3	19.2 \pm 0.3
	5	889 \pm 146	6.6 \pm 0.1	2.2 \pm 0.4	7.0 \pm 0.2
	6	894 \pm 189	28.5 \pm 0.1	-1.9 \pm 0.4	28.6 \pm 0.1
	7		44.5 \pm 0.1	-13.3 \pm 0.3	46.0 \pm 0.1
	P	17 \pm 1	41.0 \pm 1.0	0.4 \pm 0.4	41.0 \pm 1.0
370087	1	1400 \pm 500	-52.1 \pm 0.1	-5.4 \pm 0.4	52.3 \pm 0.1
	2	4052 \pm 789	-4.8 \pm 0.1	3.3 \pm 0.4	5.8 \pm 0.2
	3	3642 \pm 588	-2.6 \pm 0.1	4.0 \pm 0.4	4.8 \pm 0.3
	4	462 \pm 49	10.8 \pm 0.1	-2.3 \pm 0.4	11.0 \pm 0.1
	5		10.3 \pm 0.1	13.4 \pm 0.4	16.8 \pm 0.3
	6		20.7 \pm 0.1	-10.4 \pm 0.4	23.1 \pm 0.2
	7		44.1 \pm 0.1	-11.8 \pm 0.3	45.3 \pm 0.1
	P		85.0 \pm 0.1	-14.9 \pm 0.3	85.2 \pm 0.1
380094	1		-67.2 \pm 0.1	59.7 \pm 0.1	78.7 \pm 0.1
	2	839 \pm 203	-19.8 \pm 0.1	6.1 \pm 0.4	20.7 \pm 0.1
	3	517 \pm 85	-9.3 \pm 0.1	-2.9 \pm 0.4	9.7 \pm 0.2
	4	1071 \pm 379	-2.3 \pm 0.1	2.8 \pm 0.4	3.6 \pm 0.3
	5	8198 \pm 2218	0.6 \pm 0.1	2.5 \pm 0.4	2.6 \pm 0.4
	6	4480 \pm 960	5.7 \pm 0.1	-4.1 \pm 0.4	7.0 \pm 0.2
	7		17.2 \pm 0.1	-22.1 \pm 0.3	27.7 \pm 0.2
	P	300 \pm 210	39.2 \pm 0.1	49.6 \pm 0.2	59.8 \pm 0.1
461491	1	973 \pm 144	-24.2 \pm 0.1	-6.3 \pm 0.4	25.0 \pm 0.1
	2	900 \pm 165	-19.8 \pm 0.1	-6.1 \pm 0.4	20.7 \pm 0.1
	3	3858 \pm 812	-3.3 \pm 0.1	-3.9 \pm 0.4	5.1 \pm 0.3
	4	1362 \pm 155	0.2 \pm 0.1	-1.6 \pm 0.4	1.6 \pm 0.4
	5		6.5 \pm 0.1	-10.8 \pm 0.4	12.6 \pm 0.3
	6	987 \pm 201	18.0 \pm 0.1	-7.6 \pm 0.4	19.5 \pm 0.2
	7	1975 \pm 576	29.0 \pm 0.1	-8.6 \pm 0.4	30.1 \pm 0.1
	P	140 \pm 1	69.4 \pm 0.1	-12.7 \pm 0.3	69.9 \pm 0.1
481124	1		8.6 \pm 0.1	-21.6 \pm 0.3	23.2 \pm 0.3
	2		6.0 \pm 0.1	-16.1 \pm 0.3	17.2 \pm 0.3
	3	2549 \pm 288	4.4 \pm 0.1	5.5 \pm 0.4	7.0 \pm 0.3
	4	533 \pm 97	3.0 \pm 0.1	-6.7 \pm 0.4	7.3 \pm 0.4

EVENT	TRK	P (MEV)	ϕ ($^{\circ}$)	δ ($^{\circ}$)	θ ($^{\circ}$)
	5	2514 \pm 417	-6.8 \pm 0.1	-6.2 \pm 0.4	9.2 \pm 0.3
	6		-12.0 \pm 0.1	-35.4 \pm 0.2	37.1 \pm 0.2
	7		3.9 \pm 0.1	36.6 \pm 0.2	36.8 \pm 0.2
	P	96 \pm 1	42.7 \pm 0.1	-39.3 \pm 0.5	55.3 \pm 0.3
690016	1	1915 \pm 583	-7.4 \pm 0.1	14.0 \pm 0.6	15.8 \pm 0.5
	2	1307 \pm 204	-4.9 \pm 0.1	-2.0 \pm 0.6	5.3 \pm 0.2
	3		-2.0 \pm 0.1	11.2 \pm 0.5	11.4 \pm 0.5
	4		0.3 \pm 0.1	-12.6 \pm 0.6	12.6 \pm 0.6
	5		0.4 \pm 0.1	-8.3 \pm 0.6	8.3 \pm 0.6
	6		0.6 \pm 0.1	11.3 \pm 0.6	11.3 \pm 0.6
	7		5.9 \pm 0.1	-11.1 \pm 0.6	12.6 \pm 0.5
	P	81 \pm 1	-10.9 \pm 0.1	12.8 \pm 2.9	16.8 \pm 2.2
780071	1		40.2 \pm 0.1	9.5 \pm 0.3	41.1 \pm 0.1
	2	649 \pm 174	31.4 \pm 0.1	1.8 \pm 0.3	31.4 \pm 0.1
	3	5572 \pm 1201	6.6 \pm 0.1	-2.5 \pm 0.3	7.1 \pm 0.1
	4	4252 \pm 1339	3.7 \pm 0.1	-6.1 \pm 0.3	7.1 \pm 0.3
	5		-15.8 \pm 0.1	10.8 \pm 0.3	19.1 \pm 0.2
	6	1049 \pm 364	-31.6 \pm 0.1	-5.9 \pm 0.3	32.1 \pm 0.1
	7	753 \pm 109	-35.8 \pm 0.1	-1.4 \pm 0.3	35.8 \pm 0.1
	P	440 \pm 5	-63.4 \pm 0.1	-30.8 \pm 0.2	67.4 \pm 0.1
150127	1		8.4 \pm 0.1	17.5 \pm 0.3	19.4 \pm 0.3
	2	4370 \pm 901	3.8 \pm 0.1	3.5 \pm 0.4	5.2 \pm 0.3
	3	3497 \pm 335	2.9 \pm 0.1	4.8 \pm 0.4	5.6 \pm 0.3
	4		-1.4 \pm 0.1	-4.8 \pm 0.4	5.0 \pm 0.4
	5	2312 \pm 1520	-7.6 \pm 0.1	6.5 \pm 0.4	10.0 \pm 0.3
	6		-7.5 \pm 0.1	-30.5 \pm 0.3	31.3 \pm 0.3
	7		-23.4 \pm 0.1	-20.3 \pm 0.3	30.6 \pm 0.2
	8		155.1 \pm 0.1	-15.9 \pm 0.3	150.7 \pm 0.2
183144	1		-14.4 \pm 0.1	-13.9 \pm 0.3	19.9 \pm 0.2
	2		-11.2 \pm 0.1	-11.5 \pm 0.4	16.0 \pm 0.3
	3	1382 \pm 413	-0.3 \pm 0.1	-10.0 \pm 0.4	10.0 \pm 0.4
	4		2.0 \pm 0.1	12.5 \pm 0.3	12.7 \pm 0.3
	5	584 \pm 131	5.2 \pm 0.1	-5.8 \pm 0.4	7.8 \pm 0.3
	6		9.6 \pm 0.1	-11.8 \pm 0.4	15.2 \pm 0.3
	7		-19.7 \pm 0.1	11.3 \pm 0.4	22.6 \pm 0.2
	8		28.7 \pm 0.1	10.0 \pm 0.4	30.3 \pm 0.2
183238	1		-40.0 \pm 0.1	-19.8 \pm 0.3	43.9 \pm 0.1
	2	2102 \pm 406	-20.5 \pm 0.1	3.2 \pm 0.4	20.7 \pm 0.1
	3		-10.6 \pm 0.1	5.8 \pm 0.4	12.1 \pm 0.2
	4		-7.8 \pm 0.1	6.0 \pm 0.4	9.8 \pm 0.3
	5	4602 \pm 967	1.5 \pm 0.1	-4.3 \pm 0.4	4.6 \pm 0.4

EVENT	TRK	P(MEV)	$\phi(^{\circ})$	$\delta(^{\circ})$	$\theta(^{\circ})$
	6	1433± 268	8.7±0.1	-4.6± 0.4	9.8± 0.2
	7		10.2±0.1	-10.9± 0.4	14.9± 0.3
	8	651± 60	20.1±0.1	1.3± 0.4	20.1± 0.1
221703	1	606± 98	-23.0±0.1	4.3± 0.4	23.4± 0.1
	2	2159± 655	-5.7±0.1	-5.7± 0.4	8.1± 0.3
	3	2129± 363	-4.6±0.1	6.5± 0.4	8.0± 0.3
	4	3156± 164	1.9±0.1	0.0± 0.0	1.9± 0.1
	5	302± 55	11.5±0.1	1.9± 0.4	11.7± 0.1
	6	222± 24	12.4±0.1	7.5± 0.4	14.5± 0.2
	7		20.6±0.1	-15.6± 0.3	25.6± 0.2
	8		-8.8±0.1	22.4± 0.3	24.0± 0.3
240507	1		-51.6±0.1	14.2± 0.3	53.0± 0.1
	2		-10.3±0.1	-32.5± 0.3	33.9± 0.3
	3		-10.3±0.1	11.5± 0.4	15.4± 0.3
	4	3078± 480	-1.4±0.1	-2.7± 0.4	3.0± 0.4
	5	258± 31	8.3±0.1	-4.9± 0.4	9.6± 0.2
	6		9.8±0.1	9.2± 0.4	13.4± 0.3
	7	1314± 261	14.3±0.1	-7.4± 0.4	14.5± 0.1
	8	804± 103	19.1±0.1	-2.3± 0.4	19.2± 0.1
240546	1		18.9±0.1	17.6± 0.3	25.6± 0.2
	2		11.4±0.1	6.6± 0.4	13.2± 0.2
	3	457± 50	5.2±0.1	-7.4± 0.4	9.0± 0.3
	4		3.4±0.1	7.1± 0.4	7.9± 0.4
	5	582± 118	1.1±0.1	-9.7± 0.4	9.8± 0.4
	6	3369± 143	-4.3±0.1	0.0± 0.0	4.3± 0.1
	7		-15.1±0.1	8.8± 0.4	17.4± 0.2
	8		-31.7±0.1	16.2± 0.3	35.2± 0.2
262588	1	1249± 235	-18.2±0.1	8.7± 0.3	20.1± 0.2
	2	1445± 120	-16.9±0.1	0.0± 0.0	16.9± 0.1
	3	4117± 581	-0.9±0.1	2.5± 0.4	2.7± 0.4
	4		3.4±0.1	-22.6± 0.3	22.8± 0.3
	5		4.8±0.1	-6.6± 0.4	8.2± 0.3
	6	662± 154	5.7±0.1	-4.1± 0.4	7.0± 0.2
	7		5.8±0.1	17.3± 0.3	18.2± 0.3
	8		24.8±0.1	-5.5± 0.4	25.4± 0.1
310323	1		-16.0±0.1	15.0± 0.3	21.8± 0.2
	2	443± 84	-14.0±0.1	-4.3± 0.4	14.6± 0.1
	3	2481± 284	-4.7±0.1	-1.4± 0.4	4.9± 0.1
	4	5415±1210	-3.0±0.1	7.1± 0.4	7.7± 0.4
	5	2045± 519	4.0±0.1	-3.6± 0.4	5.4± 0.3

EVENT	TRK	P (MEV)	$\phi (^{\circ})$	$\delta (^{\circ})$	$\theta (^{\circ})$
	6		3.8 ± 0.1	-28.3 ± 0.3	28.5 ± 0.3
	7	2306 ± 305	7.5 ± 0.1	1.1 ± 0.4	7.6 ± 0.1
	8	1764 ± 191	24.2 ± 0.1	-1.2 ± 0.4	24.2 ± 0.1
330059	1		-162.4 ± 0.1	9.2 ± 0.4	160.2 ± 0.2
	2		-18.5 ± 0.1	-18.0 ± 0.3	25.6 ± 0.2
	3	1092 ± 287	-17.2 ± 0.1	1.9 ± 0.4	17.3 ± 0.1
	4	2420 ± 302	-13.1 ± 0.1	-2.1 ± 0.4	13.3 ± 0.1
	5	2268 ± 549	3.1 ± 0.1	-6.0 ± 0.4	6.8 ± 0.4
	6	4491 ± 430	4.8 ± 0.1	0.0 ± 0.0	4.8 ± 0.1
	7	1162 ± 260	9.2 ± 0.1	1.7 ± 0.4	9.4 ± 0.1
	8	339 ± 36	30.6 ± 0.1	0.1 ± 0.1	30.6 ± 0.1
351195	1	1446 ± 96	-11.0 ± 0.1	-1.0 ± 0.4	11.0 ± 0.1
	2		-7.5 ± 0.1	4.8 ± 0.4	8.9 ± 0.2
	3		-1.7 ± 0.1	-40.9 ± 0.2	40.9 ± 0.2
	4	551 ± 179	-0.6 ± 0.1	1.0 ± 0.4	1.2 ± 0.3
	5	1954 ± 655	-0.7 ± 0.1	1.0 ± 0.4	1.0 ± 0.4
	6		2.0 ± 0.1	11.9 ± 0.4	12.1 ± 0.4
	7	569 ± 97	6.9 ± 0.1	-5.2 ± 0.4	8.6 ± 0.3
	8		18.8 ± 0.1	19.9 ± 0.3	27.1 ± 0.2
370009	1	1105 ± 223	-1.0 ± 0.1	-5.6 ± 0.4	5.7 ± 0.4
	2		0.7 ± 0.1	3.0 ± 0.4	3.1 ± 0.4
	3		6.1 ± 0.1	-14.6 ± 0.3	15.8 ± 0.3
	4		9.5 ± 0.1	-25.0 ± 0.3	26.6 ± 0.3
	5		14.1 ± 0.1	13.6 ± 0.3	19.5 ± 0.2
	6		27.9 ± 0.1	8.3 ± 0.4	29.0 ± 0.1
	7		28.0 ± 0.1	-22.4 ± 0.3	35.3 ± 0.2
	8		36.5 ± 0.1	-27.0 ± 0.3	44.3 ± 0.2
370526	1	823 ± 103	-28.2 ± 0.1	5.5 ± 0.4	28.7 ± 0.1
	2		-22.7 ± 0.1	-9.2 ± 0.4	24.4 ± 0.2
	3		-15.0 ± 0.1	13.1 ± 0.4	19.8 ± 0.3
	4	901 ± 395	-11.6 ± 0.1	5.4 ± 0.4	12.8 ± 0.2
	5		-6.4 ± 0.1	-5.1 ± 0.4	8.2 ± 0.3
	6	2365 ± 1044	-4.7 ± 0.1	-2.3 ± 0.4	5.2 ± 0.2
	7		2.5 ± 0.1	-6.2 ± 0.4	6.7 ± 0.4
	8	567 ± 74	9.3 ± 0.1	10.2 ± 0.4	13.8 ± 0.3
380071	1		-20.0 ± 0.1	13.7 ± 0.3	24.1 ± 0.2
	2		-18.0 ± 0.1	11.9 ± 0.4	21.5 ± 0.2
	3		-16.8 ± 0.1	-17.4 ± 0.3	24.0 ± 0.2
	4		-0.3 ± 0.1	2.6 ± 0.4	2.6 ± 0.4
	5	1106 ± 235	3.7 ± 0.1	-6.7 ± 0.4	7.6 ± 0.4

EVENT	TRK	P (MEV)	$\phi(^{\circ})$	$\delta(^{\circ})$	$\theta(^{\circ})$
	6		3.8 ± 0.1	-12.9 ± 0.3	13.4 ± 0.3
	7		16.7 ± 0.1	5.4 ± 0.4	17.5 ± 0.2
	8	2976 ± 285	21.4 ± 0.1	0.0 ± 0.0	21.4 ± 0.1
392061	1		-45.2 ± 0.1	-13.5 ± 0.3	46.8 ± 0.1
	2	977 ± 91	-26.2 ± 0.1	-1.7 ± 0.4	26.3 ± 0.1
	3	4455 ± 783	-5.9 ± 0.1	-1.3 ± 0.4	6.0 ± 0.1
	4	663 ± 56	0.2 ± 0.1	9.2 ± 0.4	9.2 ± 0.4
	5	710 ± 205	0.5 ± 0.1	-3.7 ± 0.4	3.7 ± 0.4
	6	1428 ± 551	15.8 ± 0.1	-3.9 ± 0.4	16.3 ± 0.1
	7		18.5 ± 0.1	32.7 ± 0.3	37.1 ± 0.3
	8		-30.1 ± 0.1	-50.3 ± 0.2	56.5 ± 0.2
392159	1		-63.2 ± 0.1	33.6 ± 0.3	67.9 ± 0.1
	2		-24.2 ± 0.1	11.0 ± 0.4	26.4 ± 0.2
	3	1278 ± 347	-6.4 ± 0.1	-4.0 ± 0.4	7.5 ± 0.2
	4		-4.1 ± 0.1	15.1 ± 0.3	15.6 ± 0.3
	5	4807 ± 1118	2.0 ± 0.1	1.2 ± 0.4	2.3 ± 0.2
	6		3.3 ± 0.1	-7.1 ± 0.4	7.8 ± 0.4
	7		19.6 ± 0.1	23.6 ± 0.3	30.3 ± 0.2
	8		23.9 ± 0.1	-17.8 ± 0.3	29.5 ± 0.2
443428	1		-51.9 ± 0.1	13.3 ± 0.3	53.1 ± 0.1
	2	365 ± 42	-37.6 ± 0.1	3.7 ± 0.4	37.8 ± 0.1
	3		-17.6 ± 0.1	16.4 ± 0.3	23.9 ± 0.2
	4		-8.5 ± 0.1	-9.9 ± 0.4	13.0 ± 0.3
	5	4802 ± 944	-1.9 ± 0.1	-1.3 ± 0.4	2.3 ± 0.2
	6		0.4 ± 0.1	-3.8 ± 0.4	3.8 ± 0.4
	7	4174 ± 544	5.6 ± 0.1	5.8 ± 0.4	8.1 ± 0.3
	8		17.2 ± 0.1	-5.7 ± 0.4	18.1 ± 0.2
461931	1		-29.6 ± 0.1	13.8 ± 0.3	32.4 ± 0.1
	2	3055 ± 273	-0.6 ± 0.1	-2.0 ± 0.4	2.1 ± 0.4
	3	2559 ± 196	1.9 ± 0.1	-2.7 ± 0.4	3.3 ± 0.3
	4	2139 ± 388	3.4 ± 0.1	-2.6 ± 0.4	4.3 ± 0.3
	5	2218 ± 398	4.7 ± 0.1	-1.2 ± 0.4	4.9 ± 0.1
	6	2391 ± 343	9.1 ± 0.1	-1.8 ± 0.4	9.3 ± 0.1
	7		11.2 ± 0.1	10.8 ± 0.4	15.5 ± 0.3
	8	369 ± 96	36.0 ± 0.1	-5.7 ± 0.4	36.4 ± 0.1
780079	1		69.0 ± 0.1	36.6 ± 0.2	73.3 ± 0.1
	2		30.5 ± 0.1	6.0 ± 0.3	31.0 ± 0.1
	3	1785 ± 253	8.4 ± 0.1	-2.0 ± 0.3	8.6 ± 0.1
	4	5462 ± 2359	7.5 ± 0.1	-4.8 ± 0.3	8.9 ± 0.2
	5	2114 ± 345	-2.2 ± 0.1	-1.0 ± 0.3	2.4 ± 0.2

EVENT	TRK	P (MEV)	$\phi(^{\circ})$	$\delta(^{\circ})$	$\theta(^{\circ})$
221679	6	839± 204	-9.7±0.1	-4.2± 0.3	10.6± 0.1
	7		-11.4±0.1	-15.4± 0.3	19.1± 0.2
	8		-44.1±0.1	12.1± 0.3	45.4± 0.1
221679	1	245± 81	-36.6±0.1	8.7± 0.4	37.5± 0.1
	2		-12.6±0.1	16.6± 0.3	20.7± 0.2
	3		-10.6±0.1	20.9± 0.3	23.3± 0.3
	4	788± 160	1.6±0.1	-11.3± 0.4	11.4± 0.4
	5	446± 86	4.3±0.1	-10.8± 0.4	11.6± 0.4
	6	361± 91	7.9±0.1	14.2± 0.3	16.2± 0.3
	7	930± 230	20.9±0.1	13.9± 0.3	24.9± 0.2
	8		35.7±0.1	-14.1± 0.3	38.0± 0.1
	9	280± 91	39.8±0.1	-11.8± 0.4	41.2± 0.1
	P	181± 2	-55.3±0.1	18.9± 0.3	57.4± 0.1
400265	1	2825± 910	-25.3±0.1	-6.2± 0.4	26.0± 0.1
	2		-23.1±0.1	13.4± 0.3	26.5± 0.2
	3		-16.3±0.1	13.0± 0.3	20.7± 0.2
	4	3124±1237	-7.2±0.1	5.0± 0.4	8.8± 0.2
	5		-4.0±0.1	-29.6± 0.3	29.8± 0.3
	6	3886±1000	8.5±0.1	6.5± 0.4	10.7± 0.3
	7	2256± 256	9.3±0.1	-2.2± 0.4	9.6± 0.1
	8	519± 65	13.9±0.1	-2.5± 0.4	14.1± 0.1
	9		14.5±0.1	-11.3± 0.4	18.3± 0.3
	P	427± 5	10.7±0.1	0.2± 0.2	10.7± 0.1
480844	1		-25.6±0.1	-3.5± 0.4	25.8± 0.1
	2		-20.5±0.1	-24.7± 0.3	31.7± 0.2
	3	549± 44	-15.7±0.1	5.0± 0.4	16.5± 0.2
	4	1694± 244	-3.2±0.1	2.7± 0.4	4.2± 0.3
	5	3501± 343	-1.1±0.1	-1.9± 0.4	2.2± 0.3
	6		-0.5±0.1	16.5± 0.3	16.5± 0.3
	7		2.7±0.1	-11.0± 0.4	11.3± 0.4
	8		9.7±0.1	-7.8± 0.4	12.4± 0.3
	9		98.7±0.1	38.1± 0.2	96.8± 0.1
	P		3.0±0.1	74.8± 0.1	74.8± 0.1
850041	1		20.2±0.1	18.3± 0.3	27.0± 0.2
	2		15.9±0.1	-18.7± 0.3	24.4± 0.2
	3		10.3±0.1	-10.6± 0.3	14.7± 0.2
	4	679± 302	8.9±0.1	1.7± 0.3	9.1± 0.1
	5	2673± 696	2.3±0.1	-1.5± 0.3	2.7± 0.2
	6	869± 346	-14.6±0.1	7.5± 0.3	16.4± 0.2
	7		-22.7±0.1	12.5± 0.3	25.8± 0.2

EVENT	TRK	P (MEV)	ϕ ($^{\circ}$)	δ ($^{\circ}$)	θ ($^{\circ}$)
	8		-47.1 ± 0.1	-24.0 ± 0.3	51.5 ± 0.1
	9		-50.8 ± 0.1	-6.8 ± 0.3	51.1 ± 0.1
	P		-103.0 ± 0.1	71.7 ± 0.1	94.1 ± 0.0
190087	1	598 ± 124	-15.0 ± 0.1	5.3 ± 0.4	15.9 ± 0.2
	2	2642 ± 394	-11.3 ± 0.1	-1.8 ± 0.4	11.4 ± 0.1
	3	2461 ± 479	-7.4 ± 0.1	-2.5 ± 0.4	7.8 ± 0.2
	4	4775 ± 2393	-2.5 ± 0.1	-3.2 ± 0.4	4.1 ± 0.3
	5	1431 ± 353	0.4 ± 0.1	-4.3 ± 0.4	4.3 ± 0.4
	6		2.3 ± 0.1	24.9 ± 0.3	25.0 ± 0.3
	7	1415 ± 62	8.1 ± 0.1	-1.7 ± 0.4	8.3 ± 0.1
	8		8.1 ± 0.1	8.0 ± 0.4	11.4 ± 0.3
	9	721 ± 161	15.0 ± 0.1	-3.7 ± 0.4	15.4 ± 0.1
	10		15.9 ± 0.1	-14.9 ± 0.3	21.7 ± 0.2
370180	1	875 ± 231	-19.8 ± 0.1	-3.6 ± 0.4	20.1 ± 0.1
	2		-17.0 ± 0.1	7.1 ± 0.4	18.4 ± 0.2
	3	860 ± 134	-12.8 ± 0.1	2.6 ± 0.4	13.1 ± 0.1
	4	1700 ± 610	4.9 ± 0.1	-2.5 ± 0.4	5.5 ± 0.2
	5		5.7 ± 0.1	2.2 ± 0.4	6.1 ± 0.2
	6	601 ± 167	7.8 ± 0.1	7.5 ± 0.4	10.8 ± 0.3
	7		9.8 ± 0.1	-15.7 ± 0.3	18.4 ± 0.3
	8		9.8 ± 0.1	23.9 ± 0.3	25.7 ± 0.3
	9	438 ± 116	19.0 ± 0.1	-4.9 ± 0.4	19.6 ± 0.1
	10	514 ± 106	20.5 ± 0.1	-8.6 ± 0.4	22.2 ± 0.2
461324	1	574 ± 123	-6.5 ± 0.1	-1.6 ± 0.4	6.7 ± 0.1
	2		-5.7 ± 0.1	-7.4 ± 0.4	9.3 ± 0.3
	3	843 ± 97	-4.7 ± 0.1	5.0 ± 0.4	6.9 ± 0.3
	4		-1.5 ± 0.1	-8.3 ± 0.4	8.4 ± 0.4
	5		-1.5 ± 0.1	11.4 ± 0.4	11.5 ± 0.4
	6		0.8 ± 0.1	8.5 ± 0.4	8.5 ± 0.4
	7		1.0 ± 0.1	-6.1 ± 0.4	6.2 ± 0.4
	8		5.3 ± 0.1	8.5 ± 0.4	10.0 ± 0.3
	9	1652 ± 382	17.3 ± 0.1	-3.8 ± 0.4	17.7 ± 0.1
	10	468 ± 80	17.3 ± 0.1	6.7 ± 0.4	18.5 ± 0.2
350628	1		-62.3 ± 0.1	-30.3 ± 0.3	66.3 ± 0.1
	2	1019 ± 169	-10.5 ± 0.1	5.3 ± 0.4	11.7 ± 0.2
	3	1261 ± 186	-3.5 ± 0.1	2.9 ± 0.4	4.5 ± 0.3
	4	1557 ± 292	-1.8 ± 0.1	5.1 ± 0.4	5.4 ± 0.4
	5	3204 ± 617	-0.2 ± 0.1	2.1 ± 0.4	2.1 ± 0.4
	6		3.8 ± 0.1	18.1 ± 0.3	18.5 ± 0.3
	7		8.6 ± 0.1	0.0 ± 0.0	8.6 ± 0.1

EVENT	TRK	P (MEV)	$\phi (^{\circ})$	$\delta (^{\circ})$	$\theta (^{\circ})$
	8		8.6 ± 0.1	-7.5 ± 0.4	11.4 ± 0.3
	9		9.9 ± 0.1	0.0 ± 0.0	9.9 ± 0.1
	10		12.1 ± 0.1	-11.9 ± 0.4	16.9 ± 0.3
	11		31.2 ± 0.1	-3.8 ± 0.4	31.4 ± 0.1
	P	109 ± 1	35.9 ± 0.1	16.8 ± 0.3	39.2 ± 0.1

TABLE C2

DATA ON INELASTIC π^- -n EVENTS

EVENT	TRK	P(MEV)	$\phi(^{\circ})$	$\delta(^{\circ})$	$\theta(^{\circ})$
221626	1	3012± 381	-0.9±0.1	-1.2± 0.4	1.5± 0.3
	2	3751± 700	-0.6±0.1	-5.0± 0.4	5.0± 0.4
	P	108± 1	50.9±0.1	11.3± 0.7	51.8± 0.1
221814	1	1197± 119	-49.8±0.1	0.0± 0.0	49.8± 0.1
	2	6571± 736	1.8±0.1	-1.5± 0.4	2.3± 0.3
	P	380± 120	26.9±0.1	2.4± 0.4	27.0± 0.1
240547	1	2040± 207	-2.1±0.1	0.9± 0.4	2.3± 0.2
	2		-6.9±0.1	47.7± 0.2	48.1± 0.2
	P	282± 3	-4.9±0.1	46.4± 0.2	46.6± 0.2
330156	1	1855± 210	-9.6±0.1	2.8± 0.4	10.0± 0.1
	2	523± 51	18.5±0.1	5.5± 0.4	19.3± 0.1
	P	137± 1	29.8±0.1	40.2± 0.5	48.5± 0.4
370068	1	11166±1458	-3.3±0.1	-3.6± 0.4	4.9± 0.3
	2	2820± 330	0.8±0.1	0.0± 0.0	0.8± 0.1
	P	159± 2	6.2±0.1	56.5± 0.2	56.7± 0.2
370469	1	3491± 254	4.1±0.1	1.5± 0.4	4.4± 0.2
	2		16.8±0.1	-5.4± 0.4	17.6± 0.2
	P	337± 4	-58.6±0.1	11.1± 0.4	59.3± 0.1
370524	1	4645± 847	1.0±0.1	0.1± 0.1	1.0± 0.1
	2		64.4±0.1	-33.4± 0.3	68.9± 0.1
	P	112± 1	-12.4±0.1	-19.5± 0.3	23.0± 0.3
400251	1		-43.4±0.1	9.1± 0.4	44.2± 0.1
	2	3751± 244	1.7±0.1	0.0± 0.0	1.7± 0.1
	P	505± 6	1.7±0.1	8.7± 0.4	8.9± 0.4
400298	1	981± 185	-1.7±0.1	9.2± 0.4	9.4± 0.4
	2		8.0±0.1	11.4± 0.4	13.9± 0.3
	P	135± 1	-15.7±0.1	-10.5± 0.4	18.8± 0.2
400438	1	9659±1685	-1.9±0.1	0.0± 0.0	1.9± 0.1
	2	10918±2381	4.3±0.1	-1.5± 0.4	4.6± 0.2
	P	215± 2	-0.5±0.1	-2.7± 0.4	2.7± 0.4
461330	1	8067±1311	3.2±0.1	0.1± 0.1	3.2± 0.1
	2	4833± 652	3.8±0.1	0.1± 0.1	3.8± 0.1
	P		-31.5±0.1	-11.9± 0.4	33.5± 0.2
461440	1	3461± 599	4.4±0.1	1.9± 0.4	4.8± 0.2
	2	1569± 391	4.8±0.1	-6.2± 0.4	7.8± 0.3
	P	350± 25	-40.5±0.1	37.0± 0.2	52.6± 0.1

EVENT	TRK	P (MEV)	$\phi (^{\circ})$	$\delta (^{\circ})$	$\theta (^{\circ})$
461477	1	4788 \pm 734	-0.7 \pm 0.1	0.0 \pm 0.0	0.7 \pm 0.1
	2	5455 \pm 519	1.8 \pm 0.1	1.4 \pm 0.4	2.3 \pm 0.3
	P	26 \pm 1	-22.1 \pm 5.5	0.4 \pm 0.4	22.1 \pm 5.5
461486	1	441 \pm 22	0.1 \pm 0.1	6.2 \pm 0.4	6.2 \pm 0.4
	2	946 \pm 334	44.1 \pm 0.1	0.0 \pm 0.0	44.1 \pm 0.1
	P	113 \pm 1	-32.9 \pm 0.1	-20.5 \pm 0.3	38.1 \pm 0.2
481177	1		2.0 \pm 0.1	24.8 \pm 0.3	24.9 \pm 0.3
	2	752 \pm 511	109.6 \pm 0.1	-10.6 \pm 0.4	109.3 \pm 0.1
	P		-16.8 \pm 0.1	3.1 \pm 0.4	17.1 \pm 0.1
150129	1	4621 \pm 1010	-1.4 \pm 0.1	0.0 \pm 0.0	1.4 \pm 0.1
	2	3140 \pm 390	-0.4 \pm 0.1	-1.5 \pm 0.4	1.6 \pm 0.4
	3	2763 \pm 1145	5.9 \pm 0.1	-3.4 \pm 0.4	6.8 \pm 0.2
182905	1		-4.0 \pm 0.1	-9.4 \pm 0.4	10.2 \pm 0.4
	2		6.4 \pm 0.1	-8.7 \pm 0.4	10.8 \pm 0.3
	3	899 \pm 165	46.3 \pm 0.1	3.6 \pm 0.4	46.4 \pm 0.1
182925	1	2856 \pm 595	-8.3 \pm 0.1	-2.9 \pm 0.4	8.8 \pm 0.2
	2	11909 \pm 3282	2.0 \pm 0.1	3.3 \pm 0.4	3.9 \pm 0.3
	3	3376 \pm 381	15.2 \pm 0.1	-3.6 \pm 0.4	15.6 \pm 0.1
182952	1	2287 \pm 357	-9.1 \pm 0.1	-2.9 \pm 0.4	9.5 \pm 0.2
	2	3348 \pm 1424	-4.9 \pm 0.1	-5.0 \pm 0.4	7.0 \pm 0.3
	3		-8.3 \pm 0.1	27.1 \pm 0.3	28.2 \pm 0.3
182981	1	1124 \pm 181	-30.2 \pm 0.1	9.0 \pm 0.4	31.4 \pm 0.1
	2	2077 \pm 428	-1.2 \pm 0.1	4.7 \pm 0.4	4.9 \pm 0.4
	3	669 \pm 55	4.3 \pm 0.1	0.0 \pm 0.0	4.3 \pm 0.1
182988	1	6629 \pm 1270	-1.2 \pm 0.1	-1.0 \pm 0.4	1.6 \pm 0.3
	2	6562 \pm 1262	0.4 \pm 0.1	0.0 \pm 0.0	0.4 \pm 0.1
	3		6.4 \pm 0.1	4.9 \pm 0.4	8.1 \pm 0.3
183077	1	2222 \pm 454	-9.6 \pm 0.1	-6.5 \pm 0.4	11.6 \pm 0.2
	2	7694 \pm 613	1.7 \pm 0.1	-1.2 \pm 0.4	2.1 \pm 0.2
	3	8750 \pm 1431	2.6 \pm 0.1	0.0 \pm 0.0	2.6 \pm 0.1
183160	1	2930 \pm 346	-2.4 \pm 0.1	2.1 \pm 0.4	3.2 \pm 0.3
	2	8538 \pm 5467	-0.7 \pm 0.1	0.0 \pm 0.0	0.7 \pm 0.1
	3		11.5 \pm 0.1	12.7 \pm 0.3	17.1 \pm 0.2
183213	1	2118 \pm 567	-10.0 \pm 0.1	-4.5 \pm 0.4	11.0 \pm 0.2
	2	3570 \pm 900	-9.4 \pm 0.1	1.4 \pm 0.4	9.5 \pm 0.1
	3	4107 \pm 488	1.1 \pm 0.1	3.9 \pm 0.4	4.1 \pm 0.4

EVENT	TRK	P (MEV)	ϕ ($^{\circ}$)	δ ($^{\circ}$)	θ ($^{\circ}$)
183233	1	1180 \pm 140	-1.2 \pm 0.1	-2.2 \pm 0.4	2.5 \pm 0.4
	2	4473 \pm 430	0.1 \pm 0.1	-1.7 \pm 0.4	1.7 \pm 0.4
	3	7944 \pm 1077	2.0 \pm 0.1	6.3 \pm 0.4	6.6 \pm 0.4
183247	1	942 \pm 127	-3.5 \pm 0.1	-8.3 \pm 0.4	9.0 \pm 0.4
	2	11405 \pm 6076	-0.9 \pm 0.1	0.0 \pm 0.0	0.9 \pm 0.1
	3	1746 \pm 134	5.7 \pm 0.1	0.0 \pm 0.0	5.7 \pm 0.1
190027	1	1702 \pm 998	0.2 \pm 0.1	-5.5 \pm 0.4	5.5 \pm 0.4
	2	1531 \pm 380	3.6 \pm 0.1	-3.5 \pm 0.4	5.0 \pm 0.3
	3	3848 \pm 244	4.8 \pm 0.1	0.0 \pm 0.0	4.8 \pm 0.1
190214	1	5444 \pm 660	-2.7 \pm 0.1	0.0 \pm 0.0	2.7 \pm 0.1
	2	7108 \pm 605	1.5 \pm 0.1	0.0 \pm 0.0	1.5 \pm 0.1
	3	1159 \pm 131	4.5 \pm 0.1	-2.6 \pm 0.4	5.2 \pm 0.2
190217	1	6935 \pm 1046	-2.6 \pm 0.1	-2.3 \pm 0.4	3.5 \pm 0.3
	2	6024 \pm 1030	1.4 \pm 0.1	-2.4 \pm 0.4	2.8 \pm 0.3
	3	5091 \pm 772	1.6 \pm 0.1	1.6 \pm 0.4	2.3 \pm 0.3
221577	1	7374 \pm 3500	-4.0 \pm 0.1	-5.7 \pm 0.4	7.0 \pm 0.3
	2	864 \pm 67	2.7 \pm 0.1	1.1 \pm 0.4	2.9 \pm 0.2
	3	1461 \pm 304	3.4 \pm 0.1	3.4 \pm 0.4	4.8 \pm 0.3
221601	1		-7.6 \pm 0.1	6.6 \pm 0.4	10.1 \pm 0.3
	2	4045 \pm 700	-1.5 \pm 0.1	1.0 \pm 0.4	1.8 \pm 0.2
	3	4494 \pm 590	2.1 \pm 0.1	-2.0 \pm 0.4	2.9 \pm 0.3
221616	1	4576 \pm 527	-2.5 \pm 0.1	-1.0 \pm 0.4	2.7 \pm 0.2
	2	7577 \pm 1593	-0.7 \pm 0.1	2.4 \pm 0.4	2.5 \pm 0.4
	3	4656 \pm 759	3.2 \pm 0.1	-3.5 \pm 0.4	4.7 \pm 0.3
221695	1	8701 \pm 2199	-6.1 \pm 0.1	-2.4 \pm 0.4	6.6 \pm 0.2
	2	9181 \pm 2156	0.9 \pm 0.1	-1.3 \pm 0.4	1.6 \pm 0.3
	3	3085 \pm 190	9.4 \pm 0.1	0.0 \pm 0.0	9.4 \pm 0.1
221705	1	1309 \pm 217	-6.6 \pm 0.1	-4.5 \pm 0.4	8.0 \pm 0.2
	2	3947 \pm 655	-2.5 \pm 0.1	3.6 \pm 0.4	4.4 \pm 0.3
	3	904 \pm 243	1.1 \pm 0.1	9.1 \pm 0.4	9.2 \pm 0.4
221822	1	5248 \pm 1229	-9.4 \pm 0.1	-3.8 \pm 0.4	10.1 \pm 0.2
	2	1489 \pm 610	6.2 \pm 0.1	6.1 \pm 0.4	8.7 \pm 0.3
	3		-18.4 \pm 0.1	-17.8 \pm 0.4	25.4 \pm 0.3
221832	1	1867 \pm 538	-6.6 \pm 0.1	2.3 \pm 0.4	7.0 \pm 0.2
	2	4672 \pm 537	-2.6 \pm 0.1	-0.7 \pm 0.4	2.7 \pm 0.1
	3	2353 \pm 428	4.9 \pm 0.1	-4.3 \pm 0.4	6.5 \pm 0.3

EVENT	TRK	P (MEV)	$\phi(^{\circ})$	$\delta(^{\circ})$	$\theta(^{\circ})$
221859	1		-4.1 ± 0.1	8.6 ± 0.4	9.5 ± 0.4
	2	5552 ± 511	-1.0 ± 0.1	0.0 ± 0.0	1.0 ± 0.1
	3	6149 ± 517	2.4 ± 0.1	-2.9 ± 0.4	3.8 ± 0.3
221860	1		-3.0 ± 0.1	16.6 ± 0.3	16.9 ± 0.3
	2	8014 ± 2539	0.5 ± 0.1	-2.8 ± 0.4	2.6 ± 0.4
	3	1355 ± 397	1.5 ± 0.1	2.2 ± 0.4	2.7 ± 0.3
240458	1	4097 ± 906	-0.6 ± 0.1	0.9 ± 0.4	1.1 ± 0.3
	2	3141 ± 374	0.7 ± 0.1	1.9 ± 0.4	2.0 ± 0.4
	3	4438 ± 688	1.5 ± 0.1	-1.8 ± 0.4	2.3 ± 0.3
240508	1	3218 ± 822	-7.3 ± 0.1	1.4 ± 0.4	7.4 ± 0.1
	2	5402 ± 552	-1.8 ± 0.1	0.0 ± 0.0	1.8 ± 0.1
	3	7336 ± 680	2.7 ± 0.1	0.0 ± 0.0	2.7 ± 0.1
262593	1	5962 ± 1096	-3.6 ± 0.1	-2.2 ± 0.4	4.2 ± 0.2
	2	1520 ± 322	50.0 ± 0.1	2.9 ± 0.4	50.1 ± 0.1
	3		66.0 ± 0.1	-10.2 ± 0.4	66.4 ± 0.1
262699	1	1545 ± 495	-0.4 ± 0.1	3.8 ± 0.4	3.8 ± 0.4
	2	5434 ± 504	-0.4 ± 0.1	0.0 ± 0.0	0.4 ± 0.1
	3	3797 ± 394	1.6 ± 0.1	-1.3 ± 0.4	2.1 ± 0.3
300197	1		-9.6 ± 0.1	-2.3 ± 0.4	9.9 ± 0.1
	2		-1.2 ± 0.1	-6.8 ± 0.4	6.9 ± 0.4
	3	882 ± 111	9.7 ± 0.1	0.1 ± 0.1	9.7 ± 0.1
300241	1		-5.5 ± 0.1	7.5 ± 0.4	9.3 ± 0.3
	2	5270 ± 532	0.3 ± 0.1	-1.4 ± 0.4	1.4 ± 0.4
	3	10119 ± 1559	1.1 ± 0.1	0.1 ± 0.1	1.1 ± 0.1
310307	1	3961 ± 1087	-2.2 ± 0.1	1.3 ± 0.4	2.6 ± 0.2
	2	7724 ± 1635	0.1 ± 0.1	0.4 ± 0.4	0.4 ± 0.4
	3	1392 ± 227	7.6 ± 0.1	-5.9 ± 0.4	9.6 ± 0.3
320111	1		-15.1 ± 0.1	-57.4 ± 0.2	58.7 ± 0.2
	2		-13.1 ± 0.1	-6.1 ± 0.4	14.4 ± 0.2
	3	9338 ± 2575	0.9 ± 0.1	1.3 ± 0.4	1.6 ± 0.3
320112	1	10109 ± 2670	-1.1 ± 0.1	0.9 ± 0.4	1.4 ± 0.3
	2	8447 ± 4567	0.9 ± 0.1	0.0 ± 0.0	0.9 ± 0.1
	3		8.5 ± 0.1	-11.5 ± 0.4	14.3 ± 0.3
330049	1		-21.9 ± 0.1	-10.5 ± 0.3	24.2 ± 0.2
	2	2077 ± 429	-3.6 ± 0.1	3.3 ± 0.4	4.9 ± 0.3
	3	3170 ± 2417	2.8 ± 0.1	2.8 ± 0.4	4.0 ± 0.3

EVENT	TRK	P (MEV)	ϕ ($^{\circ}$)	δ ($^{\circ}$)	θ ($^{\circ}$)
330137	1	3118 \pm 958	-10.4 \pm 0.1	2.3 \pm 0.4	10.6 \pm 0.1
	2	5781 \pm 429	-0.5 \pm 0.1	-1.1 \pm 0.4	1.2 \pm 0.4
	3	7829 \pm 1154	2.7 \pm 0.1	0.0 \pm 0.0	2.7 \pm 0.1
330204	1	5353 \pm 642	-4.0 \pm 0.1	-2.5 \pm 0.4	4.7 \pm 0.2
	2	2754 \pm 810	1.4 \pm 0.1	1.6 \pm 0.4	2.1 \pm 0.3
	3	6766 \pm 785	1.7 \pm 0.1	0.0 \pm 0.0	1.7 \pm 0.1
330240	1	6045 \pm 2566	-5.3 \pm 0.1	-4.4 \pm 0.4	6.9 \pm 0.3
	2	2728 \pm 797	1.0 \pm 0.1	4.0 \pm 0.4	4.1 \pm 0.4
	3	8595 \pm 956	1.9 \pm 0.1	0.0 \pm 0.0	1.9 \pm 0.1
330244	1		-2.6 \pm 0.1	-2.6 \pm 0.4	3.7 \pm 0.3
	2	2946 \pm 668	2.4 \pm 0.1	6.5 \pm 0.4	6.9 \pm 0.4
	3	5120 \pm 814	3.1 \pm 0.1	0.0 \pm 0.0	3.1 \pm 0.1
330333	1	3053 \pm 324	-5.9 \pm 0.1	0.0 \pm 0.0	5.9 \pm 0.1
	2	1350 \pm 277	-4.6 \pm 0.1	2.1 \pm 0.4	5.1 \pm 0.2
	3	3386 \pm 1015	2.5 \pm 0.1	0.1 \pm 0.1	2.5 \pm 0.1
330440	1	2956 \pm 374	-4.7 \pm 0.1	3.8 \pm 0.4	6.0 \pm 0.3
	2	2474 \pm 413	2.5 \pm 0.1	-2.1 \pm 0.4	3.3 \pm 0.3
	3		21.2 \pm 0.1	-13.1 \pm 0.3	24.8 \pm 0.2
350623	1	6711 \pm 636	2.0 \pm 0.1	1.1 \pm 0.4	2.3 \pm 0.2
	2	5016 \pm 1166	-0.9 \pm 0.1	-3.0 \pm 0.4	3.1 \pm 0.4
	3	3244 \pm 155	-4.1 \pm 0.1	0.1 \pm 0.1	4.1 \pm 0.1
350634	1		3.4 \pm 0.1	13.7 \pm 0.3	14.1 \pm 0.3
	2	4044 \pm 423	0.4 \pm 0.1	0.2 \pm 0.2	0.4 \pm 0.1
	3	7850 \pm 2018	-2.5 \pm 0.1	1.9 \pm 0.4	3.1 \pm 0.3
350659	1	1721 \pm 142	2.7 \pm 0.1	-0.8 \pm 0.4	2.8 \pm 0.1
	2		-6.2 \pm 0.1	15.0 \pm 0.3	16.2 \pm 0.3
	3		-43.6 \pm 0.1	-20.3 \pm 0.3	47.2 \pm 0.1
350670	1	10887 \pm 3217	-0.5 \pm 0.1	0.0 \pm 0.0	0.5 \pm 0.1
	2	750 \pm 111	-6.3 \pm 0.1	3.7 \pm 0.4	7.3 \pm 0.2
	3	648 \pm 129	28.9 \pm 0.1	-6.8 \pm 0.4	29.6 \pm 0.1
350716	1		-5.3 \pm 0.1	3.9 \pm 0.4	6.6 \pm 0.2
	2	8546 \pm 2704	-5.5 \pm 0.1	-1.8 \pm 0.4	5.8 \pm 0.2
	3		21.7 \pm 0.1	11.9 \pm 0.4	24.6 \pm 0.2
350726	1	3582 \pm 449	1.9 \pm 0.1	-1.4 \pm 0.4	2.4 \pm 0.3
	2		-4.6 \pm 0.1	-14.6 \pm 0.3	15.3 \pm 0.3
	3		-56.3 \pm 0.1	40.0 \pm 0.2	64.8 \pm 0.1

EVENT	TRK	P (MEV)	ϕ (°)	δ (°)	θ (°)
351230	1	5004± 887	3.7±0.1	0.0± 0.0	3.7± 0.1
	2	4361± 974	-2.9±0.1	-1.2± 0.4	3.1± 0.2
	3		-20.9±0.1	16.4± 0.4	26.3± 0.3
370003	1		-25.5±0.1	25.2± 0.3	35.2± 0.2
	2	7983±1619	-2.8±0.1	-1.8± 0.4	3.3± 0.2
	3	403± 174	49.1±0.1	5.2± 0.4	49.3± 0.1
370050	1	3627± 548	-4.1±0.1	2.8± 0.4	5.0± 0.2
	2	1600± 426	-0.8±0.1	-2.7± 0.4	2.8± 0.4
	3	5656± 880	6.6±0.1	-2.5± 0.4	7.1± 0.2
370052	1	6316± 734	-2.8±0.1	-1.7± 0.4	3.3± 0.2
	2	5331± 837	3.8±0.1	0.0± 0.0	3.8± 0.1
	3	1082± 120	5.4±0.1	2.6± 0.4	6.0± 0.2
370091	1		-6.8±0.1	-14.3± 0.3	15.8± 0.3
	2	2227± 993	-0.1±0.1	0.0± 0.0	0.1± 0.1
	3	429± 24	10.3±0.1	1.4± 0.4	10.4± 0.1
370101	1	7962±1158	-2.4±0.1	2.5± 0.4	3.5± 0.3
	2	8291±1680	1.8±0.1	-1.4± 0.4	2.3± 0.3
	3	1057± 293	4.6±0.1	-1.1± 0.4	4.7± 0.1
370110	1		-5.5±0.1	5.1± 0.4	7.5± 0.3
	2	6773±1022	-0.9±0.1	0.0± 0.0	0.9± 0.1
	3	4229± 370	3.1±0.1	-1.1± 0.4	3.3± 0.2
370306	1	2220± 183	-2.9±0.1	1.2± 0.4	3.1± 0.2
	2	5824± 636	1.6±0.1	-2.5± 0.4	3.0± 0.3
	3	1346± 163	1.5±0.1	4.8± 0.4	5.0± 0.4
370385	1	4063± 528	-2.8±0.1	0.8± 0.4	2.9± 0.1
	2	4791± 481	-0.7±0.1	0.0± 0.0	0.7± 0.1
	3	1747± 508	5.7±0.1	-5.7± 0.4	8.1± 0.3
370416	1	2737± 477	-1.4±0.1	-1.2± 0.4	1.8± 0.3
	2	1424± 456	4.5±0.1	5.3± 0.4	6.9± 0.3
	3	2437± 583	6.8±0.1	-4.4± 0.4	8.1± 0.2
370424	1	313± 42	-21.8±0.1	4.4± 0.4	22.2± 0.1
	2	5526± 879	-9.9±0.1	-3.5± 0.4	10.5± 0.2
	3		11.3±0.1	-9.8± 0.4	14.9± 0.3
370507	1	2216± 460	-2.3±0.1	0.0± 0.0	2.3± 0.1
	2		2.2±0.1	-4.0± 0.4	4.6± 0.4
	3	2470± 455	7.5±0.1	4.6± 0.4	8.8± 0.2

EVENT	TRK	P (MEV)	ϕ ($^{\circ}$)	δ ($^{\circ}$)	θ ($^{\circ}$)
380011	1	944 \pm 326	-7.0 \pm 0.1	-4.7 \pm 0.4	8.4 \pm 0.2
	2	3034 \pm 329	-0.6 \pm 0.1	1.5 \pm 0.4	1.6 \pm 0.4
	3	975 \pm 144	5.5 \pm 0.1	-2.7 \pm 0.4	6.1 \pm 0.2
380071	1		-36.0 \pm 0.1	12.5 \pm 0.3	37.8 \pm 0.1
	2	2916 \pm 329	-3.2 \pm 0.1	-1.2 \pm 0.4	3.4 \pm 0.2
	3	2941 \pm 1483	5.9 \pm 0.1	-6.2 \pm 0.4	8.6 \pm 0.3
380275	1	3177 \pm 929	-1.3 \pm 0.1	-1.2 \pm 0.4	1.8 \pm 0.3
	2	3336 \pm 453	-0.7 \pm 0.1	-2.0 \pm 0.4	2.1 \pm 0.4
	3	2913 \pm 860	3.4 \pm 0.1	2.6 \pm 0.4	4.3 \pm 0.3
392031	1	2211 \pm 502	-3.9 \pm 0.1	3.7 \pm 0.4	5.4 \pm 0.3
	2	562 \pm 78	-3.2 \pm 0.1	7.4 \pm 0.4	8.1 \pm 0.4
	3		8.2 \pm 0.1	-15.1 \pm 0.3	17.1 \pm 0.3
392102	1		-28.3 \pm 0.1	-57.6 \pm 0.1	61.8 \pm 0.1
	2	2990 \pm 861	-4.9 \pm 0.1	1.0 \pm 0.4	5.0 \pm 0.1
	3		-0.9 \pm 0.1	-5.7 \pm 0.4	5.8 \pm 0.4
392106	1	836 \pm 56	-28.9 \pm 0.1	5.0 \pm 0.4	29.3 \pm 0.1
	2		-5.5 \pm 0.1	19.2 \pm 0.3	19.9 \pm 0.3
	3	4661 \pm 745	2.9 \pm 0.1	-1.5 \pm 0.4	3.3 \pm 0.2
392131	1	4404 \pm 434	-1.3 \pm 0.1	1.1 \pm 0.4	1.7 \pm 0.3
	2	2004 \pm 241	2.1 \pm 0.1	-5.9 \pm 0.4	6.3 \pm 0.4
	3		4.9 \pm 0.1	-2.5 \pm 0.4	5.5 \pm 0.2
392190	1	521 \pm 85	-10.5 \pm 0.1	1.9 \pm 0.4	10.7 \pm 0.1
	2	339 \pm 35	-8.9 \pm 0.1	-4.8 \pm 0.4	10.1 \pm 0.2
	3	1752 \pm 357	1.2 \pm 0.1	1.0 \pm 0.4	1.6 \pm 0.3
400203	1		-11.9 \pm 0.1	-9.0 \pm 0.4	14.9 \pm 0.3
	2		4.4 \pm 0.1	6.5 \pm 0.4	7.8 \pm 0.3
	3		4.7 \pm 0.1	-12.4 \pm 0.3	13.2 \pm 0.3
400257	1	2097 \pm 455	-4.2 \pm 0.1	-2.6 \pm 0.4	4.9 \pm 0.2
	2	4670 \pm 679	-2.1 \pm 0.1	1.4 \pm 0.4	2.5 \pm 0.2
	3	5469 \pm 933	4.5 \pm 0.1	2.3 \pm 0.4	5.1 \pm 0.2
400330	1	4600 \pm 2393	-2.2 \pm 0.1	-4.4 \pm 0.4	4.9 \pm 0.4
	2	4447 \pm 642	1.9 \pm 0.1	-1.7 \pm 0.4	2.5 \pm 0.3
	3	1547 \pm 317	6.3 \pm 0.1	4.0 \pm 0.4	7.5 \pm 0.2
443374	1	6397 \pm 2296	-0.9 \pm 0.1	2.2 \pm 0.4	2.4 \pm 0.4
	2	1538 \pm 603	2.1 \pm 0.1	2.7 \pm 0.4	3.4 \pm 0.3
	3	2206 \pm 327	4.6 \pm 0.1	-1.5 \pm 0.4	4.8 \pm 0.2

EVENT	TRK	P (MEV)	$\phi (^{\circ})$	$\delta (^{\circ})$	$\theta (^{\circ})$
443389	1	3625 \pm 704	-9.2 \pm 0.1	0.0 \pm 0.0	9.2 \pm 0.1
	2	2672 \pm 153	-4.5 \pm 0.1	0.0 \pm 0.0	4.5 \pm 0.1
	3	1909 \pm 228	11.7 \pm 0.1	1.9 \pm 0.4	11.9 \pm 0.1
443486	1	756 \pm 178	-40.7 \pm 0.1	4.3 \pm 0.4	40.9 \pm 0.1
	2	1555 \pm 202	-11.6 \pm 0.1	2.6 \pm 0.4	11.9 \pm 0.1
	3		2.4 \pm 0.1	-17.7 \pm 0.3	17.9 \pm 0.3
443513	1		-29.4 \pm 0.1	-19.3 \pm 0.3	34.7 \pm 0.2
	2		-5.3 \pm 0.1	6.7 \pm 0.4	8.5 \pm 0.3
	3	921 \pm 104	12.3 \pm 0.1	0.0 \pm 0.0	12.3 \pm 0.1
443514	1	4786 \pm 1241	-1.3 \pm 0.1	1.4 \pm 0.4	1.9 \pm 0.3
	2		0.9 \pm 0.1	-6.8 \pm 0.4	6.9 \pm 0.4
	3	1504 \pm 379	6.4 \pm 0.1	-2.1 \pm 0.4	6.7 \pm 0.2
461357	1		-0.1 \pm 0.1	-5.7 \pm 0.4	5.7 \pm 0.4
	2		0.8 \pm 0.1	-5.1 \pm 0.4	5.2 \pm 0.4
	3	2253 \pm 358	4.7 \pm 0.1	0.0 \pm 0.0	4.7 \pm 0.1
461383	1	3726 \pm 344	-3.3 \pm 0.1	0.0 \pm 0.0	3.3 \pm 0.1
	2		-0.3 \pm 0.1	-0.9 \pm 0.4	0.9 \pm 0.4
	3	1549 \pm 119	5.6 \pm 0.1	1.6 \pm 0.4	5.8 \pm 0.1
461443	1		-2.6 \pm 0.1	-8.2 \pm 0.4	8.6 \pm 0.4
	2		3.6 \pm 0.1	-1.2 \pm 0.4	3.8 \pm 0.2
	3	1353 \pm 96	20.6 \pm 0.1	1.2 \pm 0.4	20.6 \pm 0.1
461952	1	2173 \pm 243	-2.8 \pm 0.1	-1.9 \pm 0.4	3.4 \pm 0.2
	2	2559 \pm 408	5.4 \pm 0.1	2.4 \pm 0.4	5.9 \pm 0.2
	3	2352 \pm 244	7.5 \pm 0.1	2.6 \pm 0.4	7.9 \pm 0.2
461989	1	1069 \pm 237	-9.1 \pm 0.1	5.0 \pm 0.4	10.4 \pm 0.2
	2	4721 \pm 880	-0.4 \pm 0.1	-1.9 \pm 0.4	1.9 \pm 0.4
	3	1234 \pm 257	3.3 \pm 0.1	3.1 \pm 0.4	4.5 \pm 0.3
480801	1	8938 \pm 1521	3.1 \pm 0.1	-2.0 \pm 0.4	3.7 \pm 0.2
	2	3660 \pm 372	-3.1 \pm 0.1	-1.2 \pm 0.4	3.3 \pm 0.2
	3	1463 \pm 244	-3.2 \pm 0.1	7.0 \pm 0.4	7.7 \pm 0.4
480837	1	2179 \pm 492	9.3 \pm 0.1	-3.7 \pm 0.4	10.0 \pm 0.2
	2	8162 \pm 606	-0.7 \pm 0.1	0.0 \pm 0.0	0.7 \pm 0.1
	3	1309 \pm 459	-2.3 \pm 0.1	3.1 \pm 0.4	3.9 \pm 0.3
480869	1		23.5 \pm 0.1	-7.7 \pm 0.4	24.7 \pm 0.2
	2	10645 \pm 1391	1.0 \pm 0.1	2.0 \pm 0.4	2.2 \pm 0.4
	3	1293 \pm 718	-35.3 \pm 0.1	6.1 \pm 0.4	35.8 \pm 0.1

EVENT	TRK	P (MEV)	$\phi(^{\circ})$	$\delta(^{\circ})$	$\theta(^{\circ})$
480883	1		5.5 ± 0.1	-7.7 ± 0.4	9.5 ± 0.3
	2	8078 ± 720	0.8 ± 0.1	2.3 ± 0.4	2.4 ± 0.4
	3	6524 ± 913	0.8 ± 0.1	-1.7 ± 0.4	1.9 ± 0.4
480921	1	358 ± 65	27.4 ± 0.1	5.4 ± 0.4	27.9 ± 0.1
	2	1723 ± 237	20.2 ± 0.1	-1.9 ± 0.4	20.3 ± 0.1
	3	767 ± 175	-9.3 ± 0.1	-73.4 ± 0.0	73.6 ± 0.0
481089	1	3027 ± 401	-13.0 ± 0.1	4.0 ± 0.4	13.6 ± 0.2
	2		0.7 ± 0.1	22.0 ± 0.3	22.0 ± 0.3
	3	2971 ± 251	8.2 ± 0.1	2.3 ± 0.4	8.5 ± 0.1
481152	1	729 ± 23	3.6 ± 0.1	-8.3 ± 0.4	9.0 ± 0.4
	2		-2.0 ± 0.1	15.8 ± 0.3	15.9 ± 0.3
	3	5647 ± 1020	-3.9 ± 0.1	-1.5 ± 0.4	4.2 ± 0.2
481158	1	6244 ± 1256	3.0 ± 0.1	-1.8 ± 0.4	3.5 ± 0.2
	2	4254 ± 513	-2.1 ± 0.1	1.7 ± 0.4	2.7 ± 0.3
	3	510 ± 41	-11.8 ± 0.1	-3.0 ± 0.4	12.2 ± 0.1
481164	1		14.6 ± 0.1	-6.0 ± 0.5	15.8 ± 0.2
	2	539 ± 103	-0.3 ± 0.1	10.7 ± 0.4	10.7 ± 0.4
	3		-4.7 ± 0.1	-3.7 ± 0.4	6.0 ± 0.3
513291	1	1142 ± 400	-0.8 ± 0.1	0.0 ± 0.0	0.8 ± 0.1
	2		2.4 ± 0.1	-8.1 ± 0.4	8.4 ± 0.4
	3	786 ± 63	4.6 ± 0.1	8.7 ± 0.4	9.8 ± 0.4
182993	1		-50.5 ± 0.1	8.5 ± 0.4	51.0 ± 0.1
	2	6780 ± 3356	-2.0 ± 0.1	2.1 ± 0.4	2.9 ± 0.3
	3	3942 ± 1265	-0.6 ± 0.1	1.3 ± 0.4	1.4 ± 0.4
	4	384 ± 89	-0.3 ± 0.1	1.3 ± 0.4	1.3 ± 0.4
	P	129 ± 1	64.4 ± 0.1	25.0 ± 0.3	66.9 ± 0.1
183003	1	1270 ± 743	-7.8 ± 0.1	6.0 ± 0.4	9.8 ± 0.3
	2	6830 ± 2240	-3.1 ± 0.1	-5.8 ± 0.4	6.6 ± 0.4
	3	3054 ± 233	1.0 ± 0.1	3.6 ± 0.4	3.7 ± 0.4
	4	1255 ± 183	9.0 ± 0.1	3.7 ± 0.4	9.7 ± 0.2
	P	24 ± 1	68.0 ± 1.5	4.1 ± 4.1	68.1 ± 1.5
221606	1	1906 ± 270	-6.5 ± 0.1	0.0 ± 0.0	6.5 ± 0.1
	2		-1.4 ± 0.1	-16.2 ± 0.3	16.3 ± 0.3
	3	1990 ± 324	13.5 ± 0.1	3.2 ± 0.4	13.9 ± 0.1
	4	2432 ± 715	14.0 ± 0.1	9.7 ± 0.4	17.0 ± 0.2
	P	253 ± 3	-44.1 ± 0.1	-33.9 ± 0.3	53.4 ± 0.2

EVENT	TRK	P (MEV)	$\phi (^{\circ})$	$\delta (^{\circ})$	$\theta (^{\circ})$
221746	1	2317± 686	-20.4±0.1	4.5± 0.4	20.9± 0.1
	2	2266± 424	-1.5±0.1	-1.8± 0.4	2.3± 0.3
	3	3835±1172	0.6±0.1	4.5± 0.4	4.5± 0.4
	4	2530±1371	7.2±0.1	-4.0± 0.4	8.2± 0.2
	P	420± 30	-13.7±0.1	-29.9± 0.3	32.6± 0.3
310320	1		-12.3±0.1	25.7± 0.3	28.3± 0.3
	2	4579± 672	-1.4±0.1	1.3± 0.4	1.9± 0.3
	3	4544± 654	1.7±0.1	0.0± 0.0	1.7± 0.1
	4		18.8±0.1	-19.4± 0.3	26.8± 0.2
	P	390± 40	9.1±0.1	52.2± 0.1	52.8± 0.1
330462	1		-12.9±0.1	21.6± 0.3	25.0± 0.3
	2		-9.5±0.1	-12.2± 0.4	15.4± 0.3
	3	11938±2874	2.5±0.1	-2.8± 0.4	3.8± 0.3
	4		77.6±0.1	21.7± 0.3	78.5± 0.1
	P	34± 1	-64.9±0.1	1.7± 1.7	64.9± 0.1
350594	1		-46.5±0.1	-20.7± 0.3	49.9± 0.1
	2		-1.3±0.1	5.1± 0.4	5.3± 0.4
	3		1.3±0.1	-1.4± 0.4	1.9± 0.3
	4		3.9±0.1	4.0± 0.4	5.6± 0.3
	P	134± 1	-23.4±0.1	12.8± 0.3	26.5± 0.2
351313	1		-73.6±0.1	-48.5± 0.2	79.2± 0.1
	2	1659± 634	4.6±0.1	7.3± 0.4	8.6± 0.3
	3	7822±3101	13.2±0.1	3.5± 0.4	13.6± 0.1
	4	1201± 73	18.3±0.1	-1.3± 0.4	18.3± 0.1
	P		-74.7±0.1	-54.6± 0.1	81.2± 0.1
392136	1	5767± 802	-3.9±0.1	0.0± 0.0	3.9± 0.1
	2	3097± 906	1.2±0.1	5.0± 0.4	5.1± 0.4
	3	2741± 305	1.7±0.1	-1.6± 0.4	2.3± 0.3
	4	1563± 174	33.1±0.1	0.0± 0.0	33.1± 0.1
	P	610± 430	-44.6±0.1	-9.3± 0.4	45.4± 0.1
150106	1		-85.6±0.1	15.0± 0.4	85.7± 0.1
	2	5098± 671	-0.6±0.1	0.0± 0.0	0.6± 0.1
	3		-0.2±0.1	-11.4± 0.3	11.4± 0.3
	4		9.5±0.1	-4.3± 0.4	10.4± 0.2
	5	2466± 251	14.8±0.1	3.1± 0.4	15.1± 0.1
150186	1		-22.8±0.1	-13.6± 0.3	26.4± 0.2
	2	4603± 465	-5.8±0.1	5.9± 0.4	8.3± 0.3
	3	1570± 907	-1.8±0.1	-5.9± 0.4	6.2± 0.4
	4		-0.4±0.1	12.4± 0.3	12.4± 0.3

EVENT	TRK	P (MEV)	ϕ ($^{\circ}$)	δ ($^{\circ}$)	θ ($^{\circ}$)
	5	395 \pm 134	34.5 \pm 0.1	-5.0 \pm 0.4	34.8 \pm 0.1
182959	1	1284 \pm 263	-8.9 \pm 0.1	9.6 \pm 0.4	13.1 \pm 0.3
	2	3348 \pm 280	-5.1 \pm 0.1	0.0 \pm 0.0	5.1 \pm 0.1
	3		1.3 \pm 0.1	-6.4 \pm 0.4	6.5 \pm 0.4
	4		5.2 \pm 0.1	12.6 \pm 0.3	13.6 \pm 0.3
	5		35.3 \pm 0.1	-23.5 \pm 0.3	41.5 \pm 0.2
183065	1		-15.1 \pm 0.1	5.7 \pm 0.4	16.1 \pm 0.2
	2	3511 \pm 869	-5.7 \pm 0.1	2.8 \pm 0.4	6.3 \pm 0.2
	3		1.5 \pm 0.1	6.4 \pm 0.4	6.6 \pm 0.4
	4	4730 \pm 300	8.4 \pm 0.1	4.5 \pm 0.4	9.5 \pm 0.2
	5		-11.1 \pm 0.1	-28.2 \pm 0.3	30.1 \pm 0.3
183134	1		-35.3 \pm 0.1	22.6 \pm 0.3	41.1 \pm 0.2
	2	3778 \pm 478	-23.1 \pm 0.1	0.0 \pm 0.0	23.1 \pm 0.1
	3	1214 \pm 214	-9.3 \pm 0.1	-6.2 \pm 0.4	11.2 \pm 0.2
	4		17.3 \pm 0.1	11.6 \pm 0.4	20.7 \pm 0.2
	5	1515 \pm 247	43.0 \pm 0.1	-7.9 \pm 0.4	43.6 \pm 0.1
183177	1		-39.0 \pm 0.1	-12.7 \pm 0.3	40.7 \pm 0.1
	2		5.5 \pm 0.1	2.9 \pm 0.4	6.2 \pm 0.2
	3		22.4 \pm 0.1	9.4 \pm 0.4	24.2 \pm 0.2
	4	2151 \pm 192	36.0 \pm 0.1	-2.6 \pm 0.4	36.1 \pm 0.1
	5	549 \pm 76	-13.1 \pm 0.1	-6.9 \pm 0.4	14.8 \pm 0.2
262546	1	2959 \pm 499	-8.2 \pm 0.1	1.8 \pm 0.4	8.4 \pm 0.1
	2	4018 \pm 826	-2.1 \pm 0.1	-3.6 \pm 0.4	4.2 \pm 0.3
	3	474 \pm 29	6.1 \pm 0.1	18.0 \pm 0.3	19.0 \pm 0.3
	4		42.8 \pm 0.1	-10.4 \pm 0.4	43.8 \pm 0.1
	5		49.2 \pm 0.1	2.8 \pm 0.4	49.3 \pm 0.1
262600	1		-55.4 \pm 0.1	-39.5 \pm 0.2	64.0 \pm 0.1
	2		-14.8 \pm 0.1	37.8 \pm 0.2	40.2 \pm 0.2
	3	1316 \pm 250	-11.5 \pm 0.1	-5.6 \pm 0.4	12.8 \pm 0.2
	4	3081 \pm 581	-5.1 \pm 0.1	-4.0 \pm 0.4	6.5 \pm 0.3
	5	819 \pm 86	11.1 \pm 0.1	-1.0 \pm 0.4	11.1 \pm 0.1
350729	1		-25.2 \pm 0.1	14.0 \pm 0.3	28.6 \pm 0.2
	2	4351 \pm 788	-5.2 \pm 0.1	2.6 \pm 0.4	5.8 \pm 0.2
	3	3092 \pm 496	-5.0 \pm 0.1	5.1 \pm 0.4	7.1 \pm 0.3
	4	8280 \pm 2151	7.3 \pm 0.1	0.0 \pm 0.0	7.3 \pm 0.1
	5		95.9 \pm 0.1	-25.0 \pm 0.4	95.3 \pm 0.1
370041	1	180 \pm 8	-23.6 \pm 0.1	-3.5 \pm 0.4	23.8 \pm 0.1
	2	6187 \pm 1599	-8.5 \pm 0.1	0.0 \pm 0.0	8.5 \pm 0.1
	3	6167 \pm 678	1.3 \pm 0.1	0.9 \pm 0.4	1.6 \pm 0.2

EVENT	TRK	P (MEV)	$\phi (^{\circ})$	$\delta (^{\circ})$	$\theta (^{\circ})$
	4	3448 \pm 558	3.4 \pm 0.1	-2.9 \pm 0.4	4.5 \pm 0.3
	5		8.8 \pm 0.1	-11.6 \pm 0.4	14.5 \pm 0.3
370095	1	2525 \pm 648	-11.7 \pm 0.1	3.2 \pm 0.4	12.1 \pm 0.1
	2	4042 \pm 2383	0.9 \pm 0.1	0.0 \pm 0.0	0.9 \pm 0.1
	3	947 \pm 128	2.6 \pm 0.1	-6.1 \pm 0.4	6.6 \pm 0.4
	4		14.1 \pm 0.1	10.9 \pm 0.4	17.8 \pm 0.3
	5		158.5 \pm 0.1	-29.8 \pm 0.3	143.8 \pm 0.2
370249	1		-12.9 \pm 0.1	-28.3 \pm 0.3	30.9 \pm 0.3
	2	761 \pm 148	-6.8 \pm 0.1	-3.9 \pm 0.4	7.8 \pm 0.2
	3	3658 \pm 1913	0.1 \pm 0.1	-2.2 \pm 0.4	2.2 \pm 0.4
	4	341 \pm 58	2.1 \pm 0.1	4.6 \pm 0.4	5.1 \pm 0.4
	5	1465 \pm 377	15.3 \pm 0.1	6.4 \pm 0.4	16.6 \pm 0.2
370305	1		-26.9 \pm 0.1	-3.2 \pm 0.4	27.1 \pm 0.1
	2		-7.1 \pm 0.1	15.3 \pm 0.3	16.8 \pm 0.3
	3	3047 \pm 181	-4.1 \pm 0.1	0.0 \pm 0.0	4.1 \pm 0.1
	4		3.3 \pm 0.1	-7.5 \pm 0.4	8.2 \pm 0.4
	5	565 \pm 75	18.2 \pm 0.1	-0.8 \pm 0.4	18.2 \pm 0.1
380058	1	1014 \pm 102	-10.6 \pm 0.1	1.8 \pm 0.4	10.7 \pm 0.1
	2		1.6 \pm 0.1	-10.7 \pm 0.4	10.8 \pm 0.4
	3		19.8 \pm 0.1	12.3 \pm 0.4	23.2 \pm 0.2
	4	623 \pm 82	27.6 \pm 0.1	3.5 \pm 0.4	27.8 \pm 0.1
	5		61.9 \pm 0.1	-5.4 \pm 0.4	62.0 \pm 0.1
400160	1	3740 \pm 2289	-11.3 \pm 0.1	-2.9 \pm 0.4	11.7 \pm 0.1
	2	3079 \pm 712	-2.4 \pm 0.1	4.9 \pm 0.4	5.5 \pm 0.4
	3		-0.5 \pm 0.1	2.9 \pm 0.4	2.9 \pm 0.4
	4		0.0 \pm 0.1	-5.2 \pm 0.4	5.2 \pm 0.4
	5	1311 \pm 146	23.1 \pm 0.1	2.7 \pm 0.4	23.2 \pm 0.1
400237	1		-9.4 \pm 0.1	-14.8 \pm 0.3	17.5 \pm 0.3
	2	2479 \pm 437	-8.8 \pm 0.1	0.3 \pm 0.3	8.8 \pm 0.1
	3		4.7 \pm 0.1	-2.9 \pm 0.4	5.5 \pm 0.2
	4		13.9 \pm 0.1	-30.3 \pm 0.9	33.1 \pm 0.8
	5		14.7 \pm 0.1	15.1 \pm 0.4	21.0 \pm 0.3
400267	1		-30.0 \pm 0.1	10.3 \pm 0.4	31.6 \pm 0.2
	2	790 \pm 232	-10.9 \pm 0.1	3.6 \pm 0.4	11.5 \pm 0.2
	3		-3.9 \pm 0.1	11.0 \pm 0.4	11.7 \pm 0.4
	4	2076 \pm 239	-2.6 \pm 0.1	-2.5 \pm 0.4	3.6 \pm 0.3
	5		-1.6 \pm 0.1	18.2 \pm 0.3	18.3 \pm 0.3
400319	1		-19.5 \pm 0.1	-11.5 \pm 0.4	22.5 \pm 0.2
	2		-6.0 \pm 0.1	11.0 \pm 0.3	12.5 \pm 0.3
	3	3940 \pm 1180	-2.3 \pm 0.1	2.3 \pm 0.4	3.3 \pm 0.3

EVENT	TRK	P (MEV)	$\phi(^{\circ})$	$\delta(^{\circ})$	$\theta(^{\circ})$
	4		23.4 ± 0.1	11.9 ± 0.4	26.1 ± 0.2
	5		138.9 ± 0.1	-30.8 ± 0.3	130.3 ± 0.2
443373	1		-7.9 ± 0.1	24.1 ± 0.3	25.3 ± 0.3
	2	2086 ± 240	-3.6 ± 0.1	4.1 ± 0.4	5.5 ± 0.3
	3	1805 ± 329	2.2 ± 0.1	5.1 ± 0.4	5.6 ± 0.4
	4		3.4 ± 0.1	-20.4 ± 0.3	20.7 ± 0.3
	5		4.6 ± 0.1	-8.6 ± 0.4	9.7 ± 0.4
443450	1		-34.4 ± 0.1	-15.7 ± 0.3	37.4 ± 0.1
	2	5189 ± 576	-0.4 ± 0.1	2.4 ± 0.4	2.4 ± 0.4
	3	6487 ± 898	3.0 ± 0.1	2.4 ± 0.4	3.8 ± 0.3
	4		16.4 ± 0.1	-30.9 ± 0.3	34.6 ± 0.3
	5		23.7 ± 0.1	34.2 ± 0.3	40.8 ± 0.2
461335	1	4223 ± 672	-2.0 ± 0.1	0.0 ± 0.0	2.0 ± 0.1
	2	4012 ± 696	-2.7 ± 0.1	0.0 ± 0.0	2.7 ± 0.1
	3	2403 ± 256	-21.3 ± 0.1	0.0 ± 0.0	21.3 ± 0.1
	4	478 ± 100	-20.9 ± 0.1	0.0 ± 0.0	20.9 ± 0.1
	5	361 ± 55	46.7 ± 0.1	0.0 ± 0.0	46.7 ± 0.1
480939	1	1020 ± 125	-7.8 ± 0.1	-6.0 ± 0.4	9.8 ± 0.3
	2		-5.5 ± 0.1	10.2 ± 0.4	11.6 ± 0.4
	3	4217 ± 644	-4.9 ± 0.1	0.0 ± 0.0	4.9 ± 0.1
	4	7347 ± 1118	-1.7 ± 0.1	0.0 ± 0.0	1.7 ± 0.1
	5	299 ± 43	14.8 ± 0.1	4.2 ± 0.4	15.4 ± 0.1
480942	1	614 ± 26	5.7 ± 0.1	-1.5 ± 0.4	5.9 ± 0.1
	2	1239 ± 146	1.8 ± 0.1	1.7 ± 0.4	2.5 ± 0.3
	3	1058 ± 79	0.4 ± 0.1	-2.0 ± 0.4	2.0 ± 0.4
	4	1385 ± 339	-12.3 ± 0.1	5.8 ± 0.4	13.6 ± 0.2
	5		-4.5 ± 0.1	-14.8 ± 0.3	15.5 ± 0.3
481138	1		-35.9 ± 0.1	18.7 ± 0.3	39.9 ± 0.1
	2	1346 ± 263	-4.3 ± 0.1	7.4 ± 0.4	8.6 ± 0.3
	3		1.6 ± 0.1	-11.4 ± 0.4	11.5 ± 0.4
	4		4.1 ± 0.1	-4.8 ± 0.4	6.3 ± 0.3
	5	1476 ± 426	6.7 ± 0.1	6.6 ± 0.4	9.4 ± 0.3
513335	1		-6.3 ± 0.1	9.7 ± 0.4	11.5 ± 0.3
	2	4165 ± 310	-1.4 ± 0.1	0.0 ± 0.0	1.4 ± 0.1
	3	1098 ± 168	-0.5 ± 0.1	0.7 ± 0.4	0.9 ± 0.3
	4	2251 ± 298	0.1 ± 0.1	-5.9 ± 0.4	5.9 ± 0.4
	5	1557 ± 186	3.4 ± 0.1	-1.1 ± 0.4	3.6 ± 0.2
221715	1	368 ± 42	-10.8 ± 0.1	5.4 ± 0.4	12.1 ± 0.2
	2	4499 ± 2226	-10.3 ± 0.1	-8.5 ± 0.4	13.3 ± 0.3
	3	2788 ± 839	-5.6 ± 0.1	-2.8 ± 0.4	6.3 ± 0.2

EVENT	TRK	P (MEV)	ϕ ($^{\circ}$)	δ ($^{\circ}$)	θ ($^{\circ}$)
	4		4.0 ± 0.1	17.3 ± 0.3	17.7 ± 0.3
	5	1927 ± 342	16.9 ± 0.1	0.0 ± 0.0	16.9 ± 0.1
	6		-2.6 ± 0.1	34.5 ± 0.3	34.6 ± 0.3
	P	280 ± 3	-2.6 ± 0.1	37.6 ± 0.2	37.7 ± 0.2
330150	1		-18.6 ± 0.1	11.4 ± 0.4	21.7 ± 0.2
	2		-13.7 ± 0.1	7.7 ± 0.4	15.7 ± 0.2
	3	3726 ± 284	-0.2 ± 0.1	0.0 ± 0.0	0.2 ± 0.1
	4		9.9 ± 0.1	18.6 ± 0.3	21.0 ± 0.3
	5		35.0 ± 0.1	19.4 ± 0.3	39.4 ± 0.2
	6		43.0 ± 0.1	23.0 ± 0.3	47.7 ± 0.1
	P	540 ± 6	0.5 ± 0.1	-1.3 ± 0.4	1.4 ± 0.4
330433	1		-65.7 ± 0.1	-14.6 ± 0.4	66.5 ± 0.1
	2	1708 ± 298	-7.5 ± 0.1	-3.5 ± 0.4	8.3 ± 0.2
	3		1.9 ± 0.1	6.6 ± 0.4	6.9 ± 0.4
	4		2.9 ± 0.1	3.6 ± 0.4	4.6 ± 0.3
	5	2400 ± 825	3.2 ± 0.1	-8.1 ± 0.4	8.7 ± 0.4
	6	1416 ± 129	15.7 ± 0.1	0.0 ± 0.0	15.7 ± 0.1
	P	520 ± 360	66.4 ± 0.1	1.3 ± 0.4	66.4 ± 0.1
461374	1		-9.3 ± 0.1	-1.8 ± 0.4	9.5 ± 0.1
	2		-6.9 ± 0.1	31.7 ± 0.3	32.4 ± 0.3
	3	1428 ± 149	-1.4 ± 0.1	2.0 ± 0.4	2.4 ± 0.3
	4		2.6 ± 0.1	29.8 ± 0.3	29.9 ± 0.3
	5		4.2 ± 0.1	-13.6 ± 0.3	14.2 ± 0.3
	6	4994 ± 611	4.8 ± 0.1	0.0 ± 0.0	4.8 ± 0.1
	P	44 ± 1	-56.4 ± 0.1	41.0 ± 2.1	65.3 ± 0.8
461424	1		-35.3 ± 0.1	5.5 ± 0.6	35.7 ± 0.1
	2		-8.9 ± 0.1	-13.7 ± 0.3	16.3 ± 0.3
	3		-2.8 ± 0.1	-8.2 ± 0.4	8.7 ± 0.4
	4	460 ± 53	-0.7 ± 0.1	-1.4 ± 0.4	1.6 ± 0.4
	5		17.7 ± 0.1	-25.4 ± 0.3	30.6 ± 0.2
	6		48.8 ± 0.1	-13.3 ± 0.3	50.1 ± 0.1
	P	193 ± 2	-16.4 ± 0.1	-27.1 ± 0.3	31.4 ± 0.3
481159	1		-22.3 ± 0.1	-3.7 ± 0.4	22.6 ± 0.1
	2	2571 ± 681	-17.3 ± 0.1	5.9 ± 0.4	18.2 ± 0.2
	3		-11.3 ± 0.1	13.4 ± 0.4	17.5 ± 0.3
	4	416 ± 140	-2.2 ± 0.1	4.9 ± 0.4	5.4 ± 0.4
	5		1.7 ± 0.1	-17.9 ± 0.3	18.0 ± 0.3
	6	903 ± 108	38.2 ± 0.1	2.9 ± 0.4	38.3 ± 0.1
	P	226 ± 3	-5.8 ± 0.1	3.5 ± 0.4	6.8 ± 0.2

EVENT	TRK	P (MEV)	$\phi(^{\circ})$	$\delta(^{\circ})$	$\theta(^{\circ})$
201027	1	3855± 570	-9.3±0.1	1.5± 0.4	9.4± 0.1
	2	4203± 647	-4.3±0.1	0.0± 0.0	4.3± 0.1
	3		-3.4±0.1	12.0± 0.4	12.5± 0.4
	4	513± 37	0.1±0.1	1.9± 0.4	1.9± 0.4
	5		5.0±0.1	11.6± 0.4	12.6± 0.4
	6	672± 89	6.1±0.1	-2.6± 0.4	6.6± 0.2
	7	2796± 909	16.0±0.1	-4.0± 0.4	16.5± 0.1
221770	1	874± 179	-19.2±0.1	4.2± 0.4	19.6± 0.1
	2	4467± 450	1.1±0.1	-1.0± 0.4	1.5± 0.3
	3	10272±2936	1.7±0.1	0.0± 0.0	1.7± 0.1
	4		2.7±0.1	-5.4± 0.4	6.0± 0.4
	5	1653± 281	3.3±0.1	-4.0± 0.4	5.2± 0.3
	6		26.9±0.1	-21.7± 0.3	34.0± 0.2
	7		3.2±0.1	-12.8± 0.3	13.2± 0.3
262594	1		-28.0±0.1	-28.9± 0.3	39.4± 0.2
	2		-4.3±0.1	10.7± 0.4	11.5± 0.4
	3		-2.8±0.1	-18.7± 0.3	18.9± 0.3
	4		-2.0±0.1	-20.8± 0.3	20.9± 0.3
	5		0.5±0.1	-19.0± 0.3	19.0± 0.3
	6	2047± 282	6.1±0.1	0.0± 0.0	6.1± 0.1
	7	649± 127	18.9±0.1	-9.6± 0.4	21.1± 0.2
400244	1	810± 91	-47.2±0.1	0.0± 0.0	47.2± 0.1
	2		-26.6±0.1	-26.8± 0.3	37.0± 0.2
	3	9253±4811	-2.2±0.1	-5.6± 0.4	6.0± 0.4
	4		-2.6±0.1	10.3± 0.4	10.6± 0.4
	5		-0.1±0.1	-14.4± 0.3	14.4± 0.3
	6		4.0±0.1	3.4± 0.4	5.2± 0.3
	7	4674± 440	6.4±0.1	0.0± 0.0	6.4± 0.1
320041	1		-39.5±0.1	-15.1± 0.4	41.8± 0.2
	2		-20.4±0.1	-19.6± 0.5	28.0± 0.3
	3	985± 222	-15.9±0.1	10.1± 0.4	18.8± 0.2
	4	1212± 358	-3.5±0.1	4.3± 0.4	5.5± 0.3
	5	1030± 240	0.9±0.1	6.0± 0.4	6.1± 0.4
	6		12.6±0.1	-5.5± 0.4	13.7± 0.2
	7	1096± 103	15.6±0.1	3.6± 0.4	16.0± 0.1
	8	958± 252	19.6±0.1	7.0± 0.4	20.8± 0.2
	9		-17.2±0.1	-11.5± 0.4	20.6± 0.2

EVENT	TRK	P (MEV)	$\phi (^{\circ})$	$\delta (^{\circ})$	$\theta (^{\circ})$
370245	1	3071± 501	-8.7±0.1	-1.6± 0.4	8.8± 0.1
	2		-4.2±0.1	-2.4± 0.4	4.8± 0.2
	3		-1.6±0.1	-6.0± 0.4	6.2± 0.4
	4	1739± 869	-1.0±0.1	5.9± 0.4	6.0± 0.4
	5		-0.5±0.1	5.9± 0.4	5.9± 0.4
	6		1276± 220	-0.5±0.1	-3.8± 0.4
	7	1168± 195	2.7±0.1	2.7± 0.4	3.8± 0.3
	8	1389± 357	11.2±0.1	3.4± 0.4	11.7± 0.1
	9		14.9±0.1	5.7± 0.4	15.9± 0.2
461406	1		-58.2±0.1	-73.4± 0.1	81.3± 0.1
	2		-25.6±0.1	20.9± 0.3	32.6± 0.2
	3		-1.5±0.1	14.3± 0.3	14.4± 0.3
	4		0.1±0.1	-10.3± 0.4	10.3± 0.4
	5	947± 169	4.0±0.1	-1.7± 0.4	4.3± 0.2
	6		11.8±0.1	11.7± 0.4	16.6± 0.3
	7		17.7±0.1	-22.9± 0.3	28.6± 0.2
	8		44.0±0.1	20.1± 0.3	47.5± 0.1
	9		-25.6±0.1	-12.5± 0.4	28.3± 0.2
351220	1	694± 120	-26.3±0.1	-5.4± 0.4	26.8± 0.1
	2		-7.9±0.1	-8.5± 0.4	11.6± 0.3
	3		-4.0±0.1	-8.4± 0.4	9.3± 0.4
	4	839± 172	-0.8±0.1	-6.5± 0.4	6.5± 0.4
	5	1308± 132	1.0±0.1	2.6± 0.4	2.8± 0.4
	6		2.0±0.1	-7.9± 0.4	8.1± 0.4
	7		16.1±0.1	20.9± 0.3	26.2± 0.2
	8		18.7±0.1	52.0± 0.1	54.3± 0.1
	9	748± 150	25.8±0.1	6.7± 0.4	26.6± 0.1
	10	602± 72	43.3±0.1	5.4± 0.4	43.6± 0.1
	ii		55.1±0.1	-8.6± 0.4	55.5± 0.1
481115	1		-15.7±0.1	24.5± 0.3	28.8± 0.3
	2		-12.6±0.1	9.8± 0.4	15.9± 0.3
	3		-9.3±0.1	24.9± 0.3	26.5± 0.3
	4		-5.7±0.1	7.2± 0.4	9.2± 0.3
	5		-3.7±0.1	-21.2± 0.3	21.5± 0.3
	6		17.7±0.1	-27.6± 0.3	32.4± 0.3
	7	500± 46	17.7±0.1	0.0± 0.0	17.7± 0.1
	8		29.8±0.1	-9.4± 0.4	31.1± 0.1
	9		36.9±0.1	-18.4± 0.3	40.6± 0.1

EVENT	TRK	P(MEV)	$\phi(^{\circ})$	$\delta(^{\circ})$	$\theta(^{\circ})$
	10		40.7 ± 0.1	-15.4 ± 0.3	43.0 ± 0.1
	11		66.1 ± 0.1	42.2 ± 0.2	72.5 ± 0.1

LIST OF REFERENCES

1. Lindenbaum, S. J. and Sternheimer, R. M., Phys. Rev., 105, 1874 (57)
2. Ferrari, E. and Selleri, F., Nuovo Cim Suppl., 24, 453 (62)
3. Fermi, E., Phys. Rev. 81, 683 (51)
4. Takagi, S., Progr. Theort. Phys. 7, 123 (52)
5. Howard, R. A.: Nuclear Physics, (Calif.: Wadsworth, 63)
6. Laverriere, R. and Grea, J., Nuclear Phys., 41, 660 (63)
7. Powell, Fowler, and Perkins: Study of the Elementary Particles by the Photographic Method, (N.Y.: Pergamon, 59)
8. Barkas, W. H., Private Communications
9. Barkas, W. H.: Nuclear Research Emulsion, (N.Y.: Academic, 63)
10. Fowler, P.H. and Perkins, D. H., Phil Mag., 46, 587 (55)
11. Burwell, J.R., Proceedings of the VI Int. Conf. on Corpuscular Photography, 1966.
12. Dilworth, C. et al, Nuovo Cim, 11, 113 (54)
13. Bartke, J. et al, Proc. of the 10th Int. Conf. on High Energy Phys., Rochester, 1960
14. Wang, C.P., Phys Rev, 180, 1463 (69)
15. Segre, E.: Nuclei and Particles (N.Y.: W. A. Benjamin, 1964)

LIST OF REFERENCES (Cont.)

16. Baudinet-Robinet, Y. et al, Nuclear Phys. 32, 452 (62)
17. Ciurlo, S., et al, Nuovo Cim 27, 791 (63)
18. Bellini, G., et al, Nuovo Cim 27, 816 (63)
19. Block, M., Nuovo Cim 28, 1825 (63)
20. Ferrari, E. and Selleri, F., Nuovo Cim Suppl. 27, 1450 (63)
21. Bartke, J., Nuclear Phys. 82, 673 (66)
22. Kamal, A. A. et al, Nuclear Phys. B6, 523 (68)
23. Goldsack, S. J., et al, Nuovo Cim, 23, 941 (62)
24. Fast, G., and Hagedorn, R., Nuovo Cim, 27, 208 (63)
25. Minakowa, O., et al Nuovo Cim Suppl. 11, 125 (59)
26. Spergel, M.S. et al, Nuovo Cim, 42, 255 (66)
27. Malhotra, P. K., Nuclear Phys. 59, 551 (64)
28. Friedlander, E. M., Nuovo Cim 41A, 417 (66)
29. Aly, H. H., et al, Nuovo Cim, 32, 905 (64)
30. Ho, S. K.: M. S. Thesis, University of Oklahoma (68)
31. Lohrmann, E., Suppl. Nuovo Cim 1, 1226 (63)
32. Fowler, and Perkins, Proc. Roy. Soc. 278A, 401 (64)
33. Orear, J., Phys. Letters, 13, 120 (64)
34. Imaeda, K., Nuovo Cim, 48A, 482 (67)
35. Birger, N. G., and Smorodin, Yu. A., JETP 9, 823 (59)
36. Lim, Y. K., Nuovo Cim 28, 1228 (63)
37. Birger, N.G., and Smorodin, Y. A., Nuclear Phys. 30, 350 (62)
38. Jain, P. L., Phys. Rev., 122, 1890 (61)

LIST OF REFERENCES (Cont.)

39. Birger, N. G., et al, Proc. Moscow Cosmic Ray Conf. Vol. 1, p. 154 (Moscow, 1960)
40. Awunor-Renner, E., et al, Nuovo Cim 17, 134 (60)
41. Birger, N. G., and Smorodin, Yu. A., JETP 10, 964 (60)
42. Gainotti, A. et al, Nuovo Cim 29, 1209 (63)
43. Kaplon, M.K. and Shen, M. L., Nuovo Cim 37, 423 (64)
44. Koba, Z., and Krzywicki, A., Nuovo Cim, 21, 1078 (61)
45. Friedlander, E. M. et al, Nuovo Cim 18, 593 (60)
46. Castagnoli, C. et al, Nuovo Cim 10, 1439 (53)
47. Oleson, C. A., M.S. Thesis, University of Oklahoma (1966)
48. Bartke, J. et al, Acat Phys. Polan. 27, 869 (65)
49. Jain, P. L., Nuovo Cim 31, 764 (64)
50. Wang, P. Y., and Jain, P. L., Nuovo Cim 61A, 567 (69)
51. Proceedings of Second Topical Conference, Resonant Particles, Ohio U., Athens, Ohio, 1965
52. Williams, W. S. C.: Introduction to Elementary Particles, (N.Y.: Academic Press, 1961)
53. Samimi, J.: M. S. Thesis, University of Oklahoma (66)
54. Rosenfeld, A. H. et al, Rev. Mod. Phys., 40, 77 (68)
55. Citron, A., et al, Phys. Rev. 144, 1101 (66)
56. Kallen, G.: Elementary Particle Physics (London: Addison-Wesley, 1964)
57. O'Reilly, P. D.: Ph. D. Dissertation, University of Oklahoma (69)
58. Widgoff, M.: Techniques of High Energy Physics (Interscience, N. Y. 1961)